

---

# A quantum memory for light in nuclear spins of a quantum dot

Heike Schwager

---

MAX-PLANCK-INSTITUT  
FÜR QUANTENOPTIK



EBERHARD KARLS  
UNIVERSITÄT  
TÜBINGEN



Garching, den 2. Januar 2008



---

# **A quantum memory for light in nuclear spins of a quantum dot**

**Heike Schwager**

---

Diplomarbeit  
an der Fakultät für Physik  
der Eberhard–Karls–Universität  
Tübingen

angefertigt am  
Max-Planck Institut für Quantenoptik  
Garching

vorgelegt von  
Heike Schwager

Garching, den 2. Januar 2008

Erstgutachter: Prof. Dr. Ignacio Cirac

Zweitgutachter: Prof. Dr. Claus Zimmermann

# Contents

<b>Introduction</b>	<b>vii</b>
<b>Einleitung</b>	<b>x</b>
<b>1 Fundamentals</b>	<b>1</b>
1.1 Quantum wells and quantum dots . . . . .	1
1.1.1 Band structure of bulk semiconductor . . . . .	2
1.1.2 Quantum wells . . . . .	5
1.1.3 Quantum dots . . . . .	7
1.2 Hyperfine interaction between electrons and nuclei . . . . .	12
1.2.1 Polarization of nuclear spins in quantum dots . . . . .	15
1.2.2 Bosonic behavior of the collective nuclear spin operators . . . . .	17
1.3 Quantum memory . . . . .	20
1.3.1 Characterization of a quantum memory . . . . .	20
1.3.2 Experimental realization of a quantum memory with atoms . . . . .	22
1.4 Cavity Quantum Electrodynamics with quantum dots . . . . .	23
1.4.1 Photonic crystal nanocavities . . . . .	23
1.4.2 Strong coupling of the quantum dot-cavity system . . . . .	25
<b>2 The physical system</b>	<b>29</b>
2.1 Basic properties of the system . . . . .	29
2.2 Adiabatic elimination of the trion . . . . .	34
2.3 Adiabatic elimination of the electronic states . . . . .	35
<b>3 Landau-Zener transitions</b>	<b>37</b>
3.1 The Landau-Zener formula . . . . .	37
3.2 Landau-Zener transitions for operators . . . . .	38
3.2.1 Storage fidelity of a Fock state . . . . .	41
3.2.2 Storage fidelity of coherent states . . . . .	41
3.2.3 Storage of a two-mode squeezed state . . . . .	44
3.2.4 Mapping time . . . . .	47
<b>4 Generation of a two-mode squeezed state</b>	<b>49</b>

<b>5</b>	<b>Stimulated Raman adiabatic passage (STIRAP)</b>	<b>53</b>
5.1	Short review of STIRAP . . . . .	53
5.2	Mapping the light state to nuclear spins using STIRAP . . . . .	55
5.3	Error processes . . . . .	58
5.3.1	”Always-on” character of $g_n$ . . . . .	59
5.3.2	Non-perfect polarization of the nuclei . . . . .	61
5.3.3	Non-adiabaticity due to finite time . . . . .	61
5.4	Numerical integration of the Schrödinger equation . . . . .	63
5.5	Monte Carlo wavefunction simulation of the cavity decay . . . . .	69
<b>6</b>	<b>Summary and Perspectives</b>	<b>73</b>
<b>A</b>	<b>Adiabatic elimination</b>	<b>75</b>
A.1	Rotating frame . . . . .	75
A.2	Adiabatic elimination of the trion . . . . .	77
A.3	Adiabatic elimination of the electronic states . . . . .	80
<b>B</b>	<b>Gaussian states and transformations</b>	<b>83</b>
B.1	Preliminaries . . . . .	83
B.2	Gaussian states . . . . .	84
B.2.1	Coherent states . . . . .	85
B.2.2	Squeezed states . . . . .	86
B.3	Gaussian unitaries . . . . .	86
B.3.1	Passive transformations . . . . .	87
B.3.2	Active transformations . . . . .	88
B.4	Bipartite Gaussian states . . . . .	89
<b>C</b>	<b>Entanglement</b>	<b>93</b>
C.1	The positive partial transpose criterion . . . . .	94
C.2	Positive maps and entangled states . . . . .	95
C.3	Entanglement measures . . . . .	96
C.4	Entanglement of Gaussian states . . . . .	96
C.4.1	Pure entangled Gaussian states . . . . .	97
C.4.2	Mixed entangled Gaussian states . . . . .	97
C.4.3	Entanglement measure for Gaussian states . . . . .	98
	<b>Bibliography</b>	<b>99</b>
	<b>Acknowledgement</b>	<b>104</b>
	<b>Erklärung</b>	<b>107</b>

# Introduction

A quantum memory is an essential building block for quantum information and communication applications. Whereas light arguably serves as the preferred quantum system for information transport, it is rather unsuitable for localized storage. For the latter, material systems are more appropriate. As many quantum information applications require both transport and storage of information, an interface between the preferred quantum systems is highly desirable. Classical means of storing information cannot, even in principle, store the complete information of a quantum mechanical state. The principle of detection and subsequent storage would destroy part of the information as a measurement disturbs a quantum mechanical state.

An example for a quantum interface between light and matter that has experimentally been implemented is a quantum memory of light in atomic ensembles [1]. A quantum interface between light and matter in the solid state has not been achieved so far, although recent years have shown that, e.g., semiconductor quantum dots offer interesting possibilities for quantum information applications. The rapid progress in their production and application opens up new interesting possibilities to manipulate the electrons and the nuclear spins of the quantum dot.

The ability to trap single charges in quantum dots led to the famous Loss-DiVincenzo proposal to use single electron spins confined to quantum dots as qubits [2]. These qubits allow for local gating operations and controllable interaction through exchange interaction between neighboring spins and promise a scalable implementation of a quantum computer. Later it was proposed to use optical means to couple, manipulate, and read out qubits implemented in optically active quantum dots, where the coupling to a mode of a microcavity mediates the interaction between different qubits [3]. This also enables a coherent interface between the spin qubit and the cavity mode.

A serious problem of quantum computation with electron spin qubits in quantum dots, however, is decoherence and, in particular, the hyperfine coupling between electrons and nuclei which constitutes the main decoherence source. This decoherence could be in principle suppressed by polarizing the nuclei, but due to their small magnetic moment, the thermal state of the nuclear spins is unpolarized even at the strongest magnetic fields and lowest temperatures available in laboratories.

A solution in this respect is provided by the concept of "dynamical nuclear polarization" (DNP) which uses a bath of polarized electron spins to polarize the nuclei

[4, 5]. Thus, advantage can be taken of the "undesired" hyperfine coupling between the electron and the nuclear spins as the electrons can be used to manipulate the state of the nuclei. A quantum memory for electron spin qubits in the nuclear spins of a quantum dot has been proposed in recent years [6, 7]. But direct coherent coupling between the optical field and the nuclear spins in a QD, enabling the storage of photonic states while avoiding electron spin decoherence, has not been studied to date.

In this thesis, an interface between the light field of a microcavity and the nuclear spins of a semiconductor quantum dot is studied. To this end, the hyperfine interaction between the electron of the singly charged quantum dot and the nuclear spins is used as a mediator for an interaction between light and the nuclei. This enables the storage of light to the nuclear spins, which are, due to their exceptionally long decoherence times, an ideal candidate for such a quantum memory of light.

We show that various states of light can be mapped to the nuclear spins with a fidelity close to one. The times needed for the storage process as proposed here are of the order of  $\mu\text{s}$  and exceed today's cavity lifetimes, however, we hope that future technologies will enable longer cavity photon lifetimes.

This thesis is structured as follows. In Chapter 1, basic principles of quantum dots, cavity QED with quantum dots, hyperfine interaction between electrons and nuclear spins and fundamental concepts of a quantum memory will be introduced. Basic principles of Gaussian states and entanglement that are useful for the understanding of this thesis are introduced in Appendices B and C.

Next, the system proposed in this work, a field of an optical microcavity coupled to the highly polarized nuclear spins of a singly charged quantum dot by a detuned Raman process, will be discussed. The large detuning of the electron-trion transition allows, as will be shown in Chapter 2, the adiabatic elimination of the trion. The additional assumption of large detuning between the electronic states allows their subsequent adiabatic elimination, yielding an effective interaction between light and nuclear spins. We show in Chapter 3, that "Landau-Zener transitions" enable the mapping of the light field of the cavity to the nuclear spins. High fidelity storage, beyond standard quantum benchmarks, of different kinds of states such as Fock and coherent states can be achieved, and we show, that our memory is capable of storing part of an entangled state while preserving the entanglement.

In Chapter 4 we show that similar techniques can be used to generate two-mode squeezed states of the nuclear spin-cavity system, enabling e.g., a light-matter interface through teleportation.

The times needed to map a state of light onto the nuclear spins via "Landau-Zener transitions" are in the  $\mu\text{s}$  range and thus much longer than today's cavity lifetimes.

To achieve shorter storage times we abandon the assumption of large detuning between the electronic states and consider the system where only the trion has adiabatically been eliminated. In Chapter 5, we show that the "Stimulated Raman Adiabatic Passage" (STIRAP)-method allows for shorter mapping times of the state of light to the nuclear spins. By numerically integrating the Schrödinger equation, we

show that various states of light can be mapped with high fidelity onto the nuclear spins. Moreover, we compute entanglement fidelity and average fidelity of our memory process. Finally, we study different errors affecting the memory process such as non-adiabaticity due to the finite time of the mapping, non-perfect polarization of the nuclear spins and the cavity decay, which we model with a Monte-Carlo wavefunction simulation.



# Einleitung

Ein Quantenspeicher ist ein grundlegendes Element für Quanteninformations- und Quantenkommunikationsanwendungen. Während sich Photonen als „fliegende“ Quantenbits zur Übermittlung von Daten eignen, sind sie für deren Speicherung denkbar ungeeignet. Für letzteres sind verschiedene Formen von Materie besser geeignet. Da viele Anwendungen in der Quanteninformation jedoch sowohl die Übermittlung als auch die Speicherung von Information erfordern, ist eine Schnittstelle zwischen den dafür jeweils bevorzugten Systemen von entscheidender Bedeutung. Klassische Verfahren sind grundsätzlich nicht in der Lage, die Information eines quantenmechanischen Zustands vollständig zu speichern. Die damit verbundene Messung und anschließende Speicherung zerstört unweigerlich Teile der zu speichernden Information. Grund hierfür ist die Tatsache, dass jede Messung das zu messende System in einer zustandsverändernden Weise stört. Die Anforderung an einen Quantenspeicher besteht somit darin, einen Quantenzustand zuverlässig zu speichern, ohne die in ihm enthaltene Information zu zerstören.

Erste Quantenspeicher wurden bereits experimentell implementiert, ein Beispiel hierfür ist die Speicherung von Licht in atomaren Ensembles [1]. Eine Schnittstelle zwischen Licht und Festkörpern konnte jedoch bisher nicht realisiert werden, obwohl sich in den letzten Jahren gezeigt hat, dass zum Beispiel Halbleiterquantenpunkte vielversprechende Kandidaten für Quanteninformationsanwendungen sind. Die rasante Entwicklung bei der Herstellung und Anwendung von Halbleiterquantenpunkten in den letzten Jahren eröffnet interessante Möglichkeiten im Hinblick auf die Manipulation der Elektronen und Kernspins dieser „künstlichen Atome“. Ein berühmter Vorschlag von Loss und DiVincenzo sieht vor, Quantenpunkte mit einzelnen Elektronen zu besetzen, deren Spins als Träger von Quanteninformation dienen können [2]. Auf diese Weise implementierte Quantenbits erlauben lokale Gatteroperationen und können über die Austauschwechselwirkung benachbarter Spins kontrolliert werden. Darüber hinaus versprechen sie eine skalierbare Realisierung eines Quantencomputers. Spätere Ideen sehen vor, Qubits in optisch aktiven Quantenpunkten optisch zu koppeln, zu manipulieren und auszulesen, wobei die Wechselwirkung zwischen verschiedenen Qubits mittels der Kopplung an eine Mode eines Mikroresonators realisiert wird [3].

Ein vorrangiges Problem von Elektronen-Qubits in Quantenpunkten ist jedoch die Dekohärenz der Elektronenspins, die vor allem durch die Hyperfeinwechselwirkung der Elektronen mit den unpolarisierten Kernspins des Quantenpunktes verursacht wird. Polarisierung der Kernspins würde dieses Problem beheben, aufgrund der kleinen magnetischen Kernmomente ist der thermische Zustand der Kernspins jedoch selbst bei den größtmöglichen Magnetfeldern und niedrigsten Temperaturen, die im Labor erreicht werden können, unpolarisiert. Eine Möglichkeit, Kernspins zu polarisieren bietet das Konzept der „Dynamischen Kern Polarisierung“ (DNP) [4, 5]. Hier wird die Polarisierung der Kernspins mit Hilfe eines Reservoirs von polarisierten Elektronen erreicht. Die zunächst „unerwünschte“ Hyperfeinwechselwirkung zwischen Elektron und Kernspins kann also gezielt genutzt werden, um den Zustand der Kerne zu manipulieren.

Ein Vorschlag zur Realisierung eines Quantenspeichers, der die Speicherung von Elektronenspin-Qubits in den Kernspins von Quantenpunkten erlaubt, existiert seit einigen Jahren [6, 7]. Was jedoch bisher nicht untersucht wurde, ist die kohärente Kopplung zwischen einem optischen Feld und den Kernspins in einem Quantenpunkt, welche die Speicherung von Lichtzuständen ermöglicht ohne von der Dekohärenz der Elektronenspins betroffen zu sein.

Diese Arbeit beschäftigt sich daher mit der theoretischen Untersuchung einer Schnittstelle zwischen dem Lichtfeld eines Mikroresonators und den Kernspins von Halbleiterquantenpunkten. Zu diesem Zweck wird die Hyperfeinwechselwirkung zwischen dem Elektron eines einfach geladenen Quantenpunktes und den Kernspins als Vermittler für eine Wechselwirkung zwischen Licht und Kernen eingesetzt. Dies ermöglicht die Speicherung von Licht in Kernspins, die aufgrund ihrer außergewöhnlich langen Dekohärenzzeiten ein ideales Speichermedium für Licht darstellen.

Es wird gezeigt, dass verschiedene Lichtzustände mit nahezu perfekter Güte auf die Kernspins abgebildet werden können. Die Zeiten für den hier vorgeschlagenen Speichervorgang liegen im Bereich von  $\mu\text{s}$  und übersteigen somit leider die Lebenszeiten heutiger Resonatoren. Dieses Problem könnte jedoch durch eine Weiterentwicklung der Resonator-Technologien gelöst werden.

Die vorliegende Arbeit gliedert sich wie folgt:

Kapitel 1 führt in die Grundlagen von Quantenpunkten, Hohlraumquantenelektrodynamik mit Quantenpunkten, Hyperfeinwechselwirkung zwischen Elektronen und Kernspins sowie grundlegende Prinzipien von Quantenspeichern ein. In den Anhängen B und C werden grundlegende Konzepte von Gaußschen Zuständen und Verschränkung, welche für das Verständnis der Arbeit von Bedeutung sind, behandelt. In Kapitel 2 wird zunächst das in dieser Arbeit vorgeschlagene System, in dem die Kopplung des Lichtfelds eines optischen Mikroresonators an die stark polarisierten Kernspins eines Quantenpunktes über einen stark verstimzten Raman Übergang realisiert wird, eingeführt. Die starke Verstimmung des Überganges zwischen den

elektronischen Zuständen eines einfach geladenen Quantenpunktes und einem Trion-Zustand ermöglicht, wie in Kapitel 2 gezeigt, die adiabatische Elimination des Trions. Die Annahme einer großen Aufspaltung der elektronischen Zustände erlaubt eine weitere Elimination der elektronischen Zustände. Somit erhalten wir eine direkte, effektive Kopplung zwischen Lichtfeld und Kernspins, die, wie in Kapitel 3 gezeigt wird, Landau-Zener Übergänge ermöglicht. Diese Übergänge bieten die Möglichkeit, eine Vielzahl von Lichtzuständen mit hoher Güte (Fidelity) auf kollektive Zustände der Kernspins abzubilden. Die hier untersuchten Zustände sind Fock-Zustände und kohärente Zustände. Außerdem wird gezeigt, dass unser Quantenspeicher in der Lage ist, einen Teil eines verschränkten Zustandes zu speichern, ohne dabei die Verschränkung mit einem weiteren System zu zerstören.

In Kapitel 4 wird gezeigt, dass eine kleine Modifikation des eben besprochenen Systems die Erzeugung eines zwei-Moden gequetschten Zustandes erlaubt, der beispielsweise eine Licht-Materie Schnittstelle mit Hilfe von Teleportation ermöglicht.

Die Zeiten, die für die Speicherung eines Zustandes mit Hilfe von Landau-Zener Übergängen erreicht werden können, liegen im Bereich von  $\mu\text{s}$  und sind somit deutlich länger als die bisher erreichten Lebensdauern eines Photons in einem Mikroresonator. Um kürzere Speicherzeiten zu erreichen, wird ein System betrachtet, in dem nur das Trion adiabatisch eliminiert wurde. Somit kann die bisherige Anforderung an das System, dass die elektronischen Zustände stark verstimmt sein müssen, entfallen. In Kapitel 5 wird gezeigt, dass mit Hilfe der Methode der „Stimulierten Raman Adiabatischen Passage“ (STIRAP), Lichtzustände auf die kollektiven Kernspinzustände abgebildet werden können und sich damit Speicherzeiten erzielen lassen, die eine Größenordnung unter denen der Landau-Zener Übergänge liegen. Durch numerische Integration der Schrödinger Gleichung wird gezeigt, dass auch mit dieser Methode verschiedenste Lichtzustände mit hoher Güte auf die Kernspins abgebildet werden können. Außerdem werden die „entanglement fidelity“ (Verschränkungsgüte) und die „average fidelity“ (mittlere Güte) berechnet. Schließlich betrachten wir verschiedene Fehlerquellen, die bei diesem Speicherverfahren auftreten können. Beispiele hierfür sind Fehler durch Nicht-Adiabatizität aufgrund der endlichen Zeit der Abbildung, unvollständige Polarisierung der Kernspins und der Zerfall des optischen Resonators, der mit einer Monte-Carlo Wellenfunktion Simulation modelliert wird.



# Chapter 1

## Fundamentals

The system studied in this work is a semiconductor quantum dot embedded in an optical microcavity. In this Chapter, we set the stage for the detailed discussions in the main part of the thesis. To facilitate the understanding of the physical system, basic principles of quantum dots and optical transitions in quantum dots shall be introduced in Section 1.1.

The aim of this thesis is to achieve faithful storage of the state of an optical microcavity in the nuclear spins of a quantum dot. The interaction between light and nuclear spins is mediated by the hyperfine interaction between the singly charged quantum dot electron and the nuclear spins. Section 1.2 introduces basic concepts used in this work to describe the hyperfine interaction between the electron and the nuclear spin ensemble. In the present work, high polarization of the nuclear spins is assumed. Thus, state of the art techniques for polarizing nuclear spins in quantum dots shall be discussed. Next, assuming high polarization of the nuclei, an approximation enabling the description of collective spin operators in terms of bosonic operators will be reviewed.

In Section 1.3, requirements on a quantum memory will be discussed and the experimental realization of a quantum memory with atomic ensembles will be reviewed.

For the storage of a cavity field in the nuclear spins of a quantum dot, strong coupling of the quantum dot-cavity system has to be achieved. Experimental implementations of such systems consist of self-assembled quantum dots embedded in photonic crystal microcavities. In Section 1.4, basic concepts of photonic crystal microcavities will be discussed and one specific experimental realization of a strongly coupled quantum-dot cavity system will be reviewed.

### 1.1 Quantum wells and quantum dots

In order to understand the properties of quantum dots it is instructive to review some properties of bulk semiconductor material first. When the effective dimension of three dimensional bulk material is reduced to quasi-two dimensional quantum well systems,

quasi-one dimensional quantum wires and quasi-zero dimensional quantum dots, the properties of these systems change. These mesoscopic semiconductor structures will be studied next, first a quantum well system with strong confinement in one direction and then a quantum dot system with confinement in all three dimensions.

### 1.1.1 Band structure of bulk semiconductor

In this Section, basic features of bulk semiconductor material are studied. Semiconductors are crystals with properties intermediate between those of insulators and metals. In the ground state (at  $T = 0$ ) the valence band of a semiconductor is completely filled whereas the conduction band is empty. In this state, the semiconductor is an insulator. When the crystal temperature rises, the size of the band gap separating valence band and conduction band decreases. Some of the electrons are thermally excited from the valence band to the conduction band leaving holes that can be treated as free positively charged quasi-particles. Both these electrons and holes can carry electric charge and make the material conducting. An electron can also be excited by electromagnetic radiation incident upon the semiconductor. Optical transitions in semiconductor material are of high importance for this work and will be studied in Section 1.1.3.

First, the bandstructure of bulk semiconductors shall be reviewed briefly. Electrons in crystals have energies within certain energy bands, resulting from an effective periodic potential due to the superposition of the Coulomb potentials of the periodic array of nuclei. For a single electron moving in an effective lattice potential  $V_0(\mathbf{r})$ , the Schrödinger equation reads

$$H\psi(\mathbf{k}, \mathbf{r}) = \left[ \frac{p^2}{2m_0} + V_0(\mathbf{r}) \right] \psi(\mathbf{k}, \mathbf{r}) = E\psi(\mathbf{k}, \mathbf{r}), \quad (1.1)$$

with  $m_0$  denoting the free electron mass. The solutions of this equation, i.e., the electronic orbital wave functions in the lattice, are given by the well known Bloch wave functions

$$\psi(\mathbf{k}, \mathbf{r}) = \frac{e^{i\mathbf{k}\cdot\mathbf{r}}}{L^{3/2}} u(\mathbf{k}, \mathbf{r}), \quad (1.2)$$

where  $L^3$  is the volume of the crystal. The Bloch functions  $u(\mathbf{k}, \mathbf{r})$  reflect the periodicity of the lattice potential

$$u(\mathbf{k}, \mathbf{r}) = u(\mathbf{k}, \mathbf{r} + \mathbf{R}_n), \quad (1.3)$$

with  $\mathbf{R}_n$  denoting a vector connecting two identical sites in an infinite lattice which are  $n$  lattice cells apart. The Bloch functions describe the atomic part of the wavefunction, i.e., they have e.g., s,p character corresponding to the state of the valence band electrons of the involved atoms.

In semiconductor materials of group III-V, which will be of interest in the present work, the four outer shell electrons of the atoms populate the  $sp^3$  orbitals. The

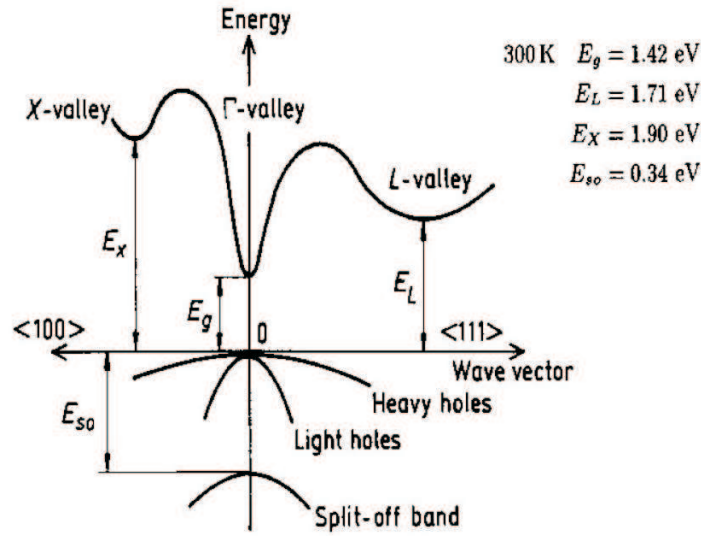


Figure 1.1: Bandstructure of GaAs [10].

conduction band Bloch wave functions have the symmetry of an atomic s-orbital, i.e., the conduction band at  $\mathbf{k} = 0$  is made up by an s-like state, while the valence band at  $\mathbf{k} = 0$  is made up of three degenerate p states (in cubic symmetry)[8, 9].

Thus, the band structure for the valence band is more complicated than for the conduction band. Here, an approximative method, namely the  $\mathbf{k} \cdot \mathbf{p}$  perturbation theory, shall be mentioned. Inserting equation (1.2) into equation (1.1) yields

$$\left[ -\frac{\hbar^2}{2m_0} \nabla^2 + \frac{\hbar}{m_0} \mathbf{k} \cdot \mathbf{p} + V_0(\mathbf{r}) \right] u(\mathbf{k}, \mathbf{r}) = \left[ E(\mathbf{k}) - \frac{\hbar^2 k^2}{2m_0} \right] u(\mathbf{k}, \mathbf{r}), \quad (1.4)$$

which is the starting point for phenomenological band structure calculations with  $\mathbf{k} \cdot \mathbf{p}$  perturbation theory. The idea is to treat the  $\mathbf{k} \cdot \mathbf{p}$  and the  $k^2$  part of the Hamiltonian in equation (1.4) in the vicinity of  $k = 0$  as a perturbation. Energy eigenvalues in second order perturbation theory can be derived, giving a good description of the band structure within certain limits.

However, for a more realistic treatment, spin orbit coupling has to be taken into account. Thus, at the center of the Brillouin zone, the cubic symmetry can be approximated by spherical symmetry for the s and p orbitals and eigenfunctions of the angular momentum can be used as basis states:  $|l = 0, m_l = 0\rangle, |l = 1, m_l = 0\rangle, |l = 1, m_l = \pm 1\rangle$  [8, 11].

Including spin orbit coupling, the three valence band states  $|l = 1, m_l = \pm 1\rangle$  and  $|l = 1, m_l = 0\rangle$  and the spin states  $|s = 1/2, m_s = \pm 1/2\rangle$  form eigenstates of the total angular momentum  $\mathbf{j} = \mathbf{l} + \mathbf{s}$  with quantum numbers  $j = 3/2, m_j = \pm 3/2, \pm 1/2$  and  $j = 1/2, m_j = \pm 1/2$ .

Due to the spin-orbit interaction obtained from relativistic quantum mechanics, states with  $j = 1/2$  are energetically shifted to lower energies, forming the "split-off" band of Figure 1.1 and will for simplicity be neglected in the following.

For the  $j = 3/2$  states, the phenomenological Luttinger Hamiltonian given by

$$H = \frac{\hbar}{2m_0} \left[ \left( \gamma_1 + \frac{5}{2}\gamma_2 \right) \mathbf{k}^2 - 2\gamma_2(\mathbf{k} \cdot \mathbf{j})^2 \right] \quad (1.5)$$

describes heavy-hole and light-hole bands in spherical approximation [8].  $\gamma_1$  and  $\gamma_2$  are phenomenological parameters that can be determined experimentally by measuring heavy and light hole masses (e.g., for GaAs,  $\gamma_1 = 6.85$  and  $\gamma_2 = 2.1$ ).

Taking the wave vector as  $\mathbf{k} = k\mathbf{e}_z$ , the two resulting energy eigenvalues are given by

$$E_{\text{hh}} = \frac{\hbar^2 k^2}{2m_{\text{hh}}} \quad \text{for } m_j = \pm 3/2 \quad (1.6)$$

and

$$E_{\text{lh}} = \frac{\hbar^2 k^2}{2m_{\text{lh}}} \quad \text{for } m_j = \pm 1/2, \quad (1.7)$$

with the effective heavy hole and light hole band masses defined by

$$m_{\text{hh}} = \frac{m_0}{\gamma_1 - 2\gamma_2} \quad (1.8)$$

and

$$m_{\text{lh}} = \frac{m_0}{\gamma_1 + 2\gamma_2}. \quad (1.9)$$

The curvature of the energy dispersion increases with decreasing mass, therefore the curvature of the light-hole band is larger than the one of the heavy-hole band.

The behavior of the wavefunction of the electron in the conduction band is much more simple. As already mentioned, the conduction band is, at  $\mathbf{k} = 0$ , made up by a s-like state and therefore there is no spin orbit coupling. In the effective mass approximation, the conduction band has parabolic shape around the wavevector  $\mathbf{k} = 0$ , i.e., the energy eigenvalues can be written as  $E = E_0 + \frac{\hbar^2 k^2}{2m_e}$ , where  $E_0$  is the energy at  $k = 0$  and  $m_e$  denotes the effective mass of the electron. Hence, the electron in the conduction band can be treated as a quasi-free particle with an effective mass  $m_e$ .

The bandstructure of GaAs is shown in Figure 1.1. The valence band, made up of p-like states, is split into heavy holes and light holes as can be seen in equation (1.6) and (1.7), both having quantum number  $j = 3/2$ . The split-off band is formed by the state with total angular momentum  $j = 1/2$ . The conduction band, made up of an s-like state, is in the effective mass approximation, in the vicinity of  $\mathbf{k} = 0$ , given by a parabolic potential.

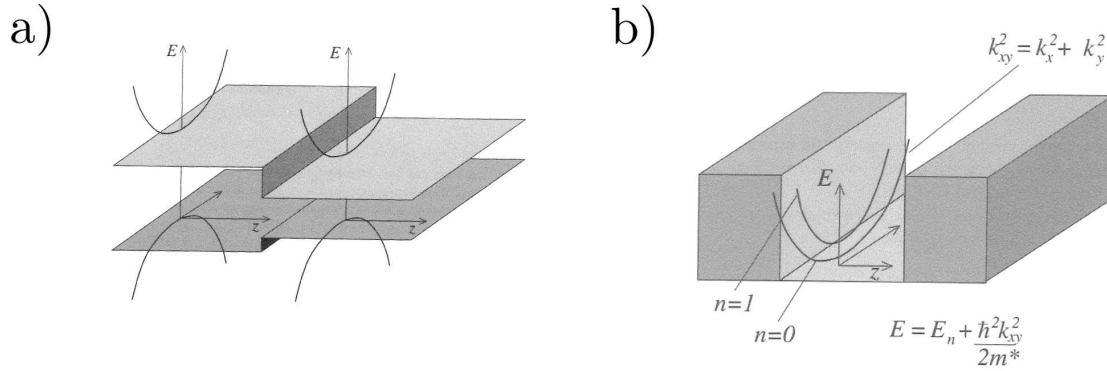


Figure 1.2: a) Heterojunction formed by two semiconductors with different band gaps. The curves represent the unrestricted motion parallel to the interface. b) In-plane dispersion curves and subband structure in a quantum well. Figures taken from P. Harrison ‘Quantum Wells, Wires and Dots’ (Wiley, 1999) reproduced with permission from the author [9].

Having introduced the bandstructure of a bulk semiconductor, the next two Sections deal with semiconductor heterostructures in which electron and hole states are confined in one or more directions. For a confinement region on the order of the quasi-free electron/hole de Broglie wave length, the motion of the quasi-particles becomes quantized. Understanding confinement in one direction is the first step to understand the three dimensional confinement of a quantum dot. Thus, quantum well systems with confinement in one direction are studied in the next Section.

### 1.1.2 Quantum wells

Quantum wells are semiconductor heterostructures in which electrons and holes are confined in one direction. A layer of one material, for example GaAs, is sandwiched between layers of a different material with a wider band gap, such as  $\text{Ga}_{1-x}\text{Al}_x\text{As}$  with  $0 < x < 0.4$  (see Figure 1.3a). The electrons of the conduction band and the holes of the valence band are confined by the potential due to the energy difference between the larger and the smaller band gap of the two different materials (see Figure 1.2b).

The confinement potential can qualitatively be approximated by an infinitely deep potential well

$$V(z) = \begin{cases} 0 & \text{for } -L_c/2 < z < L_c/2 \\ \infty & \text{for } |z| > L_c/2 \end{cases} ,$$

where  $L_c$  is the size of the confining region. Considering first the conduction band electrons in the quantum well, the  $z$ -dependent part of the plane wave envelope function in equation (1.2) has to be replaced by a quantized standing wave  $\xi_n(z)$ . For small  $\mathbf{k}$ , where the effective mass approximation and  $\mathbf{k} \cdot \mathbf{p}$  perturbation theory



Figure 1.3: Schematic view of a) a quantum well, b) single pillar containing a quantum dot.

are valid, the wavefunction reads

$$\psi(\mathbf{r}) = \xi_n(z) \frac{e^{i(k_x x + k_y y)}}{L_c} u(\mathbf{k} \simeq 0, \mathbf{r}). \quad (1.10)$$

The Schrödinger equation for the envelope function  $\xi(z)$  is given by

$$\left[ -\frac{\hbar^2}{2m_e} \frac{\partial}{\partial z^2} + V(z) \right] \xi(z) = E_z \xi(z), \quad (1.11)$$

with

$$E_z = \frac{\pi^2 \hbar^2}{2m_e L_c^2} n^2, \quad (1.12)$$

where  $m_e$  denotes the effective mass of the electron. Including the kinetic energy in the  $x$ - $y$  plane, the total energy of the electron is given by

$$E = \frac{\hbar^2}{2m_e} \left( \frac{n^2 \pi^2}{L_c^2} + k_{\perp}^2 \right). \quad (1.13)$$

The energies of the quantized envelope states, which are proportional to  $\frac{n^2}{L_c^2}$ , are similar to those of a particle in a box. Because of the additional translational motion in the  $x$ - $y$  plane, each of the energy levels forms a subband. Thus, the conduction band is split into subbands which are separated by  $\frac{\hbar^2 \pi^2}{2m_e L_c^2}$  with approximately parabolic  $k_{\perp}$  dispersion.

For the valence band holes, the situation is more complicated. Heavy-hole and light-hole band mixing occurs since the confinement leads to a reduction of the original spherical symmetry (for more details see [8]).

It is remarkable (and not the case for electrically defined quantum wells) that electron and hole can both be trapped in the same potential.

In reality, the confinement potential has finite wells, leading to a change in the eigenvalues and a finite number of bound states. However, the qualitative behavior stays the same as for the infinite well potential.

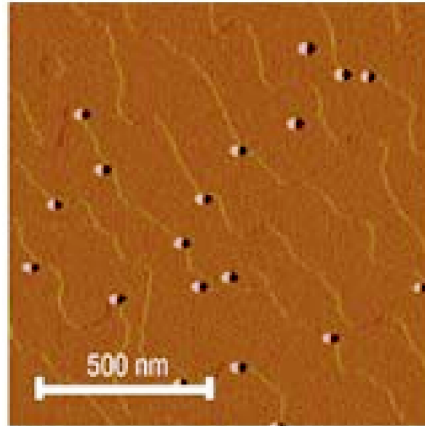


Figure 1.4: Atomic-force microscope image of a layer of InAs/GaAs self-assembled quantum dots. Each blob corresponds to a dot with typical lateral diameters of 20-30nm and a height of 4-8nm. Picture copied from [13].

### 1.1.3 Quantum dots

The dimensionality of the electrons' environment can be further reduced to a one dimensional quantum wire and to a zero dimensional quantum dot. The electron in a quantum dot is confined in all three dimensions, which leads to a discrete, "atom-like" energy spectrum.

Quantum dots can for example be manufactured by etching a quantum well to leave pillars (see Figure 1.3b). Much stronger spatial confinement can be achieved with self-assembled quantum dots. The spontaneous formation of semiconductor material droplets was discovered as a failed attempt to grow by Molecular Beam Epitaxy (MBE) InAs quantum wells embedded in a GaAs barrier [12]. InAs and GaAs have lattice constants differing by  $\cong 7\%$ . When two dimensional, strained InAs films are grown on a GaAs substrate, elastic energy is accumulated until this energy exceeds the one required to form dislocation, which happens in InAs at roughly 0.5nm. Droplets of InAs self-assemble on the GaAs layer (see Figure 1.4) in order to minimize the surface strain. Subsequently, these droplets are covered by GaAs [12] (see Figure 1.5). Concerning growth and applications of self-assembled quantum dots, one has to keep in mind that we are interested here only in low-temperature-, i.e., ground state properties of quantum dots. Experiments with self-assembled quantum dots are usually performed at liquid Helium or dilution-fridge temperatures (4.2K-100mK).

A typical InAs/GaAs self-assembled quantum dot has a base of  $\sim 20 - 30$ nm and a height of  $\sim 4 - 8$ nm and contains  $\sim 10^4 - 10^5$  atoms.

In the previous Section, it has been explained that the energy eigenvalues in a quantum well are quantized in confinement direction. The confining potential had been assumed to be a step-like potential. These assumptions are still valid for the

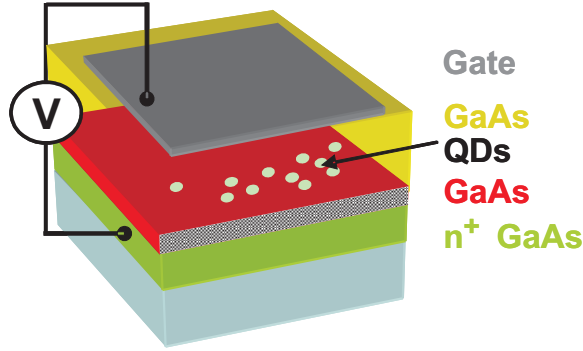


Figure 1.5: Schematic view of self-assembled quantum dots (picture by P. Maletinsky).

quantum dot, where the carrier sees a narrow, step like potential in growth direction, along the quantum dot symmetry axis  $z$ . The carriers, moving freely in the  $x-y$  direction in the quantum well, are now confined in  $x$  and  $y$  direction.

A description in terms of single-electron levels is appropriate since due to strong confinement<sup>1</sup> electron-electron interactions are only a small perturbation. The potential in the  $x-y$  plane can be modeled with a parabolic potential. The Schrödinger equation for electron (hole) describing the confinement in the  $x-y$  plane is given by [14]

$$\left[ -\frac{\hbar^2}{2m_{e,h}} \nabla_{\mathbf{r}}^2 + \frac{m_{e,h}\omega_{e,h}^2}{2} r^2 \right] \psi_{e,h}(\mathbf{r}) = E_{\parallel} \psi_{e,h}(\mathbf{r}), \quad (1.14)$$

with the effective electron (hole) masses  $m_e$  ( $m_h$ ) and the in-plane coordinate vector  $\mathbf{r} = (x, y)$ . Going to a description with 2D polar coordinates  $(r, \phi)$  where  $r = |\mathbf{r}|$  and the azimuthal coordinate  $\phi$ ,  $\Psi_{n,m}(r, \phi)$  is given by

$$\Psi_{n,m}(r, \phi) = \alpha^{-(|m|+1)} \sqrt{\frac{n!}{\pi (n + |m|)!}} e^{-im\phi} r^{|m|} e^{-r^2/2\alpha^2} \mathcal{L}_n^{|m|} \left( \frac{r^2}{\alpha^2} \right) \quad (1.15)$$

where

$$\alpha = \left( \frac{m_{e,h}\omega_{e,h}}{\hbar} \right)^{-1/2} \quad (1.16)$$

is the spatial extension of the harmonic oscillator ground state,  $n = 0, 1, 2, \dots$  is the radial and  $m = -n, -n+2, \dots, n-2, n$  the orbital quantum number.  $\mathcal{L}_n^{|m|}(x)$  denotes the generalized Laguerre polynomial in the dimensionless variable  $x = r^2/\alpha^2$ .

<sup>1</sup>To explain how strong confinement is defined, an effective exciton Bohr radius, describing the binding radius of an electron-hole pair bound by Coulomb interaction, has to be introduced. It is given by  $a_b = \frac{\epsilon\hbar^2}{m_r e^2}$  where  $\epsilon$  is the dielectric constant arising from the bulk semiconductor material and  $\frac{1}{m_r} = \frac{1}{m_e} + \frac{1}{m_h}$  is the reduced electron-hole mass. For small quantum dots, as for example for lens-shaped self-assembled quantum dots, the confinement-induced energy shift is large compared to the exciton binding energy, thus it might be a good approximation to ignore the Coulomb interaction. Note that this is a dangerous approximation which ignores important physics in the dot.

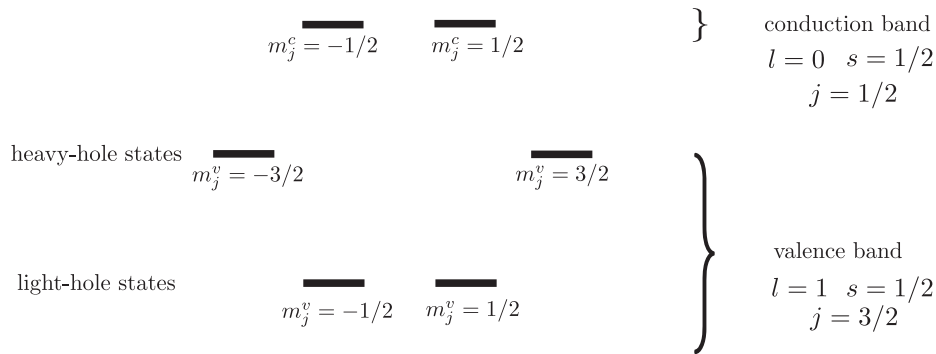


Figure 1.6: Level scheme of the lowest energy single particle states in the quantum dot

The in-plane eigenenergies are given by

$$E_{n,m} = \hbar\omega_{e,h}(2n - |m| + 1) = \hbar\omega_{e,h}(n_E + 1) \quad (1.17)$$

where  $n_E = 2n - |m|$  denotes the energy quantum number. Approximating the confining potential in  $z$ -direction as an infinitely deep potential well, the energy eigenvalues in  $z$ -direction are given by (1.12).

In the strong confinement regime, it can be assumed that the system stays in the ground state of the quantum well potential in  $z$ -direction (1.12). Thus, the problem can be reduced to the dynamics in the  $x$ - $y$  plane. With this assumption, a level scheme of the lowest-energy single-particle states in the quantum dot is shown in Figure 1.6. For the valence band holes the lowest excitations are given by heavy-hole states  $|j = 3/2, m_j^v = \pm 3/2\rangle$  and light-hole states  $|j = 1/2, m_j^v = \pm 1/2\rangle$  originating from heavy- and light-hole bands in the quantum well. For the s-conduction band electron, there are, in absence of an external magnetic field and negligible exchange interaction, two degenerate states  $|j = 1/2, m_j = \pm 1/2\rangle$ . There are also excitations with p or d orbital symmetry arising from the excited states of motion (see equation (1.1.3)) in the parabolic potential in the  $x$ - $y$  plane that has been assumed here. To keep the summary simple and brief, heavy and light-hole mixing has not been taken into account here. As usual in semiconductors at low temperature, the valence band states of a quantum dot in the ground state are completely filled whereas the conduction band states are empty.

### Optical transitions in quantum dots

Having introduced a level scheme for the lowest energy single particle states in the quantum dot, its optical properties shall be discussed now.

When an electron in a semiconductor device is excited to a conduction band state, it leaves a hole in the valence band that can be treated as a positively charged quasi-particle. The electron-hole pair, bound by the Coulomb interaction, forms a neutral

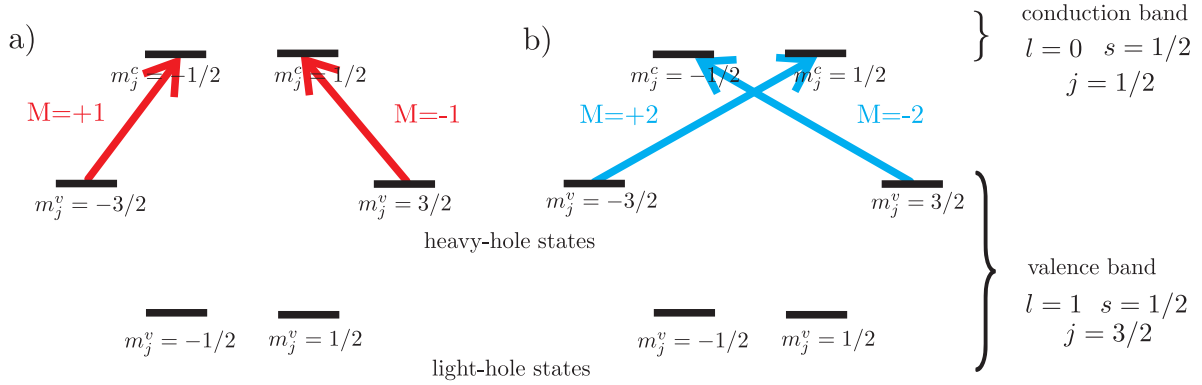


Figure 1.7: Optical transitions in a neutral quantum dot. a) Bright excitons with  $M = \pm 1$ , b) dark excitons with  $M = \pm 2$ .

exciton  $X^0$ . When the electron is excited to the s-type conduction band, the exciton is in its ground state.

In the following, light-hole band states, typically being separated from heavy-hole states by several tens of meV, can be neglected. For the ground state exciton, there are four possible configurations made up of valence band states with  $m_j^v = \pm 3/2$  and conduction band states with  $m_j^c = \pm 1/2$ . The total angular momentum projections of the exciton,  $M = m_j^v + m_j^c$ , take the values  $M = \pm 1$  and  $M = \pm 2$ . (see Figure 1.7). The states with  $M = \pm 2$  are called dark excitons as they correspond to dipole forbidden transitions, whereas the states with  $M = \pm 1$  correspond to dipole allowed transitions and are called bright excitons. They can be created by the absorption of one photon and can decay by the emission of one photon. Note that the quantum numbers refer to the electron, i.e., a valence band hole in the heavy-hole subband - being the absence of an electron with  $m_j^v = \pm 3/2$  - carries spin  $m_j^v = \mp 3/2$ .

When an additional electron is captured in the dot, the behavior of the exciton changes. In its lowest energy state, the singly charged exciton or trion, denoted by  $X^{1-}$  is made up of two electrons in the singlet-state and a hole with two possible spin orientations. Whereas there were four different configurations for the neutral exciton  $X^0$ , there are only two for the trion  $X^{1-}$ . This will be explained in the following (see Figure 1.8a). The electron excited from the  $j = 3/2$  valence band state to the s-conduction band state by the absorption of a photon, is, together with the captured electron in the  $j = 1/2$  conduction band state, in a spin-singlet state. There are two possibilities for the excitation of an electron to the conduction band: The valence band electron with  $m_j^v = +3/2$  can be excited by  $\sigma^-$  polarized light to the  $m_j^c = 1/2$  state of the conduction band, leaving a hole with  $m_j^v = -3/2$  in the valence band. An electron in the  $m_j^v = -3/2$  valence band state can be excited to the  $m_j^c = -1/2$  state of the conduction band by  $\sigma^+$  polarized light. The dashed lines in Figure 1.8 correspond to forbidden transitions with  $M = |2|$ .

A very convenient way to get transitions involving both  $m_j^v = 3/2$  and  $m_j^v = -3/2$

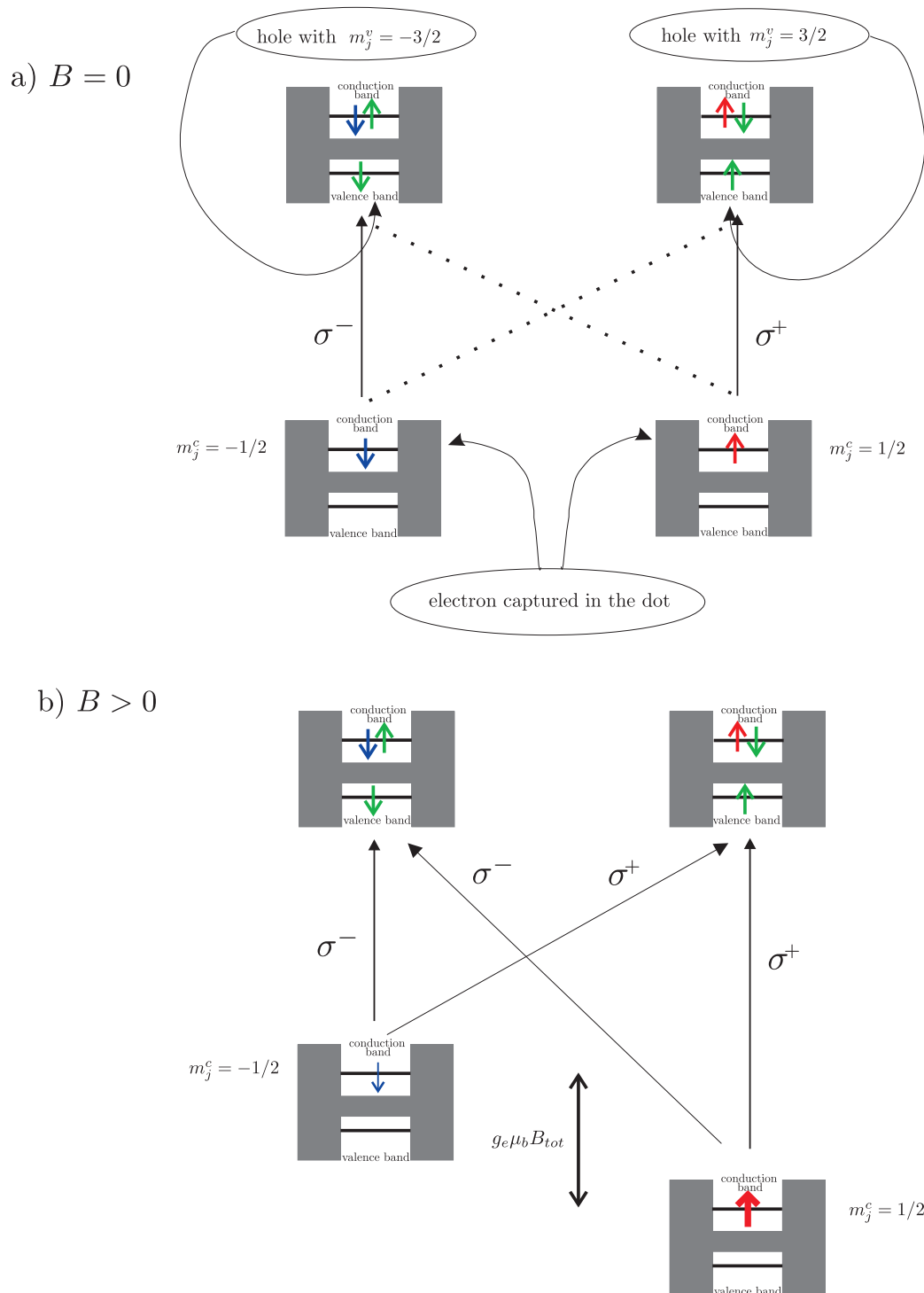


Figure 1.8: Optical transitions in the singly charged quantum dot: a) Straight lines correspond to allowed transitions from the  $m_j^v = \pm 3/2$  valence band states to the  $m_j^c = \pm 1/2$  conduction band states. Dashed lines correspond to dipole forbidden transitions with  $\Delta M = 2$ . b) In an external magnetic field that encloses an angle  $\theta > 0$  with the confinement direction, dipole forbidden transitions become allowed.

valence band electrons has been proposed in [3]. A strong magnetic field  $B_x$  in x-direction is used to completely mix the electronic spins  $m_{j,(z)} = 1/2$  and  $m_{j,(z)} = -1/2$ . Thus, single photon transitions from both  $m_j^v = 3/2$  (for the electron) to  $m_{j,(z)}^c = 1/2$  and  $m_j^v = -3/2$  to  $m_{j,(z)}^c = -1/2$  occur. This scheme will be discussed in more detail in Section 2.1.

## 1.2 Hyperfine interaction between electrons and nuclei

In this Section we consider the hyperfine contact interaction between a single electron confined in the quantum dot and the lattice nuclei<sup>2</sup>, which represents the dominant correction of the conduction band states at low temperature. Hyperfine interaction between single electrons and the surrounding nuclei in a quantum dot has attracted a lot of attention in the last years, as it constitutes the major source of decoherence for electron spin qubits.<sup>3</sup> The focus of the main part of this thesis is, in contrast, on the *use* of the hyperfine interaction for quantum information application, namely as a mediator for the interaction between light and nuclear spins enabling storage of light states in the nuclear spin degrees of freedom.

For the cases of our interest, the interaction between an s-electron spin and a single nuclear spin is given by the Fermi contact Hamiltonian [15, 16, 17]

$$H_{\text{hf}} = \frac{4\mu_0}{3I} \mu_b \mu_I |\xi(\mathbf{r})|^2 \mathbf{S} \cdot \mathbf{I}, \quad (1.18)$$

where  $\mathbf{S} = (S^x, S^y, S^z)$  denotes the electron spin,  $\xi(\mathbf{r})$  is the wavefunction of the electron at the location  $\mathbf{r}$  of the nucleus,  $I(I+1)$  is the eigenvalue of the  $z$ -component  $I_z$  of the nuclear spin  $\mathbf{I} = (I^x, I^y, I^z)$ ,  $\mu_I$  the magnetic moment,  $\mu_0$  the permeability, and  $\mu_b$  the Bohr magneton. In the semiconductor crystal, the wavefunction  $\xi(\mathbf{r})$  is approximately given by the product of a modulating envelope function  $\Psi(\mathbf{r})$  and the periodic Bloch function  $u(\mathbf{r})$ ,  $\xi(\mathbf{r}) = \Psi(\mathbf{r})u(\mathbf{r})$ . Therefore, the Hamiltonian given by equation (1.18), can be written as

$$H_{\text{hf}} = \frac{4\mu_0}{3I} \mu_b \mu_I \eta |\Psi(\mathbf{r})|^2 \mathbf{S} \cdot \mathbf{I}, \quad (1.19)$$

with  $\eta = |u(\mathbf{r})|^2$ . Whereas the Bloch function is constant for free electrons ( $|u(\mathbf{r})| = 1$ ), it has, in a realistic crystal, maxima at the locations of the nuclei leading to  $\eta > 1$ . Estimates for values of  $\eta$  can be derived from e.g., electron spin resonance experiments. For GaAs,  $\eta_{\text{Ga}} = 2.7 \cdot 10^3$  has been found [18].

For p-electrons,  $H_{\text{hf}} = 0$ , as the probability that the electron is found at the location of the nucleus vanishes.

<sup>2</sup>e.g.,  $N \sim 10^4 - 10^6$  nuclei in self assembled GaAs/InGaAs dots

<sup>3</sup>In the famous Loss-DiVincenzo proposal [2] for a solid state quantum computer, single electron spins confined to the quantum dot are used as qubits.

Considering an electron confined in the s-type conduction band of a quantum dot that interacts with the surrounding nuclei and assuming that the electron is in an orbital eigenstate of the confining potential, the Hamiltonian is given by

$$H'_{\text{hf}} = \mathbf{S} \cdot \sum_i A \nu_0 |\xi(\mathbf{r}_i)|^2 \mathbf{I}_i. \quad (1.20)$$

Here,  $\mathbf{I}_i$  is the  $i$ -th nuclear spin,  $\nu_0$  the volume of a unit cell and  $A$  the hyperfine coupling constant given by

$$A = \frac{4\mu_0}{3I} \mu_b \mu_I \eta \frac{1}{\nu_0}. \quad (1.21)$$

To give an example for the order of magnitude of  $A$ , let us consider a typical GaAs quantum dot with a volume of the order of  $10^5 \text{ nm}^3$  containing  $10^6$  nuclei. The hyperfine coupling constant  $A$  is given by  $90 \mu\text{eV}$ . With the electron g-factor  $g_e = -0.44$  in GaAs, this corresponds to a magnetic field of the order of a few Tesla [17].

If an external magnetic field is applied, the Hamiltonian is given by

$$H''_{\text{hf}} = g_e \mu_b \mathbf{S} \cdot \mathbf{B}_{\text{ext}} + \mathbf{S} \cdot \sum_i A_i \mathbf{I}_i, \quad (1.22)$$

where the first term describes the coupling of the electron spin to an external magnetic field,  $B_{\text{ext}}$ , and the second term is the coupling of the electron spin to the surrounding nuclei. The Zeeman term of the nuclear spins is neglected here, as it is 2–3 orders of magnitude smaller than the Zeeman energy of the electrons due to the small nuclear magnetic moment. We also neglect dipole-dipole interaction between nuclear spins as the timescale of the interaction between neighboring nuclei in GaAs quantum dots ( $10^{-4}$ - $10^{-5}$ s) is larger than the one for the hyperfine coupling ( $10^{-6}$ s) [17].

As the Hamiltonian in equation (1.22) describes the coherent coupling of a single electron spin to an ensemble of nuclear spins, it is useful to define a collective nuclear spin operator

$$\mathbf{A} = \sum_i \alpha_i \mathbf{I}_i \quad (1.23)$$

where

$$\alpha_i = \frac{|\Psi(\mathbf{r}_i)|^2}{\sqrt{\sum_i |\Psi(\mathbf{r}_i)|^4}}, \quad (1.24)$$

such that  $\sum_i \alpha_i^2 = 1$ .  $\alpha_i$  is proportional to the probability  $|\Psi(\mathbf{r}_i)|^2$  to find the electron at site  $i$  of nuclear spin  $\mathbf{I}_i$ .

The Hamiltonian given by equation (1.22) can now be written as

$$H''_{\text{hf}} = g_e \mu_b \mathbf{S} \cdot \mathbf{B}_{\text{ext}} + g \mathbf{S} \cdot \mathbf{A}, \quad (1.25)$$

with the coupling  $g$  given by

$$g = A \nu_0 \sqrt{\sum_i |\Psi(\mathbf{r}_i)|^4}. \quad (1.26)$$

An important special case is the homogeneous coupling of the electron spin to the nuclei. Since in this case, the collective operators  $\mathbf{A}$  are proportional to any single nuclear spin operator, the description of the hyperfine interaction is considerably simplified. Many aspects of the general hyperfine interaction are qualitatively seen already in the simple homogeneous case, where the coupling  $\alpha_i$  takes the same value at each site of the nuclei. The probability to find the electron at site  $i$  of nucleus  $I_i$  is given by  $|\Psi(\mathbf{r}_i)|^2 = \frac{1}{N}$  and the denominator of  $\alpha_i$  is given by  $\sqrt{\sum_i |\Psi(\mathbf{r}_i)|^4} = \frac{1}{\sqrt{N}}$ . Therefore,  $\alpha_i = \frac{1}{\sqrt{N}}$  and the coupling  $g$  is given by

$$g = \frac{A}{\sqrt{N}}. \quad (1.27)$$

The collective spin operator is thus given by

$$\mathbf{A}_{\text{hom}} = \frac{1}{\sqrt{N}} \sum_i \mathbf{I}_i \quad (1.28)$$

and the last part of the Hamiltonian (1.25) can be written as

$$g \mathbf{S} \cdot \mathbf{A}_{\text{hom}} = \frac{A}{N} \mathbf{S} \sum_i \mathbf{I}_i. \quad (1.29)$$

Going back to the general case, equation (1.25) can be rewritten in terms of  $S^\pm = S_x \pm iS_y$  and  $A^\pm = A_x \pm iA_y$ , leading to

$$\begin{aligned} H''_{\text{hf}} &= \frac{g}{2}(A^+S^- + S^+A^-) + gA_zS_z + g_e\mu_b\mathbf{S} \cdot \mathbf{B}_{\text{ext}} \\ &= \frac{g}{2}(A^+S^- + S^+A^-) + g_e\mu_bS_zB_{\text{tot}}, \end{aligned} \quad (1.30)$$

where we have introduced the effective magnetic field  $B_{\text{tot}}$  which is given by

$$B_{\text{tot}} = \frac{g}{\mu_b g_e} A_z + B_{\text{ext}}, \quad (1.31)$$

where the external magnetic field is assumed to be applied along the  $z$ -direction  $\mathbf{B}_{\text{ext}} = B_{\text{ext}}\mathbf{e}_z$ . The first part of the Hamiltonian is the so-called flip-flop term. It describes the exchange of spin excitation between the electron spin and the nuclear spin system. In the case of fully polarized nuclear spins, the flip-flop term couples the initial state with all nuclei in the spin down state to the superposition of states with one nuclear spin in the spin up state.

The second term of the Hamiltonian describes the coupling to the total magnetic field, which is the sum of the external magnetic field and the effective field due to the nuclei, the so-called Overhauser field. For  $\mathbf{B}_{\text{tot}} = 0$ , i.e., if the Overhauser field and the external field cancel each other, spin-exchange dominates ("resonant case"), whereas on the other hand, in the presence of a large magnetic field, spin exchange is strongly suppressed ("off-resonant case").

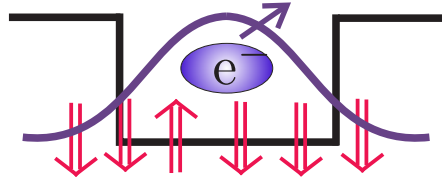


Figure 1.9: Schematic view of an electron confined in a quantum dot, interacting with the nuclear spins present in the dot.

### 1.2.1 Polarization of nuclear spins in quantum dots

In the last years, the task to polarize nuclear spins in quantum dots has received much attention [19, 20, 21]. The main interest in achieving high polarization of the nuclear spins in quantum dots lies in the fact, that the major decoherence source for electron spin qubits in quantum dots, the hyperfine interaction between single electrons and randomly oriented nuclear spins, can be suppressed by polarization of the nuclear spins. Advantage can be taken of the hyperfine interaction as it can be used to manipulate the state of the nuclear ensemble with the electrons. In this Section, an example for a way to manipulate the nuclear spins such that they become polarized, will be given. As mentioned before, in the present work, the hyperfine interaction is a mediator for an interaction between light and nuclear spins and enables storage of light states into the nuclear spin degrees of freedom. A necessary prerequisite for this scheme is high polarization of the nuclear spins. It will be shown in the following how to achieve this goal. Nuclear polarization in bulk systems has a long history and has offered many insights into the spin dynamics in solids [4, 18]. Dynamical nuclear polarization (DNP) almost always relies on providing a "bath" of polarized electrons which polarize the nuclei due to the hyperfine interaction. There are many ways in which polarization of the nuclei in quantum dots can be achieved [4]. As a specific example, we concentrate on the theoretical proposal of A. Imamoglu et al. (2003) [5] which takes quantum coherence of the nuclear spin state into account which is of importance to our quantum memory proposal later. The basic idea here is, to polarize the nuclear spins, using the hyperfine interaction with a single quantum-dot electron spin to induce controlled electron-nuclear spin-flip processes. A singly charged quantum dot where a single conduction band electron interacts with  $10^4$  nuclei is considered. A large external magnetic field ( $B = 10\text{T}$ ) is applied along the strong confinement in  $z$ -direction. The Hamiltonian of the system is the one given by equation (1.25):

$$H''_{\text{eff}} = \frac{g}{2}(A^+S^- + S^+A^-) + gA^zS_z + g_e\mu_bS_zB_z. \quad (1.32)$$

In the initial setup, nuclear spin-flip processes are forbidden by energy conservation as the Zeeman splitting between the electronic spin up and down states is large. As it is desired to achieve controlled spin-flip processes, the Zeeman splitting has to be canceled for a certain time period. It has been proposed and very recently

been demonstrated [22] that this can be achieved by applying a red detuned laser pulse that creates a "spin state dependent ac Stark shift" that effectively cancels the Zeeman splitting of the electron and allows for resonant electron-nuclear spin-flips to take place. If a spin flip process has occurred, the electron is, e.g., in the spin down state (if it was in the spin up state initially). Next, a  $\pi$  pulse excites it to a trion state, which relaxes predominantly to the electronic spin up state by spontaneous emission of a photon. If the electron-nuclear spin-flip has not taken place, the  $\pi$  pulse does not couple to any occupied state. Thus, every time a nuclear spin is flipped, the reinitialization of the electron spin leads to the emission of a photon. The nuclear spin polarization that is achieved can be measured by counting the spontaneously emitted photons. The principal limitation of this polarization scheme is the probability of the system to evolve into a dark state  $|D\rangle$ , a state that cannot be polarized any more, characterized by

$$A^-|D\rangle = 0. \quad (1.33)$$

Imamoglu et al. [5] first showed that dark states limit the polarization process and how inhomogeneous coupling can mitigate this problem. A more detailed discussion of dark states, first for the homogeneous case, where the coupling constant has the same value at all sites of the nuclei, and then for the inhomogeneous case (see [5] and [23]) follows:

*Homogeneous Case:* The operators  $A^{\pm,z}$  form a closed algebra and the system can be described by the collective angular momentum states in the well-known Dicke basis. The basis state is given by  $|A, m_A, \beta\rangle$ . Here,  $A(A+1)$  is the eigenvalue of the collective angular momentum operator  $\mathbf{A}^2$  and  $m_A$  is the eigenvalue of  $A^z$ .  $\beta$  is the permutation quantum number (see [24]). Polarizing the system corresponds to lowering  $m_A$ . This is done by the operator  $A^-$ , which decreases  $m_A$  by one when acting on the state  $|A, m_A, \beta\rangle$ . The total angular momentum  $A$  of the system is not changed during the polarization process. Thus, when  $m_A = -A$  is reached it can not be polarized any more, as  $A^-|A, -A, \beta\rangle = 0$ . However, the system can still be far from being fully polarized. Indeed, for an initially fully unpolarized system,  $A$  is of the order  $\sqrt{N} \ll \frac{N}{2}$ <sup>4</sup> [25] for the nuclear spins being initially in a completely unpolarized state given by

$$\rho = \frac{1}{2^N} \sum_A D(A)(2A+1) |A, -A\rangle\langle A, -A|, \quad (1.34)$$

where  $D(A)$  describes the degeneracy of the states  $|A, m_A\rangle$

$$D = \binom{N}{N/2 - A} - \binom{N}{N/2 - A - 1}. \quad (1.35)$$

<sup>4</sup>the maximum value for an ensemble of  $N$  nuclei with spin 1/2

<sup>5</sup>trace over  $\beta$  has been performed

The expectation value  $\langle A^z \rangle$  of the totally mixed state with  $m_A = -A$  is given by

$$\langle A^z \rangle = -\frac{1}{2^N} \sum_{A=0}^{N/2} A(2A+1)D(A). \quad (1.36)$$

An example for the limit in polarization in the homogeneous case can be given for  $N = 2$ : Here, polarization up to 75% can be achieved. This can be seen easily as there are four possible two-spin states, the three triplet states and the "dark" singlet state that cannot be polarized.

*Inhomogeneous case:* Looking at inhomogeneous coupling of the electron to the nuclei (see Figure 1.9), there is a way to mitigate the problem of the system evolving to dark states that trap excitations. In the case where the probability to find the electron at site  $i$  of nucleus  $I_i$  is not constant (see Figure 1.9), there exist as many dark states as before, however, the inhomogeneous values of  $\alpha_i$  turn most of these states bright after some time (for an example see [23]). Only subcollections of nuclear spins for which  $\alpha_k \simeq \alpha_l$  will remain dark. This effect can be further enhanced by actively introducing such inhomogeneities, e.g., by changing the electronic wavefunction such that formerly equally coupled nuclei do have different coupling strengths  $\alpha_i$ . This can be done using external electric fields that vary the spatial wave function of the electron confined in the dot. In the scheme proposed here, the measurement of the emitted photons indicates when the system has evolved into the dark state. Then, the electric field can be applied and changed until the photon detection rate increases again. A numerical simulation of this method for ten nuclear spins yields a polarization  $> 99\%$  (for details see [5]). H. Christ et al. [23] extended the study to  $N \sim 10^3$  nuclear spins by numerically integrating the master equation for the cooling process and showing that polarization larger than 90% can be achieved within a millisecond time scale.

Experimentally, polarization of  $\approx 20\%$  has been achieved in self-assembled quantum dots [26]. In smaller interface-fluctuation quantum dots, polarization  $> 65\%$  has been achieved [19].

### 1.2.2 Bosonic behavior of the collective nuclear spin operators

In the last two Sections, collective nuclear spin operators have been introduced and proposals and experimental results for the polarization of nuclear spins have been presented. In this Section, the question whether and in which cases the collective nuclear spin operators show bosonic behavior shall be discussed [27, 28].

For a highly polarized nuclear spin ensemble interacting resonantly with the electron, the spin-flip part of the Hamiltonian given by equation (1.25)

$$H_{\text{sp}} = \frac{g}{2}(A^+S^- + S^+A^-) \quad (1.37)$$

resembles the well known Jaynes-Cummings model of quantum optics. The Jaynes-Cummings model describes the interaction between a two level system (e.g. two internal states of an atom) and a bosonic mode (e.g., a cavity mode in cavity-QED). For the hyperfine interaction described by the Hamiltonian in equation (1.37) to resemble the Jaynes-Cummings interaction, the collective nuclear spin operators have to, at least in an approximation, show bosonic behavior.

To reduce the problem to a simple case first, constant coupling of the electron to all nuclei is assumed. This is the homogenous case where the operators  $\{A^+, A^-, A^z\}$  given by

$$\left\{ \frac{1}{\sqrt{N}} \sum_i I_i^+, \frac{1}{\sqrt{N}} \sum_i I_i^-, \frac{1}{\sqrt{N}} \sum_i I_i^z \right\} \quad (1.38)$$

with  $N$  denoting the number of nuclei, form a closed algebra. The collective nuclear spin operators  $A^{\pm, z}$  can be mapped to bosonic operators  $b, b^\dagger$  by the well-known Holstein Primakoff transformation [29]. The exact mapping is given by

$$A^- \rightarrow \sqrt{1 - \frac{b^\dagger b}{N}} b \quad (1.39)$$

$$A^+ \rightarrow \sqrt{1 - \frac{b^\dagger b}{N}} b^\dagger \quad (1.40)$$

and

$$A^z \rightarrow \frac{1}{\sqrt{N}} \left( b^\dagger b - \frac{N}{2} \right), \quad (1.41)$$

where  $b, b^\dagger$  are the well known bosonic creation and annihilation operators.

Thus, the action of  $A^-$  on the collective spin state made up of  $N$  spin-1/2 highly polarized nuclei with total angular momentum  $J \approx \frac{N}{2}$ , is given by

$$A^- |J, -J + n\rangle = \sqrt{n} \sqrt{1 - \frac{n}{N}} |J, -J + n - 1\rangle. \quad (1.42)$$

Note that whereas  $n$  for bosonic modes can run from 0 to  $\infty$ , it runs from 0 to  $N$  here. For  $n > N$ , equation (1.39) would yield the square root of a negative expression. However, the transition from  $n \leq N$  to  $n > N$  will never occur, as

$$A^+ |J, -J + n\rangle = \sqrt{n+1} \sqrt{1 - \frac{n}{N}} |J, -J + n + 1\rangle = 0 \quad (1.43)$$

for  $n = N$ .

In case of high polarization of the nuclei, the ratio between the average number of spins flipped to the average number of nuclei that interact with the electron is small. Thus, the action of the operators  $A^-$  and  $A^+$  corresponds to the one of bosonic creation and annihilation operators

$$A^+ |J, -J + n\rangle \approx \sqrt{n+1} |J, -J + n + 1\rangle, \quad (1.44)$$

$$A^- |J, -J + n\rangle \approx \sqrt{n} |J, -J + n - 1\rangle. \quad (1.45)$$

The correction  $\sqrt{1 - \frac{n}{N}} \approx 1$  describes the error that occurs, when the collective spin operator  $A^+$ , acting on the nuclear spin ensemble, finds a nucleus with its spin flipped. It reflects the fact, that for bosons, double occupancy is allowed. As the number of nuclei in quantum dots that will be considered in this work is of the order of  $N \sim 10^4 - 10^6$ , the deviation from the bosonic commutation relation for a small number of excitations (which are denoted by  $n$  here) is small.

In the case of inhomogeneous coupling, introducing bosonic operators is not so straightforward. The operators  $A^+, A^-, A^z$  do not form a closed algebra, as it is the case for homogeneous coupling. For the commutator  $[A^-, A^+]$ , the relation

$$[A^-, A^+] = 1 - 2 \sum_l g_l^2 \sigma_l^+ \sigma_l^- \quad (1.46)$$

holds, where the norm of  $\sum_l g_l^2 \sigma_l^+ \sigma_l^-$ , the deviation from the bosonic commutation relation, gives a measure for the non-bosonicity of the operator. This norm can be defined as a parameter  $\epsilon$ :

$$\epsilon = \left\| \sum_l g_l^2 \sigma_l^+ \sigma_l^- \right\|, \quad (1.47)$$

required to be small for the bosonic description to be valid. For a nuclear ensemble with  $m$  spins flipped, the inequality

$$\left\| \sum_l g_l^2 \sigma_l^+ \sigma_l^- \right\|_m \leq m \max_l g_l^2 = \frac{m}{N_{\text{eff}}} \quad (1.48)$$

gives an estimate for  $\epsilon$  [30]. Here,  $\|\cdot\|_m$  denotes the norm within the subspace where at most  $m$  spins are flipped and  $N_{\text{eff}} = 1/(\max_l (g_l^2))$  characterizes the number of nuclei that effectively interact with the electron. In the case of constant coupling of the electron to all nuclei, i.e., in the homogeneous case where  $g_l = 1/\sqrt{N}$ ,  $N_{\text{eff}}$  is given by  $N$ , which is obvious as all nuclei interact with the same coupling strength with the electron. In the inhomogeneous case and for a fixed number of spins flipped,  $\epsilon$  increases the more localized the electron wave function is, so the demands on polarization are stronger in inhomogeneous systems. Assuming  $\epsilon$  to be small and introducing a set of bath operators that take the correction due to non-bosonicity of the operators into account, an effective Hamiltonian resembling the Jaynes-Cummings model has been derived by H. Christ et al. [27]. The Rabi frequency and the detuning depend on the state of the bath. In a real situation where the nuclei are in a highly mixed state, the evolution of the system can be understood as a statistical mixture of Jaynes-Cummings like systems corresponding to the different parameters. This Jaynes-Cummings like description of the hyperfine coupling between a single electron spin interacting with an ensemble of nuclear spins will be the starting point for the present work.

## 1.3 Quantum memory

### 1.3.1 Characterization of a quantum memory

For many aspects of quantum information, as for example quantum networks and quantum cryptography, the implementation of an interface between light pulses, carrying quantum information, and matter, suitable for storing and processing this information, is of high importance.

Light doubtlessly serves as the preferred carrier for information transport both in classical and quantum communications. In classical communications, the information, i.e., the bits, are encoded into large average amplitudes of light pulses. The light pulses are detected by photodetectors, amplified, converted into electric signals and stored, e.g., as tiny regions of magnetization on a spinning disk. Detection and subsequent storage of information is inapplicable in quantum information as an unknown quantum state cannot be determined faithfully by a measurement.

Considering for example a state of light defined by two quadrature phase operators<sup>6</sup>  $\mathbf{x}$  and  $\mathbf{p}$  with the commutation relation  $[\mathbf{x}, \mathbf{p}] = i/2$ . A measurement of both  $\mathbf{x}$  and  $\mathbf{p}$  (for example by homodyne detection) would yield noisy results because  $\mathbf{x}$  and  $\mathbf{p}$  do not commute and thus are not simultaneously measurable.

A quantum memory however should be implemented such, that an unknown quantum state can be faithfully stored, which implies, in our example, that means, variances etc. of both  $\mathbf{x}$  and  $\mathbf{p}$  are reproduced by the stored state. A quantum memory should perform better than a classical memory, to be more precise, the quantum memory should meet the following two criteria formulated in [1]:

1. "The light pulse to be stored is sent by a third party in a state unknown to the memory party"
2. "The state of light is converted into a quantum state of the memory with a fidelity higher than that of the classical recording."

The second criterion is very important. Under realistic conditions, 100% fidelity can not be achieved and a criterion is needed in order to decide whether the fidelity achieved by the quantum memory is higher than the highest fidelity than can be achieved by classical means, so to say the classical "benchmark" fidelity. The benchmark fidelity is not known for every class of quantum states. For coherent states, K. Hammerer et al. (2005) [31] have proved a limit for the average fidelity that can be achieved classically. As storage of coherent states will be of particular interest in this work, the benchmark fidelity given in [31] shall be discussed in more detail here.

Before proceeding, a short explanation of what the term 'continuous variable systems' means in the context of quantum information and communication shall be

---

<sup>6</sup>A single frequency mode of the electric field given by  $E(\mathbf{r}, t) = E_0[ae^{i(\mathbf{k}\cdot\mathbf{r}-\omega t)} + a^\dagger e^{-i(\mathbf{k}\cdot\mathbf{r}-\omega t)}]$  can be written as  $E(\mathbf{r}, t) = 2E_0[\mathbf{x} \cos(\omega t - \mathbf{k} \cdot \mathbf{r}) + \mathbf{p} \sin(\omega t - \mathbf{k} \cdot \mathbf{r})]$  with  $\mathbf{x} = \frac{1}{2}(a+a^\dagger)$  and  $\mathbf{p} = \frac{1}{2i}(a-a^\dagger)$

given. Continuous variable systems have a continuous spectrum and are infinite dimensional. Many quantum variables as for example position, momentum and as mentioned before the quadratures of the electric field are continuous variables. However, quantum information has originally been developed for qubits, i.e., finite dimensional systems. One reason to consider infinite rather than finite systems was, that the continuous quadrature amplitudes of the quantized electromagnetic field offer efficient implementation possibilities of essential steps in quantum communication protocols, namely preparation, unitary-manipulation and measurement of (entangled) quantum states [32]. Many quantum communication protocols for qubits have been extended to continuous variable systems, as for instance the quantum teleportation protocol proposed by Bennett et al. (1993) [33] for finite dimensions, that was extended to infinite dimensions by Vaidman (1994) [34].

Let us now go back to the question which benchmark fidelity can be achieved by classical means. To be more precise, let us define the fidelity as the quality of a channel<sup>7</sup> acting on a set of input states. According to [31], the average fidelity of a channel acting on a set of predefined input states  $|\psi_x\rangle$ , where an input  $|\psi_x\rangle$  occurs with probability  $p(x)$  and the output of the channel is defined by  $E(|\psi_x\rangle)$  is given by

$$\bar{F} = \sum_x p(x) \langle \psi_x | E(|\psi_x\rangle) | \psi_x \rangle. \quad (1.49)$$

For an ideal channel that stores (or transmits) every quantum state perfectly,  $\bar{F}$  would be one. The benchmark fidelity we are interested in, is the maximal value of  $\bar{F}$  that can be achieved with a classical channel. Any channel that performs better than a classical channel leading to the maximal value of  $\bar{F}$  is then necessary quantum. A classical channel can be characterized as done in [31]: "Any classical channel can be described by a POVM [35] measurement  $\{M_x\}$  where  $y$  denotes the outcome occurring with probability  $|\langle \psi_x | M_x | \psi_x \rangle|^2$  and a reconstruction rule  $y \rightarrow \rho_y$  determining which state  $\rho_y$  is prepared when  $y$  was the measurement outcome."

A criterion for the maximal classical fidelity for finite dimensional systems has been derived in the mid-nineties. A criterion for infinite dimensional systems had been conjectured but not been proven for a long time. A rigorous proof was given in [31]. They showed, that for any classical strategy of storage and transmission, the maximal average fidelity  $F_{\max}$  for coherent states that are distributed in phase space according to a Gaussian distribution given by  $p(\alpha) = \frac{\lambda}{\pi} \exp(-\lambda|\alpha|^2)$  has to fulfill the condition

$$F_{\max} \leq \frac{1 + \lambda}{2 + \lambda}. \quad (1.50)$$

Note that this criterion holds for the maximal classical fidelity for storage or

---

<sup>7</sup>Each processing step in quantum information as for example free time evolution, controlled time evolution, preparation and measurement, can be interpreted as a channel. Defining input states and output state as  $\rho_{\text{in}}$  and  $\rho_{\text{out}}$ , a channel can be regarded as a map  $E$  which transforms the input state  $\rho_{\text{in}}$  into the output state  $\rho_{\text{out}}$ . To be more precise, each quantum channel can be described by a linear, positive, trace preserving map  $E$ .

transmission. For different demands, other criteria have to be found. For a secure channel for example, the benchmark fidelity is higher. Grangier and Grosshans (2001) [36] derived a criterion for quantum cloning and teleportation of continuous variables. When Alice teleports a quantum state to Bob, Alice's original of the state is, according to the no-cloning theorem, destroyed. It could happen that Bob receives a copy of Alice's state that is better than a copy achieved by classical means but Alice keeps a better though also imperfect copy for herself. For a secure channel, it has thus to be warranted that no copy of the input state exists that is better than the teleported state Bob receives. As shown in [36] the fidelity warranting the destruction of the initial state has to fulfill

$$F_{\text{tel}} \geq \frac{2}{3}. \quad (1.51)$$

### 1.3.2 Experimental realization of a quantum memory with atomic ensembles

Next, an example for an experimentally realized quantum memory utilizing atomic ensembles shall be given [1]. In this example, the state of light is stored in the atomic collective orientation (which is called 'spin') formed by a superposition of magnetic sublevels of the ground state of an atomic ensemble. Therefore the interface between light and atoms is given by off-resonant interaction of light pulses with spin polarized atoms. For experimental-technical reasons, two atomic ensembles are used in [1]. As the memory protocol in principle works with a single atomic ensemble, only one shall be taken in account here for reasons of simplicity. Let the initial coherent spin state of the atoms be polarized along the  $x$  axis. For a highly polarized initial collective spin state, the Holstein Primakoff approximation (see equations (1.39)-(1.41)) allows the spin operators to be described by bosonic operators. Thus, canonical atomic variables  $x_A$  and  $p_A$  corresponding to the  $y$  and  $z$  components of the collective angular momentum  $\mathbf{J}$  can be introduced where  $x_A \approx J_y / \sqrt{\langle J_x \rangle}$  and  $p_A \approx J_z / \sqrt{\langle J_x \rangle}$ .

The quantum storage of light is achieved in three steps: Firstly, the light interacts with the prepared atomic ensemble. Here a strong classical laser pulse is combined with the quantum light pulse to be stored and the combined pulse is sent through the atoms. Secondly, the transmitted light is measured and thirdly fed back into the atoms conditioned on the measurement result.

The interaction of light with the atoms leads to a polarization rotation of the light (depending on the state of the atoms) and to a Stark shift of the atomic ground states (depending on the state of light). Thus, the state of light changes depending on the state of the atoms and the atomic state changes depending on the state of the light - light and atoms become entangled!

The entanglement is reflected in the equations describing the interaction [1]:

$$x_L^{\text{out}} = x_L^{\text{in}} + kp_A^{\text{in}}, \quad p_L^{\text{out}} = p_L^{\text{in}} \quad (1.52)$$

$$x_A^{\text{out}} = x_A^{\text{in}} + kp_L^{\text{in}}, \quad p_A^{\text{out}} = p_A^{\text{in}}. \quad (1.53)$$

Here,  $x_A$  and  $p_A$  denote the canonical atomic operators,  $x_L$  and  $p_L$  denote the quadrature operators of the (quantum)light field and  $\kappa$  denotes the interaction parameter. After the interaction of the light with the atoms, the variable  $x_L^{out}$  of the transmitted light is measured. The result, given by  $x = x_L^{in} + \kappa p_A^{in}$  is fed back onto the atomic variable  $p_A$ . This results in  $p_A^{mem} = p_A^{in} - gx = p_A^{in} - g(x_L^{in} + \kappa p_A^{in}) = p_A^{in}(1 - \kappa g) - gx_L^{in}$  with gain factor  $g$ . For  $g = \kappa = 1$ , perfect mapping of  $x_L^{in}$  onto  $p_A^{mem}$  is achieved. The light operator  $p_L^{in}$  is already mapped onto the atoms by  $x_A^{out} = x_A^{in} + p_L^{in}$  without any feedback. However, the mapping is not perfect for an initial coherent spin state as the operator  $x_A$  is noisy. A storage fidelity of 82% has been achieved experimentally, which is considerably higher than the classical fidelity benchmark. Initially squeezing the atomic state reduces the noise in  $x_A$  and would for infinite squeezing lead to 100% fidelity.

## 1.4 Cavity Quantum Electrodynamics with quantum dots

As this work is dealing with a coupled quantum dot-cavity system where the aim is to store the cavity field in the collective nuclear spin state, it is important to review how such a quantum dot-cavity system could be implemented.

Cavity Quantum Electrodynamics (QED) experiments have traditionally been done on atoms in cavities with high quality factor. They allow the study of fundamental quantum-optics phenomena as for example quantum non-demolition measurements of photons, creation of entanglement and quantum decoherence. Realization of such systems in the solid state is motivated by the possibility to fix the emitter's location with respect to the maximum of the cavity mode electric field. Cavity QED with quantum dots has conventionally been done with many quantum dots embedded in the cavity. However, the indirect coupling of the quantum dots to each other leads to limiting effects. Recently, K. Hennessy et al. (2007) [37] have experimentally demonstrated a single quantum dot strongly coupled to a photonic crystal nanocavity.

Before going into details of how they show that their single quantum dot strongly couples to the cavity and that their system shows true quantum behavior, an introduction to photonic crystal nanocavities shall be given.

### 1.4.1 Photonic crystal nanocavities

Photonic crystals are periodic dielectric structures. They are formed by a periodic array of regions of different dielectric constants. A photonic crystal has a photonic band structure similar to an electronic crystal where the periodic array of atoms modifies the energy momentum relation of electrons by defining allowed and forbidden electronic energy bands. For a photonic band gap to appear, the spacing between the dielectric scatterers has to be chosen such that the microscopic scattering resonance of a unit cell of the photonic crystal occurs at the same frequency as the Bragg

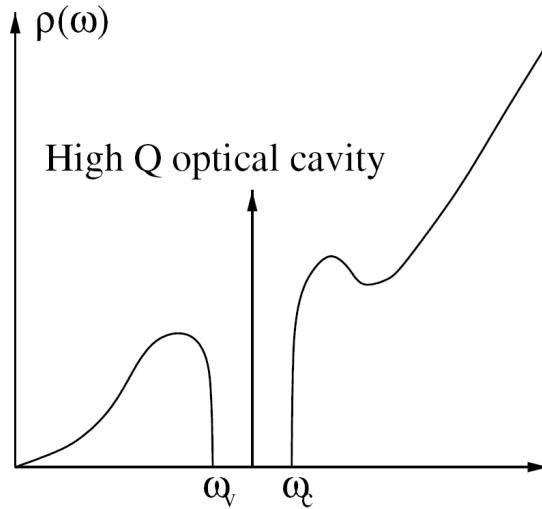


Figure 1.10: Photon density of states  $\rho(\omega)$  of a photonic crystal with a single defect. One single defect mode is present within the band gap between the band edge frequencies  $\omega_v$  and  $\omega_c$ . Picture copied from [38] with permission from the author.

resonance of the periodic array. A two dimensional photonic crystal for example, backscatters electromagnetic waves with frequencies in the band gap region incident from any direction in the plane of periodicity. Thus, the density of photon modes  $\rho(\omega)$  is zero within the band gap. The density of photon modes modifies the spontaneous emission rate. If the density of modes in the vicinity of a certain frequency is greater (smaller) than in free space, spontaneous emission will be enhanced (inhibited). This is the Purcell effect. As the density of photon modes is zero within the band gap, single photon spontaneous emission at these frequencies is completely inhibited. This means that within the band gap, the photonic crystal is emptier than the vacuum as there are not even vacuum fluctuations.

The density of states in the band gap region can be changed by the presence of a defect of the crystal. This is in analogy to a pure semiconductor crystal doped with donor (acceptor) atoms that contribute electrons to the conduction band (accept electrons from the conduction band) and lead to a donor (acceptor) mode within the band gap. In a photonic crystal a defect may be either a dielectric defect, i.e., extra dielectric material is added or an air defect, i.e., dielectric material is removed. Both can lead to a single localized state, the defect mode, within the band gap (see Figure 1.10). The dielectric defect splits a state off from the upper band edge, whereas the air defect splits a state off from the lower band edge. For increasing volume of the air defect (dielectric defect) the frequency of the defect mode increases (decreases), thus the frequency of the defect mode state can be tuned by changing the volume of the defect. In materials with a high refractive index contrast, strong confinement at

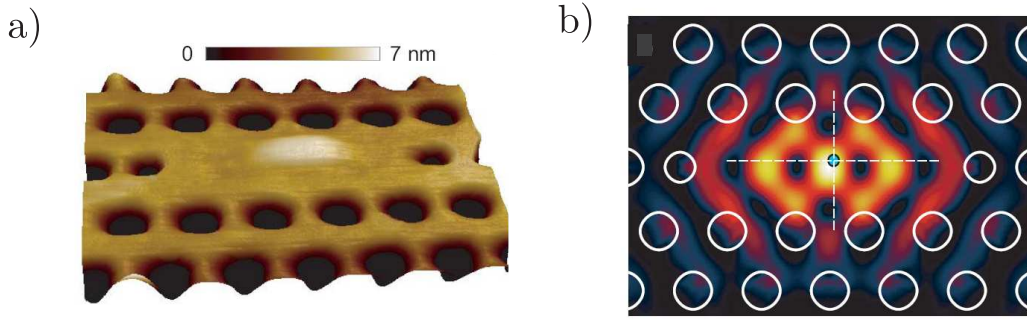


Figure 1.11: a) Atomic force microscopy of a quantum dot embedded in a photonic crystal nanocavity. b) Electric field intensity of the cavity mode. The location of the quantum dot, indicated by the blue dot, lies approximately at the electric field maximum. Pictures copied from [37] with permission from the author.

the location of a defect can be achieved. These systems act as microcavities having a very high quality factor  $Q$ . The  $Q$  factor, defined by

$$Q = \frac{\omega}{\Delta\omega}, \quad (1.54)$$

is given by the ratio of the resonance frequency to the width of the resonance curves and gives a measure for the rate of loss of the cavity. After having introduced basic properties of photonic microcavities, the coupling of a quantum dot to such a cavity shall be studied now.

### 1.4.2 Strong coupling of the quantum dot-cavity system

K. Hennessy et al. (2007) [37] achieved strong coupling of a single quantum dot to a photonic crystal nanocavity and demonstrated that their system shows true quantum behavior. The photonic crystal cavity used in this experiment is fabricated by etching a triangular lattice of air holes in a thin GaAs membrane. A single air hole supports a nondegenerate defect mode within the band gap region. A self-assembled InAs quantum dot is embedded in the photonic crystal, the top half of the photonic crystal slab is grown on the quantum dot layer. The quantum dot gives rise to a 1-2 nm hill on the surface of the photonic crystal and can be detected by atomic force microscopy (AFM)(see Figure 1.11).

High  $Q$  factors ranging from  $Q = 12000 - 30000$  are achieved with this system. The location of the quantum dot is at  $\sim 90\%$  of the electric field maximum. The cavity mode wavelength can be tuned such that the interaction of the cavity and the exciton can be studied as a function of the detuning between the cavity mode resonance wavelength and the wavelength of the exciton transition of the quantum dot,  $\Delta\lambda = \lambda_X - \lambda_c$  where  $\lambda_X$  denotes the exciton transition wavelength and  $\lambda_c$  the cavity mode frequency. When tuning the cavity into resonance with the exciton,

spectra recorded as a function of  $\Delta_\lambda$  show evidence of the strong coupling between the exciton and the cavity mode. For  $\Delta_\lambda > 0.05$  nm, two peaks, one with cavity-like spectral feature and one with excitonic nature, can be seen. For decreasing  $\Delta_\lambda$ , three peaks are observed. The two outer ones can be explained with vacuum Rabi splitting. The middle peak can be explained with fluctuations in the emitter energy due to charging centers in the vicinity of the quantum dot. The vacuum Rabi splitting of the outer peaks shows that energy is exchanged coherently between the exciton and the photon in the form of Rabi oscillations. Another confirmation of strong coupling is the measurement of the exciton lifetime. When tuning the cavity into resonance with the exciton, the lifetime of the exciton decreases to 60 ps, whereas in bulk semiconductor the lifetime is  $\approx 1$  ns. Thus, emission of a photon is enhanced by the cavity mode. For large detuning  $\Delta_\lambda$ , the lifetime increases as explained before, because emission is inhibited by the photonic crystal band gap with zero photon mode density.

Both Rabi splitting and the reduction of the exciton lifetime by a factor 145 show that the system is in the strong coupling regime, however, both effects are not sufficient to show that the system manifests true quantum behavior. The observed vacuum Rabi splitting could also be the result of the coupling behavior of two classical oscillators. The difference to the coupling of two classical oscillators can be seen in the anharmonicity of the Jaynes-Cummings ladder of energy eigenvalues. The energy eigenvalues of a coupled system formed by a two level system interacting resonantly with a light field, i.e., of the Jaynes-Cummings Hamiltonian describing this system, are given by ( $\hbar = 1$ ):

$$E_\pm = (n + 1/2)\omega_c \pm g\sqrt{n + 1}, \quad (1.55)$$

where  $\omega_c$  denotes the single mode cavity frequency/the resonance frequency of the two level system,  $g$  the cavity-two level system coupling and  $n$  the photon number. If a probe field with frequency  $\omega_p = \omega_c - g$  is tuned to excite the state  $|n = 0\rangle$  to  $|n = 1, -\rangle$  (where  $|n, \pm\rangle$  denotes the higher/lower energy eigenstate with  $n$  excitations), the absorption of a second photon of frequency  $\omega_p$  is blocked because a frequency of  $\omega'_p = \omega_0 + g - \sqrt{2}g$  would be needed to drive the transition (for a pictorial view see [39]). This effect is called the photon blockade effect. The photon statistics of the cavity output can be determined by measuring the second order correlation function  $g^{(2)}(\tau)$ . If a blockade effect due to the anharmonicity of the Jaynes-Cummings ladder spectrum occurs, the photon statistics should show non-classical behavior. K.M. Birnbaum et al. (2005) [39] measured  $g^{(2)}(\tau)$  of the cavity transmission of a strongly coupled single atom-cavity system and found that the photon statistics of the output field is sub-Poissonian and antibunched.

To get a confirmation for the quantum nature of the coupling of the quantum dot-cavity system, K. Hennessy et al. [37] apply the same method to their system. They measure quantum correlations between photons that are emitted by the strongly coupled single quantum dot-cavity system. To get a better understanding of their results, a short overview of the second order correlation function is given first.

As mentioned before, measuring the intensity correlation of the cavity output gives insights into the statistical properties of the emitted light. The measurement corresponds to the second order correlation function defined by

$$g_{c,c}^{(2)}(\tau) = \frac{\langle : I_c(t + \tau) I_c(t) : \rangle}{\langle I_c(t) \rangle \langle I_c(t) \rangle}, \quad (1.56)$$

where  $::$  represents normal ordering and  $I_c(t)$ ,  $I_c(t + \tau)$  are the intensities of the cavity photon stream at time  $t$  and time  $t + \tau$ . The second order correlation function allows to decide whether the detected photons stem from a classical field or a quantum field. In the case of a classical field, the inequality

$$g^{(2)}(\tau) \leq g^{(2)}(0) \quad (1.57)$$

holds. It is satisfied for coherent light and thermal light. For coherent light  $g^{(2)}(\tau) = g^{(2)}(0) = 1$ , meaning that the photons arrive randomly at the detector and the photon numbers obey a Poisson distribution. For multimode thermal light, the inequality  $g^{(2)}(\tau) < g^{(2)}(0)$  holds. As its distribution is wider than a Poisson distribution it is referred to as super-Poissonian light. It expresses that the probability to detect one single photon is smaller than the probability to detect two photons at the same time. This effect is called photon-bunching as the photons prefer to arrive in bunches rather than at random. For super-Poissonian light the inequality  $g^{(2)}(0) > 1$  holds, for example for thermal light  $g^{(2)}(0) = 2$ . But there are other possibilities, the case for which

$$g^{(2)}(\tau) > g^{(2)}(0) \quad (1.58)$$

and the case where

$$g^{(2)}(0) < 1. \quad (1.59)$$

Both effects are nonclassical. The effect for which  $g^{(2)}(\tau) > g^{(2)}(0)$  holds, is the opposite of photon bunching, photon antibunching. States for which  $g^{(2)}(0) < 1$  holds are sub-Poissonian. An example is a single mode field in a number state, for which  $g^{(2)}(\tau) = g^{(2)}(0) < 1$ . Both sub-Poissonian statistics and photon antibunching show that the system emitting the photons behaves nonclassical.

K. Hennessy et al. observed sub-Poissonian statistics and antibunching of the cavity output photon stream in the regime of strong exciton-cavity coupling. This gives evidence of the Jaynes-Cummings ladder spectrum that leads to the photon blockade effect that has been explained in conjunction with the experiment done by K.M. Birnbaum [39].



# Chapter 2

## The physical system

In the following Chapter, the physical system of the present work will be discussed. It will be shown, that for large detuning of the Raman transition, the trion can be adiabatically eliminated. This yields a Hamiltonian that is the starting point of Chapter 5, where mapping of the light to the nuclei using the method of "Stimulated Raman adiabatic passage" is studied. Next, assuming large splitting of the electronic states, a second adiabatic elimination of the electron will be carried out. The Hamiltonian derived this way will be the starting point for studying "Landau-Zener transitions" in Chapter 3. Furthermore, by exchanging the coupling of the laser and the cavity field, yielding a squeezing instead of a beam-splitter like Hamiltonian, it will be shown in Chapter 4 that two-mode squeezed states of the nuclear spin-cavity system can be generated.

### 2.1 Basic properties of the system

The system proposed in the present work consists of a singly charged quantum dot strongly coupled to the light field of a high-Q microcavity, a classical laser field and an external magnetic field in  $z$ -direction incident on the quantum dot (see Figure 2.1 a). A quantum dot with confinement that is strongest in  $z'$ -direction and in-plane confinement, that is large enough to guarantee that the electron will always be in the ground state orbital, is assumed here. This is for example the case in self-assembled quantum dots at low temperature (4.2K-100mK). The lowest eigenstates of a III-V semiconductor quantum dot are formed by s-type  $m_{j,z'}^c = \pm 1/2$  conduction band states and  $m_{j,z'}^v = \pm 3/2$  heavy hole valence band states. Light hole states  $m_{j,z'}^v = \pm 1/2$  can be neglected due to the large energy separation (tens of meV) to heavy hole states.

The ground states of the single conduction band electron present in the dot are assumed to be Zeeman split by the external magnetic field  $B_z$  (see Figure 2.1b). When an electron is excited from the valence band to the conduction band by the absorption of a photon of either the cavity or the laser field, the excited electron and

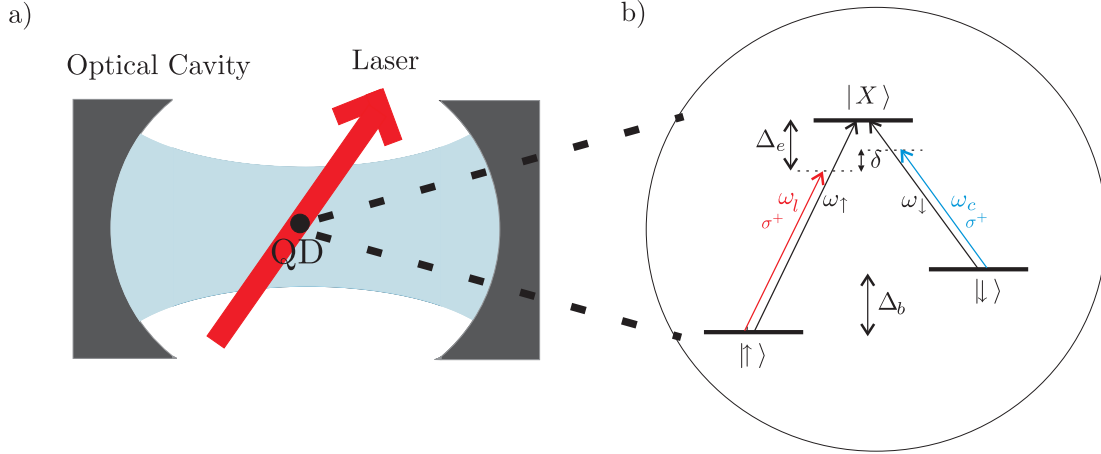


Figure 2.1: a) Schematic view of the quantum dot interacting with the light field of the cavity and a classical laser field. b) Level scheme of the optical transitions between the electronic states  $|\uparrow\rangle$ ,  $|\downarrow\rangle$  and the trion state  $|X\rangle$ .

the electron that has already been present in the ground state of the singly charged quantum dot, form a spin-singlet state. They are bound by Coulomb interaction to the hole that the excited electron leaves in the valence band and form a trion  $X^{1-}$ . It has been explained in Section 1.1.3, that if the external magnetic field and the confinement direction enclose an angle  $\theta > 0$ , the electronic spins  $m_{j,z'}^c = 1/2$  and  $m_{j,z'}^c = -1/2$  are mixed by the magnetic field. This can be seen by writing electronic states as

$$|\uparrow\rangle \equiv |\uparrow\rangle_z = \cos(\theta)|\uparrow\rangle_{z'} + \sin(\theta)|\downarrow\rangle_{z'} \quad (2.1)$$

and

$$|\downarrow\rangle \equiv |\downarrow\rangle_z = \cos(\theta)|\downarrow\rangle_{z'} - \sin(\theta)|\uparrow\rangle_{z'}. \quad (2.2)$$

As  $\sin(\theta) > 0$ , an electron in the  $m_j^v = 3/2$  valence band state can be excited by  $\sigma^+$  polarized light to both the  $m_{j,z'}^c = 1/2$  and  $m_{j,z'}^c = -1/2$  conduction band states, leaving a hole in the valence band with  $m_j^v = -3/2$ . The Hamiltonian of the system described so far is given by ( $\hbar = 1$ )

$$\begin{aligned} H_{\text{opt}} = & \omega_c a^\dagger a + \omega_\uparrow |X\rangle\langle X| + g_e \mu_b B_z |\downarrow\rangle\langle\downarrow| + \frac{\Omega_c}{2} (a^\dagger |\downarrow\rangle\langle X| + \text{h.c.}) \\ & + \frac{\Omega_l}{2} (e^{+i\omega_l t} |\uparrow\rangle\langle X| + \text{h.c.}), \end{aligned} \quad (2.3)$$

where  $\omega_\uparrow$  denotes the resonance frequency of the exciton-electron spin up transition,  $\omega_c$  and  $\omega_l$  denote the cavity and the laser frequency,  $\Omega_c$  and  $\Omega_l$  denote the Rabi frequencies of the cavity and the laser field and  $a^\dagger$  and  $a$  denote creation and annihilation operators of the cavity field. Spin up and down states of the conduction band electron present in the ground state of the quantum dot are denoted by  $|\uparrow\rangle$  and  $|\downarrow\rangle$  and the trion state is denoted by  $|X\rangle$ . The zero point energy level is set to the energy of the

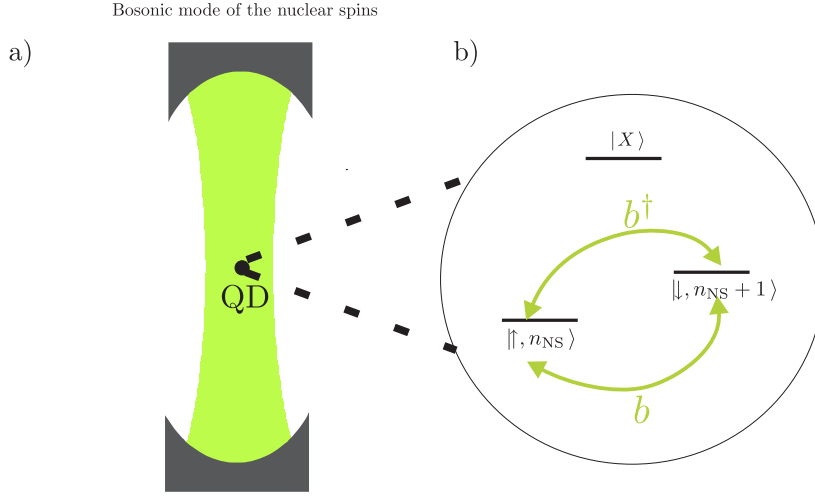


Figure 2.2: a) Schematic view of the quantum dot interacting with the bosonic mode arising from the collective nuclear spin operators. b) Level scheme illustrating the electron-nuclear spin interaction.  $|\uparrow, n_{\text{NS}}\rangle$  denotes the tensor product of the electron spin up state and the collective nuclear spin state with  $n_{\text{NS}}$  excitations, i.e.,  $n_{\text{NS}}$  spin up nuclei in case that the polarization of the sample is spin down. A flip of a spin up electron creates a nuclear spin excitation, i.e., leads to the state  $|\uparrow, n_{\text{NS}+1}\rangle$  and vice versa.

spin-up electronic state. The penultimate term of the Hamiltonian (2.3) describes the coupling to the cavity field, where a photon is destroyed when a valence band electron is excited to the valence band and vice versa. The last term describes the coupling to a classical laser field where a conduction band electron is excited to the valence band. Note that the Hamiltonian describes a system evolving in the subspace  $\mathcal{H}_N : \{|\uparrow\rangle|n-1\rangle, |\downarrow\rangle|n\rangle, |X\rangle|n\rangle\}$ , with  $|n\rangle$  being the  $n$ -photon Fock state of the cavity.

So far, optical transitions in the quantum dot due to the laser and the cavity field have been considered. However, there is another interaction process that has to be taken into account, namely the hyperfine interaction between the single electron of the charged quantum dot and the nuclear spins present in the dot. In a typical GaAs quantum dot, the number of Ga and As nuclei lies between  $N \sim 10^4$ - $10^6$ . The Hamiltonian describing the hyperfine interaction between a single electron spin  $\mathbf{S}$  and the collective spin of the nuclei defined by  $A^{\pm,z} = \sum_k \alpha_k I_k^{\pm,z}$ , where  $\alpha_k$  is proportional to the probability to find the electron at site of nuclear spin  $I_k$ , has been discussed in detail in Section 1.2. It was shown to be given by equation (1.32) and is rewritten here with the only difference, that the external magnetic field does not appear in the Hamiltonian as it is already included in the Hamiltonian  $H_{\text{opt}}$  given by equation (2.3). The Hamiltonian thus reads

$$H_{\text{hf}} = \frac{g_n}{2}(A^+ S^- + S^+ A^-) + g_n A^z S^z, \quad (2.4)$$

where we have introduced  $g_n \equiv g = A/\sqrt{N}$  (see equation (1.26)). In the following we will consider the case of fully polarized nuclear spins, where  $|0\rangle = |-I \dots -I\rangle$  denotes the state of  $N$  spin-down nuclei with angular momentum  $I$ .

As it has been discussed in Section 1.2.1, for homogeneous coupling of the electron to the nuclei, the collective nuclear spin operators  $A^{\pm,z}$  can be mapped to bosonic operators  $b, b^\dagger$  by the well-known Holstein Primakoff transformation [29], associating  $A^{\pm,z}$  with

$$A^- \rightarrow \sqrt{1 - \frac{b^\dagger b}{N}} b \quad (2.5)$$

$$A^+ \rightarrow \sqrt{1 - \frac{b^\dagger b}{N}} b^\dagger \quad (2.6)$$

and

$$A^z \rightarrow \frac{1}{\sqrt{N}} \left( b^\dagger b - \frac{N}{2} \right). \quad (2.7)$$

These equations correspond to equations (1.39)-(1.41) and are recapitulated here to remind the reader. For a low number of excited nuclear spins  $\langle b^\dagger b \rangle \ll N^1$  in a highly polarized sample,  $A^\pm$  are well-approximated by  $A^- \simeq b$  and  $A^+ \simeq b^\dagger$ .

As it has been discussed in Section (1.2.1), in the case of inhomogeneous coupling, introducing bosonic operators is more complicated as the operators  $A^+, A^-, A^z$  do not form a closed algebra. However, H. Christ et al. [27] and Song et al. [28] have shown, that for a sufficiently large number of polarized nuclei interacting with the electron spin, the collective nuclear spin operators  $A^\pm$  show bosonic behavior.

Thus, assuming highly polarized nuclear spins, the Hamiltonian given by equation (2.4) can be written as

$$\begin{aligned} H_{\text{NS}} &= \frac{g_n}{2} (b^\dagger S^- + S^+ b) + \frac{g_n \sigma_z}{2\sqrt{N}} \left( b^\dagger b - \frac{N}{2} \right) \\ &= \frac{g_n}{2} (b^\dagger S^- + S^+ b) + \frac{A}{N} \frac{\sigma_z}{2} \left( b^\dagger b - \frac{N}{2} \right), \end{aligned} \quad (2.8)$$

where the coupling in the last term arising from  $g_n A^z S^z$  reads  $g_n/\sqrt{N} = A/N$  as  $A^z = \frac{1}{\sqrt{N}} \sum_i I_i^z$  in the homogeneous case as defined in equation (1.38).

A pictorial view of a single electron spin in a quantum dot interacting with the collective nuclear spin approximated by a bosonic mode can be seen in Figure 2.2.

The Hamiltonian describing the whole system is given by

$$H = H_{\text{opt}} + H_{\text{NS}}. \quad (2.9)$$

To simplify this Hamiltonian, the time dependency of its first part  $H_{\text{opt}}$ , described by equation (2.3), can be removed by turning to a rotating frame defined by the transformation

$$H' \rightarrow U H U^\dagger + i \dot{U} U^\dagger, \quad (2.10)$$

---

<sup>1</sup>with  $N \sim 10^4$ - $10^5$

where  $U^\dagger$  is given by

$$U^\dagger = \exp[-i\omega_l t(a^\dagger a + |X\rangle\langle X|)]. \quad (2.11)$$

This transformation leaves  $H_{\text{NS}}$  unchanged whereas  $H_{\text{opt}}$  is transformed to

$$H'_{\text{opt}} = \delta a^\dagger a + \Delta_e |X\rangle\langle X| + \Delta_b |\downarrow\rangle\langle\downarrow| + \frac{\Omega_c}{2} (a^\dagger |\downarrow\rangle\langle X| + \text{h.c.}) + \frac{\Omega_l}{2} (|\uparrow\rangle\langle X| + \text{h.c.})$$

with

$$\delta = \omega_c - \omega_l, \quad (2.12)$$

$$\Delta_b = g_e \mu_b B_{\text{ext}} \quad (2.13)$$

and

$$\Delta_e = \omega_\uparrow - \omega_l \quad (2.14)$$

(for more details of the calculation, see Appendix A).

Thus the Hamiltonian  $H'$  is given by

$$H' = H'_{\text{opt}} + H_{\text{NS}}. \quad (2.15)$$

Shifting the energy in equation (2.15) by  $\frac{A}{4}\mathbb{1}$ , the Zeeman splitting of the electronic states due to both the external magnetic field and the field created by the polarized nuclear spins, the so-called Overhauser field, can be written as

$$\tilde{\Delta}_b = g_e \mu_b B_{\text{tot}}, \quad (2.16)$$

where  $B_{\text{tot}}$  is given by

$$B_{\text{tot}} = \frac{1}{g_e \mu_b} \frac{A}{2} + B_{\text{ext}} \quad (2.17)$$

with the electron g-factor denoted by  $g_e$ . Thus, the Hamiltonian given by equation (2.15) reads

$$\begin{aligned} H' = & \delta a^\dagger a + \Delta_e |X\rangle\langle X| + \tilde{\Delta}_b |\downarrow\rangle\langle\downarrow| + \frac{A}{N} \frac{\sigma_z}{2} b^\dagger b + \frac{\Omega_c}{2} (a^\dagger |\downarrow\rangle\langle X| + \text{h.c.}) \\ & + \frac{\Omega_l}{2} (|\uparrow\rangle\langle X| + \text{h.c.}) + \frac{g_n}{2} [b^\dagger |\downarrow\rangle\langle\uparrow| + \text{h.c.}]. \end{aligned} \quad (2.18)$$

It describes the interaction of the electronic levels with both the optical fields (cavity and laser field) and the collective nuclear spins in the bosonic approximation. These two processes, both leading to an effective spin-flip of the electron spin, evolve on different timescales. Whereas the coupling of the cavity to the quantum dot transition can be of the order of  $\Omega_c = 120\mu\text{eV}$  [37], the coupling constant  $g_n$  of the nuclear spins to the electron spins is given by  $g_n = A/\sqrt{N}$ . For a typical self-assembled GaAs quantum dot,  $A$  is of the order of  $100\mu\text{eV}$  and  $N$  can be assumed to be  $N = 10^4$ . This leads to  $g_n = 1\mu\text{eV}$ , which leads to a spin-flip process of one order of magnitude slower than the spin-flip processes induced by the optical fields. Thus, the slower timescale of the nucleus-electron spin-flips sets a lower limit to how long the desired coupling will at least take.

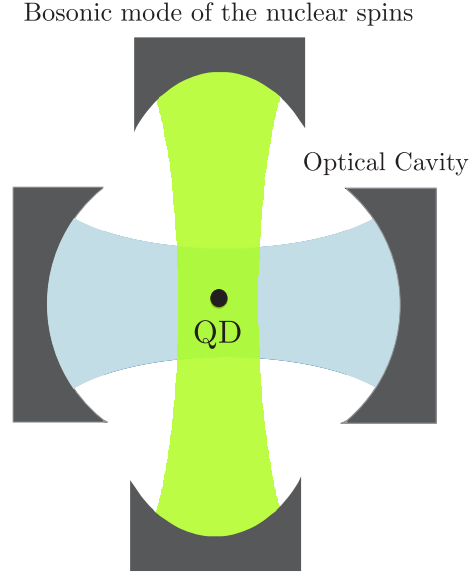


Figure 2.3: Schematic view of the quantum dot interacting with both the optical cavity field and the bosonic approximation of the collective nuclear spin operators.

## 2.2 Adiabatic elimination of the trion

The Hamiltonian given by equation (2.18) is rather complicated for the description of the interaction between light and nuclear spins. To achieve a simpler form of the Hamiltonian, the trion and the electronic states can subsequently be adiabatically eliminated. First, the trion is eliminated. This can be done if laser and cavity are sufficiently detuned from the exciton transition, so that the initially unpopulated trion state will essentially remain unpopulated. In the frame rotating with the laser frequency  $\omega_l$  (see equation (2.18)), the energy separation between the electronic state  $|\uparrow\rangle$  and the trion state  $|X\rangle$  is given by the detuning  $\Delta_e$ . If  $\Delta_e$  is large compared to the Rabi frequencies  $\Omega_c$  and  $\Omega_l$  and the splitting  $\tilde{\Delta}_b - \frac{A}{N}\langle b^\dagger b \rangle$  of the electronic states  $|\uparrow\rangle$  and  $|\downarrow\rangle$ , the timescale of the electron spin down/up - exciton transition is much more rapid than the other processes. The fast oscillating processes average over time and the dynamics of the system can be reduced to the dynamics of the subspace of the electronic states. The projection of the Schrödinger equation onto the subspace of the electronic states reads

$$i\mathbb{P}|\dot{\Psi}\rangle = \mathbb{P}H'(\mathbb{P} + \mathbb{Q})|\Psi\rangle, \quad (2.19)$$

where the projectors  $\mathbb{P}$  and  $\mathbb{Q}$  are defined by  $\mathbb{P} = \mathbb{1} - |X\rangle\langle X|$  and  $\mathbb{Q} = |X\rangle\langle X|$  and the condition

$$|\Delta_e| \gg |\tilde{\Delta}_b|, |\Omega_c|, |\Omega_l| \quad (2.20)$$

is assumed to hold.

Note, that the projector  $\mathbb{P}$  leaves  $H_{\text{NS}}$  unchanged. Following the detailed calculation in Appendix A, the resulting Schrödinger equation for

$$|\varphi\rangle \mapsto \mathbb{P}|\psi\rangle \quad (2.21)$$

is given by:

$$i|\dot{\varphi}\rangle = H_{\text{eff}}|\varphi\rangle \quad (2.22)$$

with

$$\begin{aligned} H_{\text{eff}} &= \mathbb{P}H'\mathbb{P} - \mathbb{P}H'\mathbb{Q} \frac{1}{\mathbb{Q}H'\mathbb{Q}} \mathbb{Q}H'\mathbb{P}|\Psi\rangle \\ &= \delta a^\dagger a + \left( \tilde{\Delta}_b - \frac{\Omega_c^2}{4\Delta_e} a^\dagger a - \frac{A}{2N} b^\dagger b \right) |\downarrow\rangle\langle\downarrow| - \left( \frac{\Omega_l^2}{4\Delta_e} - \frac{A}{2N} b^\dagger b \right) |\uparrow\rangle\langle\uparrow| \\ &\quad - g_a (a|\uparrow\rangle\langle\downarrow| + \text{h.c.}) + \frac{g_n}{2} (b^\dagger|\downarrow\rangle\langle\uparrow| + \text{h.c.}), \end{aligned} \quad (2.23)$$

where

$$g_a = \frac{\Omega_c \Omega_l}{4\Delta_e}. \quad (2.24)$$

Note that terms of order

$$\frac{1}{\Delta_e^2} \cdot \left\{ \frac{\Omega_c \sqrt{n} \delta n}{2}, \frac{\Omega_c \sqrt{n} \tilde{\Delta}_b}{2}, \frac{\Omega_c \sqrt{n} A}{4N}, \frac{\Omega_l \delta}{2}, \frac{\Omega_l A}{4N}, \frac{\Omega_l g_n}{4}, \frac{\Omega_c \sqrt{n} g_n}{4} \right\} \quad (2.25)$$

have been neglected here.

Shifting the energy by adding  $\frac{\Omega_l^2}{4\Delta_e} \mathbb{1}$ , leads to

$$\begin{aligned} H_{\text{eff}}'' &= \delta a^\dagger a + \left( \tilde{\Delta}_b - \frac{\Omega_c^2}{4\Delta_e} a^\dagger a - \frac{A}{2N} b^\dagger b + \frac{\Omega_l^2}{4\Delta_e} \right) |\downarrow\rangle\langle\downarrow| + \frac{A}{2N} b^\dagger b |\uparrow\rangle\langle\uparrow| \\ &\quad + \frac{g_n}{2} (b^\dagger|\downarrow\rangle\langle\uparrow| + \text{h.c.}) - g_a (a|\uparrow\rangle\langle\downarrow| + \text{h.c.}) \end{aligned} \quad (2.26)$$

The interaction part of  $H_{\text{eff}}$  is given by

$$H_{\text{int}} = -g_a (a|\uparrow\rangle\langle\downarrow| + \text{h.c.}) + \frac{g_n}{2} (b|\downarrow\rangle\langle\uparrow| + \text{h.c.}), \quad (2.27)$$

describing a linear two-mode interaction of the electron spin states with the optical fields and the nuclear spins, respectively. The dynamics arising from this Hamiltonian will be studied in more detail in Chapter 5.

## 2.3 Adiabatic elimination of the electronic states

The system can be further simplified by the additional assumption that for the detuning  $\Delta_2$ , which is essentially the splitting of electron spin up and down states, the condition

$$|\Delta_2| \gg |g_a|, |g_n| \quad (2.28)$$

holds, where  $\Delta_2$  is given by

$$\Delta_2 = \tilde{\Delta}_b - \frac{\Omega_c^2}{4\Delta_e} \langle a^\dagger a \rangle - \frac{A}{2N} \langle b^\dagger b \rangle + \frac{\Omega_l^2}{4\Delta_e}. \quad (2.29)$$

This assumption allows us to eliminate the electronic states and thus to derive a direct coupling of the light field to the nuclei that is governed by a beam-splitter type Hamiltonian.

Defining the projectors  $\mathbb{P}'$  and  $\mathbb{Q}'$  by

$$\mathbb{P}' = |\uparrow\rangle\langle\uparrow|, \quad (2.30)$$

$$\mathbb{Q}' = 1 - \mathbb{P}' = |\downarrow\rangle\langle\downarrow| \quad (2.31)$$

and projecting the Schrödinger equation on the electron spin-up subspace

$$i \mathbb{P}' |\dot{\Psi}\rangle = \mathbb{P}' H''_{\text{eff}} \overbrace{(\mathbb{P}' + \mathbb{Q}')}^{\mathbb{1}} |\Psi\rangle, \quad (2.32)$$

where  $H''_{\text{eff}}$  is the Hamiltonian given by equation (2.26), the effective Hamiltonian

$$\tilde{H}_{\text{eff}} = \mathbb{P}' H''_{\text{eff}} \mathbb{P}' - \mathbb{P}' H''_{\text{eff}} \mathbb{Q}' \frac{1}{\mathbb{Q}' H''_{\text{eff}} \mathbb{Q}'} \mathbb{Q}' H''_{\text{eff}} \mathbb{P}' \quad (2.33)$$

$$\begin{aligned} &= \delta a^\dagger a - \left( \frac{g_n}{2} b - g_a a \right) \frac{1}{\Delta_2} \left( \frac{g_n}{2} b^\dagger - g_a a^\dagger \right) \\ &= \delta a^\dagger a - \frac{g_a^2}{\Delta_2} a a^\dagger - \frac{g_n^2}{4\Delta_2} b b^\dagger + \frac{g_n g_a}{2\Delta_2} (a^\dagger b + \text{h.c.}) \end{aligned} \quad (2.34)$$

can be derived in the same way as it has been done for the adiabatic elimination of the trion.

With a shift of  $\frac{g_a^2}{\Delta_2} \mathbb{1}$ ,  $\tilde{H}_{\text{eff}}$  reads

$$\tilde{H}_{\text{eff}} = \left( \delta - \frac{g_a^2}{\Delta_2} \right) a^\dagger a - \frac{g_n^2}{4\Delta_2} b b^\dagger + \frac{g_n g_a}{2\Delta_2} (a^\dagger b + \text{h.c.}). \quad (2.35)$$

This Hamiltonian is the starting point for studying Landau-Zener transitions in Chapter 3. The second term in the Hamiltonian describes the beam-splitter like interaction between light field and nuclear spins: the annihilation of a photon leads to the creation of a nuclear spin excitation and vice versa. Letting this beam-splitter like interaction act for a time  $\frac{\pi}{g_n g_a / 2\Delta_2}$ , would, if the  $a^\dagger a$  and  $b^\dagger b$  terms of the Hamiltonian were not present, lead already to a mapping of the light state to the nuclear spins. However, to achieve the latter with the Hamiltonian given by equation (2.35), methods such as "Landau-Zener transitions" and "Stimulated Raman Adiabatic Passage" (STIRAP) have to be considered. This will be done in the following.

# Chapter 3

## Landau-Zener transitions

The Hamiltonian given by equation (2.35) describes an effective interaction between the light field of the cavity and the nuclear spins. As we aim at storing the light field in the nuclear spin degrees of freedom, it is desirable to find a transition between the light field of the cavity and the nuclei. It will be shown that this can be achieved using the Landau-Zener formula that was developed independently by L. Landau [40] and C. Zener [41] in the early 1930's<sup>1</sup>.

### 3.1 The Landau-Zener formula

Both Landau and Zener study a quantum mechanical two level system with an energy separation varying linearly in time. The Hamiltonian of the system which they consider can be written as

$$H_{\text{LZ}}(t) = \begin{pmatrix} \frac{v}{2}t & g_{12} \\ g_{12} & -\frac{v}{2}t \end{pmatrix}, \quad (3.1)$$

where  $E_{1,2} = \pm \frac{v}{2}t$  denote the energies of the states of the two level system and  $g_{12}$  denotes the coupling of the two levels, which is assumed to be time independent. As can be seen in equation (3.1), the energy difference  $E_1 - E_2 = vt$  is assumed to be a linear function of time.

The instantaneous eigenvalues of the Hamiltonian are given by  $\lambda_{1,2} = \pm \sqrt{\frac{v^2}{4}t^2 + g_{12}^2}$ . At  $t = 0$ , the eigenvalues are separated by  $2g_{12}$ , i.e., for nonzero coupling their crossing is avoided (see Figure 3.1). In case that the system starts at  $t \rightarrow -\infty$  in the lower (upper) instantaneous eigenstate  $|\phi_1\rangle$  ( $|\phi_2\rangle$ ), the Landau-Zener formula gives the probability with which the system is found in the upper (lower) eigenstate  $|\phi_2\rangle$  ( $|\phi_1\rangle$ ) at  $t \rightarrow \infty$ . If the energy separation would be changed infinitely slow, the system would, according to the adiabatic theorem, be in an instantaneous eigenstate of the Hamiltonian given by equation (3.1) at all times. Thus, if it is in the state

---

<sup>1</sup>Landau considered scattering from two atoms whereas Zener studied electronic levels of a diatomic molecule

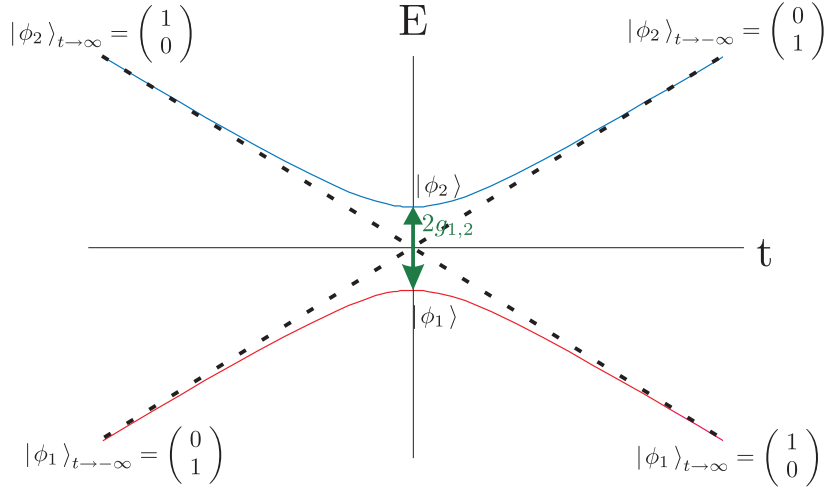


Figure 3.1: Plot of the instantaneous eigenenergies *vs.* time of the Hamiltonian given by equation (3.1). The dashed lines indicate the eigenenergies for zero coupling of the two levels,  $g_{12} = 0$ .

$|\phi_1\rangle_{t \rightarrow -\infty} = (0, 1)$  at  $t \rightarrow -\infty$ , it will be found to be in the state  $|\phi_1\rangle_{t \rightarrow \infty} = (1, 0)$  at  $t \rightarrow \infty$  (see Figure 3.1). However, for (realistic) finite times, unwanted transitions from the lower (upper) to the upper (lower) level occur. The transition probability is given by the Landau-Zener formula:

$$P = e^{-2\pi\gamma}, \quad \text{where} \quad \gamma = \frac{\left(\frac{2\pi}{\hbar}\right)^2 g_{12}^2}{\left|\frac{d}{dt}(vt)\right|} = \frac{\left(\frac{2\pi}{\hbar}\right)^2 g_{12}^2}{|v|}. \quad (3.2)$$

### 3.2 Landau-Zener transitions for operators

In the foregoing Section the basic idea behind Landau-Zener transitions has been reviewed. Here, we invoke this idea in the Heisenberg picture to achieve a mapping of the photon annihilation operator  $a$  to the collective nuclear spin operator in the bosonic approximation  $b$ , i.e.,  $a \rightarrow b$ . In the Heisenberg picture, the linear two-mode interaction between the cavity mode and the nuclear spins in the quantum dot, given by equation (2.35), is described by a set of coupled differential equations for the mode operators:

$$\frac{d}{dt} \begin{pmatrix} a \\ b \end{pmatrix} = -i \begin{pmatrix} \omega_1 & \beta \\ \beta & \omega_2 \end{pmatrix} \begin{pmatrix} a \\ b \end{pmatrix}, \quad (3.3)$$

where

$$\omega_1 = \delta - \frac{g_a^2}{\Delta_2}, \quad (3.4)$$

$$\beta = \frac{g_a g_n}{2\Delta_2} \quad (3.5)$$

and

$$\omega_2 = -\frac{g_n^2}{4\Delta_2}. \quad (3.6)$$

Equation (3.3) is already of the form of the starting point of the Landau-Zener problem given by equation (3.1). However, equation (3.3) is dealing with the annihilation operators  $a$  and  $b$  rather than with states, as in the original problem. But as the form of (3.3) is technically the same as the one in equation (3.1), the Landau-Zener formalism can be used to derive the probability for a transition from the operator  $a$  at  $t = -\infty$  to the operator  $b$  at  $t \rightarrow \infty$ . This can be made even more evident by writing

$$\begin{pmatrix} a \\ b \end{pmatrix} \text{ in the basis } a = \begin{pmatrix} 1 \\ 0 \end{pmatrix} \text{ and } b = \begin{pmatrix} 0 \\ 1 \end{pmatrix}. \quad (3.7)$$

Equation (3.3) now reads:

$$\frac{d}{dt} \begin{pmatrix} u \\ v \end{pmatrix} = iB \begin{pmatrix} u \\ v \end{pmatrix}, \quad (3.8)$$

with

$$B = -\begin{pmatrix} \omega_1 & \beta \\ \beta & \omega_2 \end{pmatrix} \text{ and } \begin{pmatrix} u \\ v \end{pmatrix} = ua + vb. \quad (3.9)$$

As it has been seen in Section 3.1, the energy separation  $\omega_1 - \omega_2$  is assumed to be a linear function in time. The control parameters of the time dependent change of  $\omega_1 - \omega_2$  are the laser Rabi frequency  $\Omega_l$  and the laser frequency  $\omega_l$ . By choosing the parameters in a right way<sup>2</sup>  $\omega_1 - \omega_2$  can be made linear dependent in time. In the adiabatic limit, this leads to the transition

$$\begin{pmatrix} u \\ 0 \end{pmatrix} \rightarrow \begin{pmatrix} 0 \\ v \end{pmatrix} \quad (3.10)$$

(see Figure 3.1), i.e., the photonic operator  $a$  is mapped to the operator  $b$  of the nuclear spins. In a rotating frame given by the transformation

$$\begin{pmatrix} u' \\ v' \end{pmatrix} \rightarrow U^\dagger \begin{pmatrix} u \\ v \end{pmatrix} \text{ with } U = \exp \left[ -i \int (k_2 \sigma_z + k_3 \mathbb{1}) dt \right], \quad (3.11)$$

---

<sup>2</sup>In the Landau-Zener problem, the coupling  $\beta = \frac{g_a g_n}{2\Delta_2}$  is assumed to be constant. The Rabi frequencies of laser and cavity can be chosen small enough so that  $\frac{\Omega_{c,l}^2}{4\Delta_e} \ll \tilde{\Delta}_b$  and thus  $\Delta_2 \approx \tilde{\Delta}_b$ . Assuming that only  $\Omega_l$  and  $\omega_l$  can be changed,  $\beta$  is constant if  $\Omega_l$  and  $\omega_l$  are changed such that  $g_a = \frac{\Omega_l \Omega_c}{4(\omega_1 - \omega_l)}$  is constant. For constant  $g_a$  and  $\Delta_2$ , the only free parameter of  $\omega_1 - \omega_2 = \delta - \frac{g_a^2}{\Delta_2} + \frac{g_n^2}{4\Delta_2}$  is  $\delta = \omega_c - \omega_l$ . Thus, changing  $\omega_l$ , and at the same time  $\Omega_l$  to keep  $g_a$  constant,  $\omega_1 - \omega_2$  can be made linear in time. Note, that transitions do occur as well for an adiabatic but nonlinear time dependence of  $\omega_1 - \omega_2$ , however the problem has no analytic solution any more.

the Heisenberg equations given by equation (3.8) transform to :

$$\dot{u}' = ik_1 e^{-2i \int k_2 dt} v', \quad (3.12)$$

$$\dot{v}' = ik_1 e^{2i \int k_2 dt} u', \quad (3.13)$$

with<sup>3</sup>  $k_0 = -\frac{1}{2}(\omega_1 + \omega_2)$ ,  $k_1 = -\beta$ , and  $k_2 = -\frac{1}{2}(\omega_1 - \omega_2)$ .

The initial boundary conditions of the coupled differential equations given by (3.12) and (3.13) are now chosen such, that the photon operator  $a$  at time  $t \rightarrow -\infty$  is mapped to the nuclear spin operator  $b$  at  $t \rightarrow \infty$

$$u'_{-\infty} = 1, \quad (3.14)$$

$$|v'_{-\infty}| = 0. \quad (3.15)$$

Eliminating  $u'$  in equations (3.12) and (3.13) leads to the single equation:

$$\ddot{v}' + \left( 2ik_2'(t) - \frac{\dot{k}_1}{k_1} \right) v' + k_1^2 v' = 0, \quad (3.16)$$

where  $k_2' \equiv -k_2$ . As mentioned before, linear time dependency of  $k_2 = -\frac{1}{2}(\omega_1 - \omega_2)$  is assumed in the transition region,

$$k_2 = \frac{\alpha_c t}{2}, \quad (3.17)$$

and the coupling is assumed to be time independent, i.e.,  $\dot{k}_1 = 0$ . Together with the substitution

$$v' = e^{-i \int k_2' dt} U_1, \quad (3.18)$$

equation (3.16) reduces to the so called Weber equation:

$$\ddot{U}_1 + \left( k_1^2 - i \frac{\alpha_c}{2} + \frac{\alpha_c^2}{4} t^2 \right) U_1 = 0. \quad (3.19)$$

Solving equation (3.19) as proposed by Zener [41] and considering the asymptotic behavior of the solution at  $t \rightarrow \infty$ , it is found to be

$$\lim_{t \rightarrow \infty} U_1(t) = -A_+ \frac{\sqrt{2\pi}}{\Gamma(i\gamma_z + 1)} e^{-\frac{1}{4}\pi\gamma_z} e^{i\alpha_c t^2} (\sqrt{\alpha_c t})^{i\gamma_z}, \quad (3.20)$$

where  $\gamma_z = \frac{k_1^2}{2k_2} = \frac{k_1^2}{\alpha_c} = \frac{\beta^2}{\alpha_c}$  and the constant  $A_+ = \sqrt{\gamma_z} \exp\left(-\frac{\gamma_z \pi}{4}\right)$ . The probability that the photonic operator  $a$  is mapped to the collective nuclear spin operator  $b$  is given by

$$|v(t = \infty)|^2 = A_+^2 U_1^\infty U_1^{\infty*} = 1 - e^{-2\pi\gamma_z} = 1 - \epsilon^2, \quad (3.21)$$

---

<sup>3</sup> $B = k_0 \mathbb{1} + k_1 \sigma_x + k_2 \sigma_z$

where  $\epsilon \equiv e^{-2\pi\gamma z}$ . We thus find, that the initial state of the system given by equations (3.14) and (3.15), is mapped according to

$$\begin{pmatrix} 1 \\ 0 \end{pmatrix} \longrightarrow \begin{pmatrix} \sqrt{\epsilon} \\ \sqrt{1-\epsilon^2} \end{pmatrix}. \quad (3.22)$$

This implies that the cavity mode operator  $a$  is mapped to

$$a_{+\infty} = \sqrt{1-\epsilon^2} b + \sqrt{\epsilon} a, \quad (3.23)$$

a dominantly nuclear operator for times large enough so that  $\epsilon$  is small.

### 3.2.1 Storage fidelity of a Fock state

To evaluate the quality of the memory, we return to the Schrödinger picture. The mapping of a  $n$  photon Fock state of the cavity to the nuclei leads to a mixture of Fock states with photon numbers  $\leq n$ . The density matrix of the mapping of the two photon Fock state  $|2\rangle$  for instance, is given by

$$\begin{aligned} \rho(M(|n\rangle)) &= \left[ \frac{a_{\infty}^{\dagger}}{\sqrt{n!}} \right]^2 |0\rangle\langle 0| \left[ \frac{a_{\infty}}{\sqrt{n!}} \right]^2 \\ &= \left[ (1-\epsilon^2)b^{\dagger} + 2\sqrt{\epsilon}\sqrt{1-\epsilon^2}a^{\dagger}b^{\dagger} + \epsilon a^{\dagger 2} \right] |0\rangle\langle 0| \left[ (1-\epsilon^2)b + 2\sqrt{\epsilon}\sqrt{1-\epsilon^2}ab + \epsilon a^2 \right], \end{aligned}$$

where  $M$  denotes the mapping operation. Tracing over the "undesired" cavity mode yields

$$\text{tr}_{\text{cavity}}(\rho(M(|n\rangle))) = \epsilon^2 |0\rangle\langle 0| + 4\epsilon(1-\epsilon^2) |1\rangle\langle 1| + (1-\epsilon^2)^2 |2\rangle\langle 2|. \quad (3.24)$$

The fidelity with which a  $n$ -photon Fock state is mapped, is given by

$$F_{\text{Fock}} = \langle n | \text{tr}_{\text{cavity}} \left( \left[ \frac{a_{\infty}^{\dagger}}{\sqrt{n!}} \right]^n |0\rangle\langle 0| \left[ \frac{a_{\infty}}{\sqrt{n!}} \right]^n \right) |n\rangle = (1 - e^{-2\pi\gamma z})^n. \quad (3.25)$$

As storage of superpositions of Fock states, especially coherent states that are used for many quantum information and communication protocols, is of high interest, we will consider in the next Section which storage fidelities can be achieved for those states.

### 3.2.2 Storage fidelity of coherent states

Up to now, only the fidelity for storage of photon number (Fock) states has been considered. In a next step, we want to know which fidelity can be achieved for the storage of coherent states, i.e., for a superposition of number states. The properties of coherent states are discussed in detail in Appendix B.2.1.

With the fidelity of a photon number state given by equation (3.25), the storage of a coherent state of light into the nuclear spins corresponds to the map

$$|\alpha\rangle \rightarrow |\eta\alpha\rangle \quad \text{with} \quad \eta = \sqrt{1 - e^{-2\pi\gamma_z}}, \quad (3.26)$$

and  $|\alpha\rangle$  as defined in equation (B.17).

As it has been discussed in detail in Section 1.3, the goal of a quantum memory is to achieve higher average fidelity than the one that can be achieved by classical means. As already explained in Section 1.3, K. Hammerer et al. (2005) [31] proved, that the classical benchmark fidelity of coherent states distributed in phase space according to

$$p(\alpha) = \frac{\lambda}{\pi} \exp(-\lambda|\alpha|^2) \quad (3.27)$$

is given by

$$F_{max} = \frac{1 + \lambda}{2 + \lambda}. \quad (3.28)$$

Averaging over the complete set of all possible coherent input states with a Gaussian distribution as given in equation (3.27), the fidelity  $\overline{F}_c$  reads

$$\begin{aligned} \overline{F}_c &= \int d^2\alpha p(\alpha) |\langle \alpha | \alpha' \rangle|^2 \\ &= \int d^2\alpha p(\alpha) \exp\left[-\frac{(1 - \sqrt{1 - \epsilon^2})^2}{2} |\alpha|^2\right] \\ &= \int d^2\alpha \lambda \pi \exp\left[-\left(1 - \sqrt{1 - \epsilon^2} - \frac{\epsilon^2}{2} + \lambda\right) |\alpha|^2\right] \\ &= \frac{\lambda}{1 - \frac{\epsilon^2}{2} - \sqrt{1 - \epsilon^2} + \lambda} \end{aligned} \quad (3.29)$$

with  $\int d^2\alpha = \int_{-\infty}^{\infty} d\text{Re}(\alpha) \int_{-\infty}^{\infty} d\text{Im}(\alpha)$  and  $|\langle \alpha | \alpha' \rangle| = \exp(-|\alpha - \alpha'|^2)$  [42].

For a flat distribution, i.e.,  $\lambda \rightarrow 0$  and therefore  $\overline{F}_c \rightarrow 0$ . This can be overcome by amplification of the coherent state either at the write in or the read out stage, thus compensating losses due to imperfect mapping.

As it has been seen in equation (B.21) a coherent state is fully described by  $(\gamma, d) = (\mathbb{1}, \alpha)$ , with  $\gamma = \mathbb{1}$  being the covariance matrix (CM) of the vacuum state and  $d = \alpha$  the displacement.

The amplification can be achieved by a two-mode squeezing operation, where one mode is amplified but at the same time entangled to a second mode. The two-mode squeezing Hamiltonian and the two mode input-output relation of the squeezing transformation can be found in Appendix B in equation (B.52) and (B.53, B.54), respectively. Thus, the transformation of the covariance matrix of the coherent state ( $\gamma = \mathbb{1}$ ) in the basis of the annihilation and creation operators of the two modes

reads

$$\gamma_{\text{amp}} = A\gamma A^T = \begin{pmatrix} \cosh(r)^2 + \sinh(r)^2 & 0 & 0 & 2\sinh(r)\cosh(r) \\ 0 & \cosh(r)^2 + \sinh(r)^2 & 2\sinh(r)\cosh(r) & 0 \\ 0 & 2\sinh(r)\cosh(r) & \cosh(r)^2 + \sinh(r)^2 & 0 \\ 2\sinh(r)\cosh(r) & 0 & 0 & \cosh(r)^2 + \sinh(r)^2 \end{pmatrix} \quad (3.30)$$

where

$$A = \begin{pmatrix} \cosh(r) & 0 & 0 & \sinh(r) \\ 0 & \cosh(r) & \sinh(r) & 0 \\ 0 & \sinh(r) & \cosh(r) & 0 \\ \sinh(r) & 0 & 0 & \cosh(r) \end{pmatrix}. \quad (3.31)$$

The reduced covariance matrix of the subsystem of the mode we want to amplify, which will be denoted by system I in the following, is given by the upper left  $2 \times 2$  submatrix of  $\gamma_{\text{amp}}$ . Thus, the amplification parameter is given by  $\kappa = \cosh(r)^2 + \sinh(r)^2$ . The displacement of the subsystem I after the amplification is given by

$$d_I = \langle \alpha | a_I | \alpha \rangle = \cosh(r)\alpha \quad (3.32)$$

where  $a_I$  denotes the annihilation operator of system I. Let us choose the squeezing parameter such that

$$\cosh(r) \stackrel{!}{=} \frac{1}{\eta}. \quad (3.33)$$

Thus, amplification and subsequent mapping can be written as

$$(\mathbb{1}, \alpha)_{\text{cavity}} \xrightarrow{\text{amplification}} (\kappa \mathbb{1}, \frac{1}{\eta} \alpha)_{\text{cavity}} \xrightarrow{\text{mapping}} ((\kappa(1 - \epsilon^2) + \epsilon^2) \mathbb{1}, \alpha)_{\text{NS}}. \quad (3.34)$$

The two expressions on the left,  $(\ )_{\text{cavity}}$ , describe the light state prior to and after amplification, respectively, whereas the system on the right,  $(\ )_{\text{NS}}$ , describes the state of the nuclear spin system.

The fidelity of the mapping of the amplified state given by equation (3.34) reads

$$F_{\text{co}} = \langle \alpha | \rho_{\text{mapped}}(\alpha) | \alpha \rangle \quad (3.35)$$

where  $\rho_{\text{mapped}}$  is the density operator of the mapped state. Scutaru (1998) [43] showed, that for an arbitrary Gaussian state with covariance matrix  $\gamma_{U_1}$  and displacement  $d_{U_1}$  and a pure Gaussian state with  $(\gamma_{U_2}, d_{U_2})$

$$|\langle \gamma_{U_1}, d_{U_1} | \gamma_{U_2}, d_{U_2} \rangle|^2 = \left[ \det \left( \frac{\gamma_{U_1} + \gamma_{U_2}}{2} \right) \right]^{-1/2} e^{-(d_{U_1} - d_{U_2})^T (\gamma_{U_1} + \gamma_{U_2})^{-1} (d_{U_1} - d_{U_2})} \quad (3.36)$$

holds. Using equation (3.36), the fidelity given by equation (3.35) reads

$$\begin{aligned} F_{\text{co}} &= |\langle \mathbb{1}, \alpha | (\kappa(1 - \epsilon^2) + \epsilon^2) \mathbb{1}, \alpha \rangle|^2 \\ &= \det \left( \frac{\kappa(2 - \epsilon^2) + \epsilon^2}{2} \mathbb{1} \right)^{-1/2} = \frac{1}{1 + \epsilon^2}. \end{aligned} \quad (3.37)$$

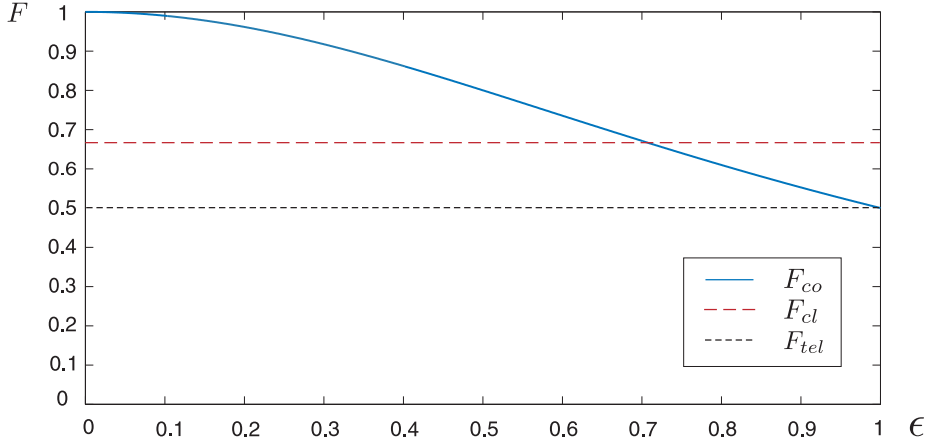


Figure 3.2: The blue line indicates the fidelity of the mapping of an amplified coherent state of light to the nuclear spins *vs.* the losses of the mapping  $\epsilon$ . The fidelity is, even for large losses, higher than the fidelity  $F_{cl}$  that can be achieved by classical means, indicated by the dashed red line. For losses  $\epsilon \gtrsim 0.7$  it is even higher than the teleportation fidelity  $F_{tel}$ , indicated by the dashed black line.

A plot of the  $F_{co}$  is shown in Figure 3.2. Here, the fidelity of the mapping of the amplified coherent state is compared to the classical benchmark fidelity  $F_{cl} = \frac{1}{2}$  of a flat distribution  $\lambda \rightarrow 0$  and the teleportation fidelity  $F_{tel} = \frac{2}{3}$  suggested by Grangier [36] which is reviewed in Section 1.3. We see that for  $\epsilon > 1/\sqrt{2}$ , the fidelity is higher than the teleportation fidelity, i.e., the quantum memory shows high performance even for large losses  $\epsilon$ .

### 3.2.3 Storage of a two-mode squeezed state

In the previous Sections we have shown that it is possible to transfer Fock and coherent states of light onto the nuclear spin memory. However, the ultimate test for a quantum memory is whether it is capable of faithfully storing part of an entangled quantum system. This will be discussed in more detail in Section 5.4. The linear mapping of equation (3.22) enables us to study how well part of a two-mode squeezed state is stored into the nuclear spin degrees of freedom. A concrete example for an entangled light state would be the two-mode squeezed state emitted by spontaneous parametric down conversion (SPDC). One of its light modes, in the following denoted by  $M1$ , is coupled into the cavity and mapped onto the nuclear spins of the quantum dot (see Figure 3.3), while the second light mode, denoted by  $M2$ , is, after the mapping of  $M1$  to the nuclear spins, entangled with the nuclear spins.

The question is now how much entanglement of the two-mode squeezed light state is left after the mapping of the light mode  $M1$  to the nuclear spins, that is, how much are the nuclear spins entangled with the light mode  $M2$ .

To quantify the entanglement, the entanglement measure "logarithmic negativity"

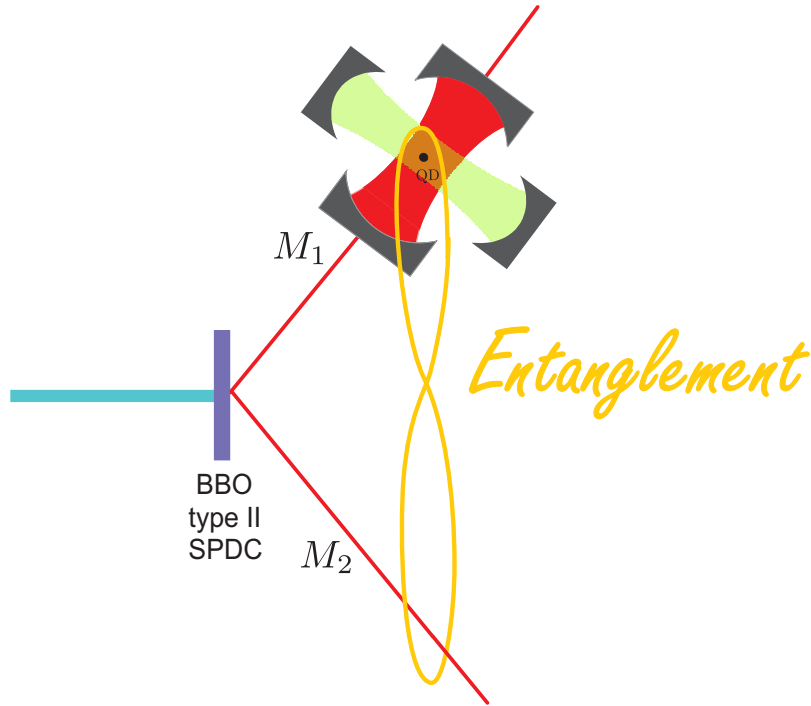


Figure 3.3: Schematic view of a two-mode squeezed state produced by spontaneous parametric down conversion, where  $M_1$  and  $M_2$  denote the light modes.  $M_1$  is mapped onto the nuclear spins of the quantum dot, whereby  $M_2$  and the nuclear spins become entangled, denoted by the yellow line.

for Gaussian states can be used [44]. As introduced in more detail in Appendix C.4.3, the logarithmic negativity  $E_{\mathcal{N}}$  for Gaussian states is given by

$$E_{\mathcal{N}} = \sum_{\alpha=1}^n F(c_{\alpha}), \quad (3.38)$$

where  $(c_1, \dots, c_n)$  is the symplectic spectrum of  $\gamma^{TA}$ , being the partial transpose of the covariance matrix  $\gamma$  of a Gaussian density operator.  $F(c)$  is defined by

$$F(c) = \begin{cases} 0 & \text{for } c \geq 1 \\ -\log_2(c) & \text{for } c < 1 \end{cases}.$$

To compute the logarithmic negativity, we need to know the symplectic eigenvalues of the partially transposed covariance matrix of the system whose entanglement we want to quantify. Thus, we first have to consider the covariance matrix of the system composed of the two-mode squeezed light state and the nuclear spins, map the light mode  $M_1$  to the nuclear spins and then trace over the system  $M_1$ . Then we know the covariance matrix of the entangled light mode  $M_2$ -nuclear spin system, and after transposing the subsystem formed by the light mode  $M_2$ , we finally calculate the symplectic spectrum and hence the logarithmic negativity.

The initial covariance matrix  $\gamma_{\text{ini}}$  of the two-mode squeezed state, formed by the two light modes  $M1$  and  $M2$  and the initial state of the nuclear spins, is given by

$$\gamma_{\text{ini}} = \begin{pmatrix} \cosh(2r) & 0 & 0 & \sinh(2r) & 0 & 0 \\ 0 & \cosh(2r) & \sinh(2r) & 0 & 0 & 0 \\ 0 & \sinh(2r) & \cosh(2r) & 0 & 0 & 0 \\ \sinh(2r) & 0 & 0 & \cosh(2r) & 0 & 0 \\ 0 & 0 & 0 & 0 & 1 & 0 \\ 0 & 0 & 0 & 0 & 0 & 1 \end{pmatrix}, \quad (3.39)$$

where the upper left  $4 \times 4$  matrix denotes the reduced subsystem of the two-mode squeezed light state and the lower right  $2 \times 2$  matrix denotes the initial state of the nuclear spins.

By doing the transformation

$$\gamma_{\text{final}} = S^T \gamma_{\text{ini}} S, \quad (3.40)$$

where  $S$  is given by

$$S = \begin{pmatrix} 1 & 0 & 0 & 0 & 0 & 0 \\ 0 & 1 & 0 & 0 & 0 & 0 \\ 0 & 0 & \epsilon & 0 & \sqrt{1-\epsilon^2} & 0 \\ 0 & 0 & 0 & \epsilon & 0 & \sqrt{1-\epsilon^2} \\ 0 & 0 & \sqrt{1-\epsilon^2} & 0 & \epsilon & 0 \\ 0 & 0 & 0 & \sqrt{1-\epsilon^2} & 0 & \epsilon \end{pmatrix}, \quad (3.41)$$

the state of light mode  $M1$  is mapped onto the nuclear spins of the quantum dot. Next, we trace over the subsystem  $M1$ ,

$$\text{tr}_{M1}(\gamma_{\text{final}}) = \gamma' \quad (3.42)$$

and calculate the partial transpose of  $\gamma'$ .

As discussed in Appendix C.4.2, partially transposing  $\gamma'$  corresponds to a time reversal (multiplying all momenta coordinates by  $-1$ ) of the part of the system to be transposed [45]. This corresponds to

$$a = x + ip \xrightarrow{p \rightarrow -p} a^\dagger. \quad (3.43)$$

Consequently, the covariance matrix of the partially transposed state is given by

$$(\gamma')^{T_{M1}} = \lambda^{-1} \gamma' \lambda \quad (3.44)$$

$$= \begin{pmatrix} y_1 & 0 & \sqrt{xy_2} & 0 \\ 0 & y_1 & 0 & \sqrt{xu_2} \\ \sqrt{xy_2} & 0 & \epsilon^2 + xy_1 & 0 \\ 0 & \sqrt{xy_2} & 0 & \epsilon^2 + xy_1 \end{pmatrix} \quad (3.45)$$

where  $y_1 = \cosh(2r)$ ,  $y_2 = \sinh(2r)$ ,  $x = 1 - \epsilon^2$  and

$$\lambda = \lambda_{a^\dagger, a} \oplus \lambda_{b^\dagger, b} = \begin{pmatrix} 0 & 1 & 0 & 0 \\ 1 & 0 & 0 & 0 \\ 0 & 0 & 1 & 0 \\ 0 & 0 & 0 & 1 \end{pmatrix} \quad (3.46)$$

To compute the logarithmic negativity  $E_{\mathcal{N}}$ , we need to determine the symplectic spectrum  $(c_1, c_2)$  of  $(\gamma')^{T_{M_1}}$ . This can be done by computing the eigenvalues of<sup>4</sup>  $\sigma^{-1}(\gamma')^{T_{M_1}}$ , which yields  $\pm ic_1, \pm ic_2$ . With the symplectic eigenvalues  $(c_1, c_2)$  of  $(\gamma')^{T_{M_1}}$ , where  $c_1 > 1$  and

$$d_2 = \frac{1}{2}(\epsilon^2 - (-2 + \epsilon^2) \cosh(2r) - \sqrt{2} \sinh(r) \sqrt{\cosh(r)^2(-2 + \epsilon^2) - \epsilon^4}) \leq 1,$$

$E_{\mathcal{N}}$  is a monotonic decreasing function for increasing mapping error  $\epsilon$ , with  $\epsilon \in [0, 1]$ . For  $\epsilon = 0$  and  $\epsilon = 1$ ,  $E_{\mathcal{N}}$  is found to be

$$E_{\mathcal{N}} = \begin{cases} 2.89 r & \text{for } \epsilon = 0 \\ 0 & \text{for } \epsilon = 1 \end{cases}$$

Hence, the nuclear spins of the quantum dot are entangled with the light mode  $M_2$ . This allows a remote access to the memory, required for e.g., quantum repeaters.

### 3.2.4 Mapping time

The times needed for a high fidelity mapping have not been discussed so far. A rough estimation for the time needed to transfer one photon to one nuclear excitation with at least 0.8 can be done as follows:

The fidelity for the mapping of one photon is given by equation (3.25)

$$F_{\text{Fock},1} = 1 - e^{-2\pi\gamma}. \quad (3.47)$$

For a mapping fidelity higher than 0.8,

$$1 - e^{-2\pi\gamma} \geq 0.8, \quad (3.48)$$

has to be fulfilled, which yields

$$k_1^2 \geq \frac{1}{4} |\alpha_c|. \quad (3.49)$$

However, at  $t \rightarrow -\infty$ ,  $|\alpha_c t|$  is much larger than the coupling,

$$\alpha_c t_0 \gg |k_1|. \quad (3.50)$$

Assuming  $\alpha_c t_0 = 10k_1$  and using condition (3.49), we get  $t_0 \gg 3.6\mu\text{s}$ . This estimation is pessimistic, as the assumption for  $k_2(t)$  being linear in time is only necessary in the transition region, while  $k_2(t)$  can e.g., have quadratic time dependence away from the transition region.

<sup>4</sup>with the symplectic matrix  $\sigma$  defined by equation (B.3) in Appendix B



# Chapter 4

## Generation of a two-mode squeezed state

In the previous Chapter we studied the scenario where one part of an entangled state of light is transferred to the nuclear spins of the quantum dot, thereby creating entanglement between the remaining subsystem of the initial light state.

Another way to create an entangled state is to directly entangle a coherent state of light with the nuclear spins. In the following we will consider the scenario where a coherent state of light is coupled into the cavity, where it interacts with the nuclear spins of the quantum dot. The output state of the cavity, which is an entangled state between light field and nuclear spins, can be used as a resource for e.g., teleportation.

In the previous chapter, we have seen that the Hamiltonian, given by equation (2.9), yielded, after the adiabatic elimination of the trion and the electronic states, a beam-splitter like coupling. Simple changes in the setting make it possible to realize a different interesting coupling, namely a squeezing Hamiltonian, that allows to entangle cavity and nuclei. To create such a two-mode squeezed state of light and nuclear spins, the coupling of the laser and the cavity field in the lambda system (see Figure 2.1b)) have to be interchanged, i.e. the electron spin up state  $|\uparrow\rangle$  is now coupled to the exciton  $|X\rangle$  via the cavity field and the spin down state  $|\downarrow\rangle$  via the laser field (see Figure 4.1).

The optical part of the Hamiltonian, given by equation (2.3), now reads

$$H_{\text{opt}}^{\text{SQ}} = \omega_c a^\dagger a + \omega_\uparrow |X\rangle\langle X| + g_e \mu_b B_z |\downarrow\rangle\langle\downarrow| + \frac{\Omega_l}{2} (e^{+i\omega_l t} |\downarrow\rangle\langle X| + \text{h.c.}) + \frac{\Omega_c}{2} (a^\dagger |\uparrow\rangle\langle X| + \text{h.c.}). \quad (4.1)$$

The electron-nuclei interaction Hamiltonian  $H_{\text{NS}}$  given by equation (2.8) is left unchanged. Adiabatic elimination of the exciton and the electronic states, as done in Appendix A, leads to

$$H_{\text{eff}}^{\text{SQ}} = \left( \tilde{\delta} - \frac{g_a^2}{\Delta_2} \right) a^\dagger a - \frac{g_n^2}{4\Delta_2} bb^\dagger + \frac{g_a g_n}{2\Delta_2} (a^\dagger b^\dagger + ba). \quad (4.2)$$

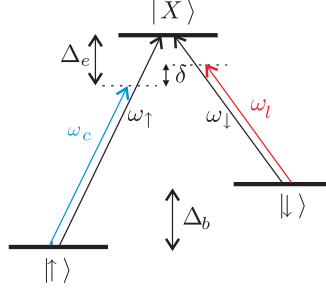


Figure 4.1: Level scheme of the optical transitions between electronic states and excitonic state, where compared to the level scheme shown in Figure (2.1), laser and cavity coupling are interchanged.

Whereas in  $\tilde{H}_{\text{eff}}$  given by equation (2.35), the creation (annihilation) of a cavity photon involves the annihilation (creation) of a nuclear spin excitation, both are created (annihilated) simultaneously in  $H_{\text{eff}}^{\text{SQ}}$ . This kind of interaction is called "squeezing".

In the Heisenberg picture we get

$$\dot{\vec{c}} = iA\vec{c}, \quad (4.3)$$

with

$$A = \begin{pmatrix} -\omega_1 & 0 & 0 & -\beta \\ 0 & \omega_1 & \beta & 0 \\ 0 & -\beta & -\omega_2 & 0 \\ \beta & 0 & 0 & \omega_2 \end{pmatrix}, \quad \vec{c} = \begin{pmatrix} a \\ a^\dagger \\ b \\ b^\dagger \end{pmatrix}.$$

$\omega_1$ ,  $\omega_2$  and  $\beta$  have been defined in Chapter 3.

The solution of equation (4.3) is given by

$$\vec{c}(t) = T e^{iA_D t} T^{-1} \vec{c}_0 = R \vec{c}_0, \quad (4.4)$$

with

$$R = T e^{iA_D t} T^{-1} \quad (4.5)$$

and

$$A_D = T^{-1} A T, \quad (4.6)$$

where  $A_D$  is the diagonal matrix formed by its eigenvalues and  $T$  the diagonalizing matrix.

To decide whether the state of the system is a two-mode squeezed state, we consider the covariance matrix, which for a bipartite system reads

$$\gamma = \begin{pmatrix} A & C \\ C^T & B \end{pmatrix}, \quad (4.7)$$

where explicit expressions of the  $2 \times 2$  matrices  $A, B, C$  can be found in Appendix B equations (B.56)-(B.58).  $A, B$  are the reduced covariance matrices of the two

subsystems and  $C$  describes the correlations between the two systems. The standard form of the covariance matrix of a two-mode squeezed state in the basis of annihilation and creation operators, defined in Appendix B equation (B.62), reads

$$\gamma_{TMSS} = \begin{pmatrix} \cosh(2r) & 0 & 0 & \sinh(2r) \\ 0 & \cosh(2r) & \sinh(2r) & 0 \\ 0 & \sinh(2r) & \cosh(2r) & 0 \\ \sinh(2r) & 0 & 0 & \cosh(2r) \end{pmatrix}, \quad (4.8)$$

where  $r$  is the squeezing parameter.

The covariance matrix of our system at time  $t$ , denoted by  $\gamma'$ , is, in the basis of annihilation and creation operator  $a, a^\dagger$  and  $b, b^\dagger$ , given by

$$\gamma'(t) = R^\dagger \mathbb{1} R = \begin{pmatrix} v & 0 & 0 & w_- \\ 0 & v & w_+ & 0 \\ 0 & w_- & v & 0 \\ w_+ & 0 & 0 & v \end{pmatrix}, \quad (4.9)$$

with

$$v = \frac{(\omega_1 + \omega_2)^2 - 4\beta^2 \cos(\sqrt{(\omega_1 + \omega_2)^2 - 4\beta^2 t})}{(\omega_1 + \omega_2)^2 - 4\beta^2} \quad (4.10)$$

and

$$w_\pm = \frac{2\beta}{(\omega_1 + \omega_2)^2 - 4\beta^2} [\omega_1 + \omega_2 - (\omega_1 + \omega_2) \cos(\sqrt{(\omega_1 + \omega_2)^2 - 4\beta^2 t}) \pm i\sqrt{(\omega_1 + \omega_2)^2 - 4\beta^2} \sin(\sqrt{(\omega_1 + \omega_2)^2 - 4\beta^2 t})] \quad (4.11)$$

For the special case of

$$\omega_1 = -\omega_2, \quad (4.12)$$

one can easily see that  $\gamma'$  can be transformed by the local transformation<sup>1</sup>  $S$  to the covariance matrix standard form

$$\gamma_s = S^\dagger \gamma' S \quad (4.13)$$

of a two-mode squeezed state given by equation (4.8):

$$\gamma_s = \begin{pmatrix} \cosh(2\beta t) & 0 & 0 & \sinh(2\beta t) \\ 0 & \cosh(2\beta t) & \sinh(2\beta t) & 0 \\ 0 & \sinh(2\beta t) & \cosh(2\beta t) & 0 \\ \sinh(2\beta t) & 0 & 0 & \cosh(2\beta t) \end{pmatrix} \quad (4.14)$$

with

$$S = \begin{pmatrix} 0 & 0 & 0 & e^{-i\phi} \\ 0 & 0 & e^{i\phi} & 0 \\ 0 & e^{-i\phi} & 0 & 0 \\ e^{i\phi} & 0 & 0 & 0 \end{pmatrix} \quad (4.15)$$

---

<sup>1</sup>A definition of local transformations can be found in Appendix B.

where  $\phi = \frac{\pi}{4}$ .

To see how long it takes to achieve a squeezing of  $2\beta t = 1$ , two different sets of parameters are discussed in the following. For both sets, a detuning of  $\Delta_e = 10^{-2}$ , such that the condition for the adiabatic elimination of the trion given by equation (2.20) is fulfilled, is assumed.

First, we will study a set of parameters that can be experimentally achieved at present. For a laser and cavity Rabi frequency of the order of  $100\mu\text{eV}$  ([37],[22]),  $g_a = \frac{\Omega_l \Omega_c}{4\Delta_e} = 2.5 \cdot 10^{-7} \text{eV}$ . In a typical self-assembled GaAs quantum dot with  $N = 10^4$  nuclear spins, the hyperfine constant  $g_n = \frac{A}{\sqrt{N}} = 10^{-6} \text{eV}$  with  $A = 100\mu\text{eV}$ . Thus, we can choose  $\Delta_2 = 10^{-5} \text{eV}$  such that condition given by equation (2.28) for the adiabatic elimination of the electronic states is fulfilled. This yields

$$\beta = \frac{g_a g_n}{2\Delta_2} = 1.25 \cdot 10^{-8} \text{eV}, \quad (4.16)$$

and for a squeezing of  $2\beta t = 1$

$$t = \frac{1}{2\beta} = 6.6 \cdot 10^{-7} \text{s}. \quad (4.17)$$

If we choose the Rabi frequencies as in Section 5.4,  $\Omega_c = 208\mu\text{eV}$  and  $\Omega_l = 1.9 \text{meV}$ , and the detuning  $\Delta_2$  such that the condition given by equation (2.28) is fulfilled, i.e.,  $\Delta_2 = 10^{-4} \text{eV}$ ,

$$\beta = 1.25 \cdot 10^{-8} \text{eV}, \quad (4.18)$$

and for a squeezing of  $2\beta t = 1$

$$t = \frac{1}{2\beta} = 4.2 \cdot 10^{-8} \text{s}. \quad (4.19)$$

The longest lifetime of a photon in a photonic crystal nanocavity at present is  $2.1 \text{ns}$  [46]. To reach squeezing of 1, longer cavity lifetimes and higher Rabi frequencies would have to be achieved in the future. However, the times required for squeezing are considerably shorter than the times required for the mapping of the light field to the nuclei. Thus, the here proposed scheme for the generation of a two-mode squeezed state of the nuclear spin-cavity system might be a more interesting candidate for experimental realization than the schemes for storing the state of light to the nuclei studied in Chapter 3 and 5.

# Chapter 5

## Stimulated Raman adiabatic passage (STIRAP)

In Section 3, Landau-Zener transitions have been studied to map the light state of the cavity to the nuclear spins. The times for the mapping required by the adiabaticity condition turned out to be in the  $\mu\text{s}$  range, i.e., longer than today's cavity lifetimes. To achieve faster storage times, we study the system described by equation (2.23), where the trion has been adiabatically eliminated, but no subsequent elimination of the electronic spin states is carried out. This system does not have to fulfill the constraint given by equation (2.28), where large splitting between the electronic states had to be assumed to adiabatically eliminate the electronic spin up and down states.

### 5.1 Short review of STIRAP

The process of storing a state of light to the nuclear spins can be achieved by the well-known technique of Stimulated Raman adiabatic passage (STIRAP) [47]. This scheme allows to completely transfer population between two suitable quantum states via at least two coherent light pulses that drive transitions of a lambda or a multilevel system. One great advantage of this method is, that it is relatively insensitive to many experimental details of the pulses. First, a three-level system will be considered. We assume that ground state  $|1\rangle$  is populated initially. The idea is, *not* to couple state  $|1\rangle$  with the excited state, denoted by  $|2\rangle$ , first, and then transfer the population to state  $|3\rangle$ , but to couple the initially unpopulated states  $|2\rangle$  and  $|3\rangle$  first, and subsequently couple the coherent superposition of  $|2\rangle$  and  $|3\rangle$  to state  $|1\rangle$  (see Figure 5.1). Thereby we get a state that allows to directly channel population into state  $|3\rangle$  without populating the excited state  $|2\rangle$ , which, in the case of atoms, might be subject to spontaneous emission.

To see how complete population transfer can be achieved using a counterintuitive pulse sequence as mentioned before, we study a system where one transition is coupled by the quantum field of a cavity, whereas the second transition is coupled by a classical

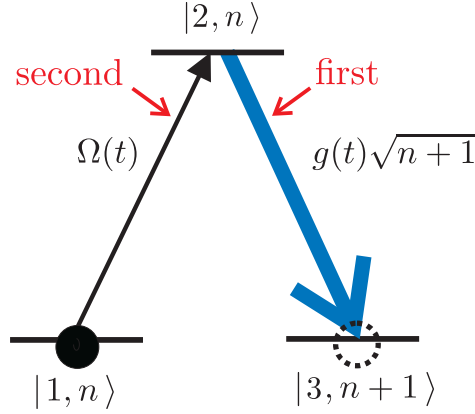


Figure 5.1: STIRAP in a three-level system as proposed in [48]. In contrast to conventional STIRAP, where two classical laser pulses are used, one of the transitions couples to a cavity field with Rabi frequency  $g(t)$ . The initially unpopulated state  $|3\rangle$  is coupled to the excited state  $|2\rangle$  first. Then the superposition of  $|3\rangle$  and  $|2\rangle$  is coupled to state  $|1\rangle$ .

laser field [48]. Note that this is a special way of implementing STIRAP. Traditionally, it is done with a counterintuitive pulse sequence of classical laser fields, which can be implemented by either spatially displaced continuous laser beams or with pulsed lasers that are time delayed. But as the system studied in the present work consists of transitions coupled by a cavity field and a classical laser field, we will study this special implementation. To go more into detail, the Hamiltonian of the system is given by ( $\hbar = 1$ )

$$H = \omega a^\dagger a + \omega_{12} |2\rangle\langle 2| - ig(t)(|2\rangle\langle 3|a - \text{h.c.}) + i\Omega(t)(|2\rangle\langle 1|e^{-i\omega t} - \text{h.c.}), \quad (5.1)$$

where  $\Omega(t)$  and  $g(t)$  are the Rabi frequencies of the laser and cavity respectively,  $a$  is the cavity field annihilation operator and  $\omega_l$  is the laser frequency (see Figure 5.1). One particular eigenstate of the Hamiltonian (5.1) is given by

$$|E_n\rangle = \frac{g(t)\sqrt{n+1}|1, n\rangle + \Omega(t)|3, n+1\rangle}{\sqrt{\Omega(t)^2 + g(t)^2(n+1)}}. \quad (5.2)$$

It does not contain any contribution of the excited state and is thus called dark state. Here,  $|1, n\rangle = |1\rangle \otimes |n\rangle$ , where  $|n\rangle$  denotes the  $n$  photon Fock state of the cavity mode. Now, we can already see what happens if a counterintuitive pulse sequence is applied. For  $\Omega(t)/g(t) \rightarrow 0$ , the energy eigenstate is  $|E_n\rangle \rightarrow |1, n\rangle$ , whereas for  $g(t)/\Omega(t) \rightarrow 0$ , the energy eigenstate is  $|E_n\rangle \rightarrow |3, n+1\rangle$ . Thus, if the atom first interacts with the cavity field and then, after some time delay, with the laser light, and if both fields have a certain overlap, population can be transferred from  $|1\rangle$  to  $|3\rangle$  in case of adiabatic evolution, i.e., if the Hamiltonian changes in time slowly enough so that the system stays in the instantaneous eigenstate  $|E_n\rangle$

at all times. The time delay between the cavity field pulse and the laser light pulse can be provided simply by the motion of the atom across the laser- and cavity field profiles. One needs not to restrict oneself to three-level systems, the same method can also be applied to multilevel systems as proposed in [48]. This method will be used in the present work to transfer population of a state of the cavity mode to the nuclear spins of the quantum dot. However, in multilevel systems compared to three-level systems, a difficulty of keeping track of the dynamical phases of the individual eigenstates arises. This will be discussed in more detail later. First, some experimental realizations of STIRAP shall be mentioned. An example for the realization of STIRAP in a three-level system is given by the experiment done by Bergmann et al. [47]. There, two metastable electronic states of Ne\* atoms that emerge from a discharge source into a vacuum are coupled to a third state, that radiatively couples to other states. The atoms travel through two spatially displaced laser beams, which couple first the unpopulated and then the populated ground state to the excited state. Subsequently, the metastable state to which the population is transferred is coupled to an unstable state and the fluorescence from this state can be measured, proving that the population transfer has been successful. To show that the intermediate state has not become populated during the process, the fluorescence from this state can be measured during the STIRAP process. The Ne\* atom can be used for multilevel STIRAP as well, by using a magnetic field that removes the degeneracy of the magnetic sublevels in the intermediate and final levels [47].

## 5.2 Mapping the light state to nuclear spins using STIRAP

In the following we consider the Hamiltonian given by equation (2.23), that has been derived in Section 2.2. It is blockdiagonal

$$H_{\text{eff}} = \bigoplus_n H_n, \quad (5.3)$$

where  $n$  denotes the initial photon number. The  $(2n + 1)$ -dimensional Hamiltonian  $H_n$ , describing the evolution of the " $n$ -excitation subspace", is given by

$$H_n = \begin{pmatrix} \Delta_{G_0} & -g_a\sqrt{n} & 0 & 0 & 0 & \dots \\ -g_a\sqrt{n} & \Delta_{E_0} & g_n\sqrt{1} & 0 & 0 & \dots \\ 0 & g_n\sqrt{1} & \Delta_{G_1} & -g_a\sqrt{n-1} & 0 & \dots \\ 0 & 0 & -g_a\sqrt{n-1} & \Delta_{E_1} & g_n\sqrt{2} & \dots \\ 0 & 0 & 0 & g_n\sqrt{2} & \Delta_{G_2} & \dots \\ \vdots & \vdots & \vdots & \vdots & \vdots & \ddots \end{pmatrix}, \quad (5.4)$$

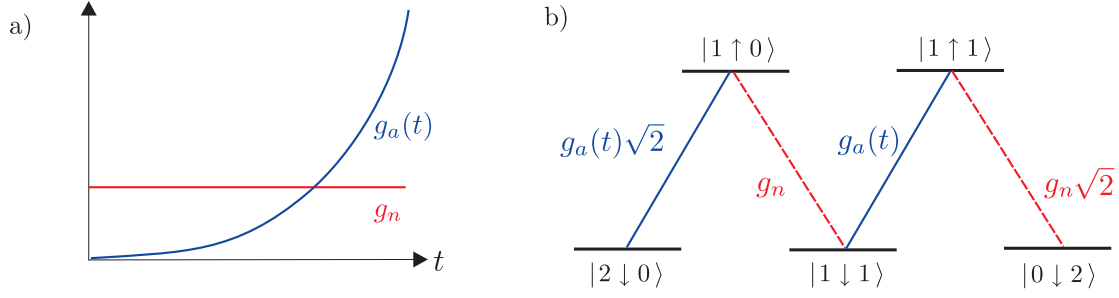


Figure 5.2: a) Schematic view of the time dependency of the coupling  $g_a$  and the constant hyperfine coupling  $g_n$ . b) Schematic view of the level scheme of the system with initially two photons. The hyperfine coupling  $g_n$  is "always on", whereas  $g_a(t)$  is an increasing function for which  $g_a(T) \gg g_n$ .

with

$$\begin{aligned}\Delta_{G_k} &= \left( \delta - \frac{\Omega_c^2}{4\Delta_e} \right) (n - k) - \frac{A}{2N}k, \\ \Delta_{E_l} &= -\tilde{\Delta}_b - \frac{\Omega_l(t)^2}{4\Delta_e} + \delta(n - l) + \frac{A}{2N}l\end{aligned}\quad (5.5)$$

for  $k \in \{0, 1, 2..n\}$  and  $l \in \{0, 1, 2..n - 1\}$ .

We denote the states with electron spin down as "ground states" and the states with electron spin up as "excited states". For, e.g., two photons (see Figure 5.2b)), the ground states are given by

$$\{|G_0\rangle, |G_1\rangle, |G_2\rangle\} = \{|2 \downarrow 0\rangle, |1 \downarrow 1\rangle, |0 \downarrow 2\rangle\}.\quad (5.6)$$

Here  $|2 \downarrow 0\rangle = |2\rangle_P \otimes |\downarrow\rangle_{e^-} \otimes |0\rangle_N$ , where  $|2\rangle_P$  represents the two photon Fock state of the cavity,  $|\downarrow\rangle_{e^-}$  denotes the spin down state of the electron and  $|0\rangle_N$  the excitation number of the nuclear spins. The excited states are given by

$$\{|E_0\rangle, |E_1\rangle\} = \{|1 \uparrow 0\rangle, |0 \uparrow 1\rangle\}.\quad (5.7)$$

By choosing the parameters such that  $\Delta_{G_k} \equiv \Delta_{G_n}$ , where  $\Delta_{G_n}$  is constant for each subspace with fixed initial photon number, i.e.,

$$\delta - \frac{\Omega_c^2}{4\Delta_e} = -\frac{A}{2N}\quad (5.8)$$

so that

$$\Delta_{G_n} = -\frac{A}{2N}n,\quad (5.9)$$

the ground states of the Hamiltonian are degenerate within each subspace. Hence, the phases of the individual eigenstates which the system acquires during the time evolution (for perfect adiabaticity), given by

$$\phi_n = \Delta_{G_n} t = -\frac{A}{2N} n t,\quad (5.10)$$

are well known and can be corrected. This can be done by applying a magnetic field for a time  $t = -\frac{A/(2N)}{g_k\mu_k B}$  after the state has been transferred to the nuclei, where  $g_k$ ,  $\mu_k$  denote the nuclear g-factor and the nuclear magnetic moment.

It can be proven by induction, that  $H_n$  has an eigenvalue  $E_{G_n} = \Delta_{G_n} \forall n$ , where  $n$  is the initial photon number, i.e. that

$$\det(H_n - E_{G_n} \mathbb{1}) = 0 \quad \text{for all } n \in \{0, 1, \dots, \infty\}. \quad (5.11)$$

To be more general, the matrix  $H_n - E_{G_n}$  is of the form of the matrix  $W_n$ , given by

$$W_n = \begin{pmatrix} 0 & x_1 & 0 & 0 & 0 & \dots \\ x_1 & z_1 & y_1 & 0 & 0 & \dots \\ 0 & y_1 & 0 & x_2 & 0 & \dots \\ 0 & 0 & x_2 & z_2 & y_2 & \dots \\ 0 & 0 & 0 & y_2 & 0 & \dots \\ \vdots & \vdots & \vdots & \vdots & \vdots & \ddots \end{pmatrix}, \quad (5.12)$$

where we assume  $x_1, x_2, \dots, y_1, y_2, \dots, z_1, z_2, \dots$  to be a set of arbitrary values. The proof for  $\det(W_n) = 0$  for all  $n$  by induction can be done as follows.

For  $n=1$ ,  $\det(W_n) = 0$  as

$$W_1 = \begin{pmatrix} 0 & x & 0 \\ x & z & y \\ 0 & y & 0 \end{pmatrix}, \quad (5.13)$$

for an arbitrary choice of  $x, y, z$ . Assuming that for  $n = k$ ,

$$\det(W_k) = 0, \quad (5.14)$$

we find that for  $n = k + 1$ ,

$$\det(W_{k+1}) = x_1'^2 \det(W_k') \stackrel{(5.14)}{=} 0, \quad (5.15)$$

as equation (5.14) holds for an arbitrary set of parameters. Having shown that  $\det W_n = 0$ , we know that  $\det(H_n - E_{G_n} \mathbb{1}) = 0$  for all  $n$ .

We have seen that by suitably choosing the parameters, the ground states of the Hamiltonian are degenerate within the subspace of a certain photon number, and that the phases the system acquires within each subspace can be corrected. We will show now, how the state of light can be transferred to the nuclear spins by applying the method of STIRAP in multilevel systems. By slowly increasing the laser Rabi frequency and thus changing  $g_a(t)$ , an initial state  $|\psi, \downarrow, 0\rangle$  with no excitations in the quantum dot and a state  $|\psi\rangle$  in the cavity, evolves under the adiabatic change of  $H_{\text{eff}}$  to  $|\psi, \downarrow, 0\rangle$ , i.e., the state where the cavity is empty and its state has been mapped to the nuclear spins:

$$|G_0\rangle = |\psi \downarrow 0\rangle_{t=0} \rightarrow |G_n\rangle = |0 \downarrow \psi\rangle_{t \rightarrow \infty}. \quad (5.16)$$

Note, that perfect adiabaticity is assumed and that phases  $\phi_n$  between states with different photon number have been corrected and the error arising from the constant hyperfine coupling  $g_n$ , which will be discussed in more detail later, has not been considered. In the ideal case, the system stays in a dark state, i.e., a superposition of all ground states, during the evolution. Thus, the dark state can be written as

$$|D\rangle = \sum_{i=0}^n c_i |G_i\rangle. \quad (5.17)$$

The coefficients  $c_i$  can be determined by solving the stationary Schrödinger equation

$$H_n |D\rangle \stackrel{!}{=} E_{G_n} |D\rangle \quad (5.18)$$

with

$$\begin{aligned} H_n = & \sum_{i=0}^{n-1} (g_a \sqrt{n-i} |E_i\rangle \langle G_i| + \text{h.c.}) + \\ & + \sum_{i=1}^n g_n \sqrt{i} |E_{i-1}\rangle \langle G_i| + \text{h.c.} + \Delta_{E_i} |E_i\rangle \langle E_i|, \end{aligned} \quad (5.19)$$

which leads to the relation

$$c_{i+1} = -\frac{g_a(t) \sqrt{n-1}}{g_n \sqrt{i+1}} c_i. \quad (5.20)$$

This means that for  $k \in 0..n$ , the corresponding coefficient is

$$c_k \sim \left( \frac{g_a(t)}{g_n} \right)^k. \quad (5.21)$$

Now, we see that population being initially in state  $|G_0\rangle$ , is, by adiabatically increasing  $g_a(t)$  to  $g_a(t) \gg g_n$  (see Figure 5.2), transferred to the state  $|G_n\rangle$ , as its coefficient  $c_n \gg c_l$  where  $l \in 0..n-1$ .

### 5.3 Error processes

Up to now, imperfections of the system, that lead to a non-perfect mapping of the state of light to the nuclear spins, have not been taken into account.

First, an "error" that is intrinsic to our system shall be studied. It arises from the fact that we do not, as it is done in conventional STIRAP, use a counterintuitive sequence of pulses, in which the pulse that drives the last transition between the "ground" and the "excited state", precedes the pulse driving the first transition. What we propose, is to adiabatically increase the coupling  $g_a(t)$  so that  $g_a(t) \gg g_n$  after a certain time period. The hyperfine coupling  $g_n$ , however, cannot be changed,

thus, even for  $g_a(t) \gg g_n$ , the mapping is imperfect due to  $g_n$  being nonzero. These imperfections will be studied in Section 5.3.1, using first order perturbation theory.

Second, the effect of the nuclear spin ensemble not being fully polarized, as assumed so far, will be studied in Section 5.3.2.

The error studied in Section 5.3.3, arising in every method where parameters are supposed to be changed adiabatically, is the non-adiabaticity due to the finite time of realistic processes. An estimate for the minimum time needed to faithfully map the state of light to the nuclear spins will be given in the following, using the well-known adiabatic theorem. Moreover, the phases arising from non-adiabaticity will be computed.

For long times, error processes such as cavity decay, which has been neglected so far, will become important. This will be studied numerically in Section 5.5, where cavity losses are implemented by a Monte Carlo wavefunction simulation of the quantum jump approach.

### 5.3.1 "Always-on" character of $g_n$

As already stated, an error arises from the fact that one of the couplings used for the STIRAP, namely the hyperfine coupling  $g_n$ , is constant and cannot be turned off. Thus, the ideal situation for which

$$|D(t \rightarrow \infty)\rangle = |G_n\rangle \text{ for } \frac{g_n}{g_a(\infty)} \rightarrow 0 \quad (5.22)$$

cannot be achieved.

Treating the coupling  $g_n$  as a small perturbation in first order perturbation theory at  $t = T$  (where  $T$  is the final time), the fidelity of the population transfer from the initial state of light to the nuclear spins can be derived.

The Hamiltonian  $H_n(T)$  given by equation (5.4), shifted by the constant  $-\Delta_{G_k} \mathbb{1}$ , is decomposed into a Hamiltonian  $H^0$ , describing the unperturbed part of the system, and a perturbation Hamiltonian denoted by  $V$ :

$$H_n(T) = H^0(T) + V(T). \quad (5.23)$$

The unperturbed Hamiltonian  $H^0$  reads

$$H^0 = \begin{pmatrix} 0 & -g_a\sqrt{n} & 0 & 0 & 0 & \dots \\ -g_a\sqrt{n} & \Delta_{E_0} - \Delta_{G_k} & 0 & 0 & 0 & \dots \\ 0 & 0 & 0 & -g_a\sqrt{n-1} & 0 & \dots \\ 0 & 0 & -g_a\sqrt{n-1} & \Delta_{E_1} - \Delta_{G_k} & 0 & \dots \\ 0 & 0 & 0 & 0 & 0 & \dots \\ \vdots & \vdots & \vdots & \vdots & \vdots & \ddots \end{pmatrix}, \quad (5.24)$$

The perturbation part  $V$  is given by

$$V = \begin{pmatrix} 0 & 0 & 0 & 0 & 0 & \dots \\ 0 & 0 & g_n & 0 & 0 & \dots \\ 0 & g_n & 0 & 0 & 0 & \dots \\ 0 & 0 & 0 & 0 & g_n\sqrt{2} & \dots \\ 0 & 0 & 0 & g_n\sqrt{2} & 0 & \dots \\ \vdots & \vdots & \vdots & \vdots & \vdots & \ddots \end{pmatrix}. \quad (5.25)$$

As it can be found in every quantum mechanics textbook (for example [49]), unnormalized eigenstates of  $H_n = H_0 + V$  are given by

$$|\xi\rangle = |\xi^0\rangle + |\xi^1\rangle + \dots, \quad (5.26)$$

where the first order correction  $|\xi_1\rangle$  due to the perturbation of one particular eigenstate  $|\xi_0\rangle$  of the unperturbed Hamiltonian is given by

$$|\xi^1\rangle = \sum_{\phi^0 \neq \xi^0} \frac{\langle \phi^0 | V | \xi^0 \rangle}{E_{\xi^0} - E_{\phi^0}} |\phi^0\rangle, \quad (5.27)$$

with  $\{|\phi^0\rangle\}$  denoting the set of all eigenstates of  $H_n$  different from  $|\xi^0\rangle$ .

It is convenient to choose

$$\langle \xi^0 | \xi \rangle = 1 \quad (5.28)$$

and thus

$$\langle \xi^0 | \xi^1 \rangle = 0. \quad (5.29)$$

The norm of  $|\xi\rangle$ , neglecting terms higher than first order, is given by

$$\langle \xi | \xi \rangle = 1 + \left( \sum_{\phi \neq \xi} \frac{\langle \phi^0 | V | \xi^0 \rangle}{E_{\xi^0} - E_{\phi^0}} \right)^2. \quad (5.30)$$

The fidelity of the mapping is given by the absolute value squared of the overlap between the ideal output state  $|\xi^0\rangle$ , for which  $g_n = 0$  (for time  $t=T$ ), and the actual output state  $|\xi\rangle$

$$F = \frac{|\langle \xi^0 | \xi \rangle|^2}{\langle \xi | \xi \rangle}, \quad (5.31)$$

which is, after some calculation, found to be

$$F = \frac{1}{1 + n g_n^2 / g_a(T)^2} \approx 1 - n \left( \frac{g_n}{g_a} \right)^2. \quad (5.32)$$

For  $g_a(T) \gg g_n$ , the error arising from  $g_n$  being nonzero is small. In Section 5.4, this error will be discussed when studying the numerical integration of  $H_{\text{eff}}$ .

### 5.3.2 Non-perfect polarization of the nuclei

As it has been discussed in Section 1.2.1, full polarization of the nuclear spins is hard to achieve as the system evolves to dark states, i.e., to states that cannot be polarized any more. Thus, the assumption that we made so far does not hold in a realistic setup and we are interested in the effect of non-perfect polarization on the mapping fidelity. When the number of polarized spins is reduced from

$$N \rightarrow PN, \quad (5.33)$$

where  $|P| = \langle A^z \rangle / |\langle A^z \rangle|_{max} < 1$  gives the polarization of the spin ensemble, the expectation values of the collective nuclear spin operators change according to

$$\langle A^z \rangle \rightarrow P \langle A^z \rangle \quad (5.34)$$

and

$$\langle A^+ \rangle \rightarrow \sqrt{P} \langle A^+ \rangle. \quad (5.35)$$

Thus, the Hamiltonian of the situation in which the nuclear spins are highly ( $> 80\%$ ) but not fully polarized is given by

$$H_{\text{pol}} = H_{\text{eff}} - (1 - P) \frac{A}{2} |\uparrow\rangle\langle\uparrow| - \frac{g_n}{2} (1 - \sqrt{P}) (S^- A^+ + \text{h.c.}) \quad (5.36)$$

where  $H_{\text{eff}}$  is given by equation (5.3) and  $P = 1$  for perfect polarization. The structure of the Hamiltonian does not change, so the only change is a small variation of the parameters. Thus, the effect on the mapping fidelity is negligibly small as confirmed numerically. Note however, that the assumption that the collective nuclear spin operators  $A^+, A^-$  can be well approximated by the bosonic operators  $b^\dagger, b$  for a small number of flipped spins is no longer that straightforward, as the exact expression for  $A^+ \rightarrow \sqrt{1 - \frac{b^\dagger b}{N}} b^\dagger$  has to be taken into account. When the corrections of the bosonic operators have to be considered, the operators do no longer form a closed algebra. A detailed study of this error goes beyond the scope of this thesis [30].

### 5.3.3 Non-adiabaticity due to finite time

Up to now, errors that can be treated analytically, namely the error arising from the hyperfine interaction being constant and the error arising from non-perfect polarization of the nuclear spins, have been considered.

An error inevitable in adiabatic processes is the non-adiabaticity due to finite time that leads to unwanted transitions between different eigenstates of the system. If the process would be perfectly adiabatic (and if conditions as continuity, noncrossing and differentiability hold), an initial instantaneous eigenstate of the Hamiltonian would evolve to the corresponding instantaneous eigenstate at a later time [50]. For finite times that are still long enough for the adiabatic approximation [50] to hold, the state

evolves to a state that is at least close to the corresponding instantaneous eigenstate at later time. The adiabatic approximation assures, that the rate of nonadiabatic coupling, i.e., the rate at that the instantaneous eigenstate in which the system is supposed to stay in couples to the other eigenstates of the system, is small compared to the separation of the corresponding eigenvalues. This condition reads

$$\left| \langle E_l(t) | \frac{d}{dt} H_{\text{eff}}(t)' | E_0(t) \rangle \right| \ll |E_l(t) - E_0(t)|^2, \quad (5.37)$$

where  $|E_0(t)\rangle$ ,  $E_0(t)$  denote the instantaneous eigenstate and eigenvalue the system is supposed to stay in at all times and  $|E_l\rangle$ ,  $E_l$  denote the set of eigenstates and eigenvalues of  $H_{\text{eff}}(t)'$  that are different to  $|E_0(t)\rangle$  and  $E_0$ . Here,  $|E_0\rangle$  is the eigenstate associated with the dark state  $|D\rangle \equiv |E_0\rangle$  given by equation (5.17), of the Hamiltonian, which we now define as  $H_{\text{eff}}(t)'$ , given by

$$H_{\text{eff}}(t)' = H_{\text{eff}}(t) - E_{G_n} \mathbb{1}. \quad (5.38)$$

Equation (5.18) reads

$$H_{\text{eff}}(t)' | E_0 \rangle = 0. \quad (5.39)$$

Thus, the eigenvalue of the Hamiltonian  $H_{\text{eff}}(t)'$  associated with the dark state is  $E_0 = 0$ .

For a quantitative estimate of the time  $T$  that is needed for adiabatic passage to occur, we use the condition given by equation (5.37) and compute numerically the minimum time fulfilling

$$\left| \langle E_l | \frac{d}{dt} H'_{\text{eff}} | E_0 \rangle \right| \leq \frac{1}{10} |E_l - E_0|^2 \quad \forall t \in [0, T]. \quad (5.40)$$

For the mapping of, e.g., one and two photons, it is found to be  $T_1 \approx 0.9\mu\text{s}$  and  $T_2 \approx 1.3\mu\text{s}$ , respectively. These estimations of the times needed for adiabatic transfer are close to  $T = 1\mu\text{s}$ , the time found to be appropriate for achieving high fidelities when numerically integrating the Schrödinger equation, as we will see in Section 5.4.

Up to now we have estimated the time for adiabatic following, however, we do not have any accurate description of the errors arising from non-adiabaticity. Shi and Yong-Shi (2004) [51] have formulated a perturbative approach to treat nonadiabatic corrections, in which the adiabatic limit is the zeroth-approximation. Supposing to be at  $t = 0$  in an nondegenerate eigenstate  $|\phi_n(0)\rangle$  of a Hamiltonian  $H$  slowly varying in time, the exact state at some later time  $t$  is given by

$$|\phi_{\text{na}(t)}\rangle = U(t) |\phi_n(0)\rangle = e^{i\eta(t)} [|\phi_n(t)\rangle + \sum_{m \neq n} \frac{|\phi_m(t)\rangle \langle \phi_m(t) | \partial_t \phi_n(t) \rangle}{E_m(t) - E_n(t)} + \dots] \quad (5.41)$$

where  $\eta = -i \int_0^t E(\tau) d\tau$  is the dynamic phase.

Using equation (5.41), we can derive the energy correction of the considered energy eigenvalue due to non-adiabaticity. The total energy of the energy eigenvalue we consider, is in first order given by

$$\begin{aligned} \langle \phi_{\text{na}}(t) | H | \phi_{\text{na}}(t) \rangle &= \langle \phi_n(t) | H | \phi_n(t) \rangle + \langle \phi_{\text{na}}^1(t) | H | \phi_{\text{na}}^1(t) \rangle \\ &+ \overbrace{\langle \phi_n(t) | H | \phi_{\text{na}}^1(t) \rangle + \text{h.c.}}^{=0}, \end{aligned} \quad (5.42)$$

where  $|\phi_{\text{na}}^1(t)\rangle$  is the first order correction of  $|\phi_n(t)\rangle$  (see equation (5.41)), which can be written as

$$|\phi_{\text{na}}^1(t)\rangle = e^{i\eta(t)} \sum_{m \neq n} \frac{|\phi_m(t)\rangle \langle \phi_m(t) | \partial_t \phi_n(t) \rangle}{E_m(t) - E_n(t)} \quad (5.43)$$

$$= e^{i\eta(t)} \sum_{m \neq n} \frac{|\phi_m(t)\rangle \langle \phi_m(t) | \frac{d}{dt} H | \phi_n(t) \rangle}{(E_m(t) - E_n(t))^2}. \quad (5.44)$$

Thus, the first order correction  $E_{\text{na}}^1$  to the eigenvalue  $E_0 = 0$  of the system, for which the phases  $\phi_n$  arising from the ground state energy  $E_{G_n}$  have been corrected, is given by

$$E_{\text{na},n} = \sum_{m \neq 0} \frac{|\langle \phi_m | \frac{d}{dt} H_n | \phi_0 \rangle|^2}{E_m^3}. \quad (5.45)$$

The phases  $\phi_{\text{na},n} = \int_0^T \frac{E_{\text{na},n}}{\hbar} dt$  the system acquires arising from non-adiabatic evolution can be found by numerical integration of  $E_{\text{na},n}$ . The phase  $\phi_{\text{na},n}$  for  $T = 1\mu\text{s}$  for  $n = 1$  (one initial photon in the cavity) is given by  $\phi_{\text{na},1} = 0.064$  and  $\phi_{\text{na},2} = 0.127$  for  $n = 2$ , respectively. Thus, as expected, the errors arising from non-adiabaticity are small for sufficiently long times  $T$ .

## 5.4 Numerical integration of the Schrödinger equation

To study the quality of the mapping of a state of the cavity to the nuclear spins of a quantum dot that can be achieved using STIRAP, we numerically integrate the Schrödinger equation given by

$$i \frac{\partial}{\partial t} |\psi(t)\rangle = H_{\text{eff}}(t) |\psi(t)\rangle, \quad (5.46)$$

where  $H_{\text{eff}}$  is the Hamiltonian given by equation (5.3, 5.4). The formal solution of equation (5.46) with known boundary conditions at  $t = t_0$  is given by

$$|\psi(t)\rangle = U(t, t_0) |\psi(t_0)\rangle, \quad (5.47)$$

where  $U(t, t_0)$  is the time evolution operator which satisfies

$$U(t, t_0) = U(t, t') U(t', t_0) \quad (5.48)$$

for any times  $t, t', t_0$ . If we divide the time interval  $t_0 \leq t \leq T$  into subintervals  $t_{k-1} \leq t \leq t_k$  where  $k = 0 \dots L$  and  $L = T/Dt$ , we can use a product of time evolution operators to get a numerical solution for the Schrödinger equation given by equation (5.46). Thus, for  $t_0 = 0$ ,  $U(T, t_0)$  is given by

$$U(T, 0) = U(T, t_{L-1})U(t_{L-1}, t_{L-2}) \dots U(t_2, t_1)U(t_1, 0) \quad (5.49)$$

$$= e^{-iH_{\text{eff}}(T)Dt} e^{-iH_{\text{eff}}(T-Dt)Dt} \dots e^{-iH_{\text{eff}}(Dt)Dt} e^{-iH_{\text{eff}}(0)Dt}. \quad (5.50)$$

The simulation, implemented with Matlab, computes

$$|\psi(t + Dt)\rangle = e^{-iH_{\text{eff}}(t+Dt)Dt} |\psi(t)\rangle \quad (5.51)$$

in  $T/Dt$  steps from  $t = 0$  to  $t = T$ .

We assume, that the change of  $g_a(t)$  is quadratic in time, ensuring an initially slow and a finally fast increase of  $g_a(t)$ . For the final time  $T$ , the fraction of  $g_a$  and  $g_n$  is chosen such that  $\frac{g_n}{g_a(T)} = \frac{1}{10}$ , i.e.,

$$g_a = 10 g_n \frac{t^2}{T^2}. \quad (5.52)$$

The parameters are chosen to be  $g_n = 1\mu\text{eV}$ ,  $N = 10^4$ ,  $\Omega_l = 1.9\text{meV}$ ,  $\Omega_c = 208\mu\text{eV}$ ,  $\Delta_e = 10\text{meV}$  and  $\Delta_b = 2.5\mu\text{eV}$ . The values chosen for the cavity and laser Rabi frequencies are significantly higher than the ones reached experimentally so far, which are of the order of  $\Omega_l$ ,  $\Omega_c = 120\mu\text{eV}$  [37],[22].

The fidelity of the mapping we are interested in, is given by the overlap of the numerically evolved state

$$\rho(t) = |\psi_{\text{si}}\rangle\langle\psi_{\text{si}}| \quad (5.53)$$

and the ideal output  $|\psi_{\text{id}}\rangle$

$$F = \langle\psi_{\text{id}}|\rho(t)|\psi_{\text{id}}\rangle = |\langle\psi_{\text{id}}|\psi_{\text{si}}\rangle|^2 \quad (5.54)$$

To achieve a fidelity close to one, the total evolution time is chosen to be  $T = 1\mu\text{s}$ . The width of the time steps is chosen to be  $Dt = 10^{-10}\text{s}$ . Different states of the cavity lead to different fidelities.

Figure 5.4 shows the fidelity plotted versus time for different kind of states that will be discussed in the following, illustrating the different aspects of mapping.

### Fock states

First, we want to consider the mapping of Fock states. The one photon Fock state  $|1\rangle$  is mapped in  $T = 1\mu\text{s}$  with a fidelity of  $F = 0.99$  to the nuclear spins. The mapping fidelities of Fock states decrease with increasing photon number. One reason is the increasing error due to the increasing hyperfine coupling at the end of the process, which arises from the fact, that the more photons are mapped, the more nuclear spins

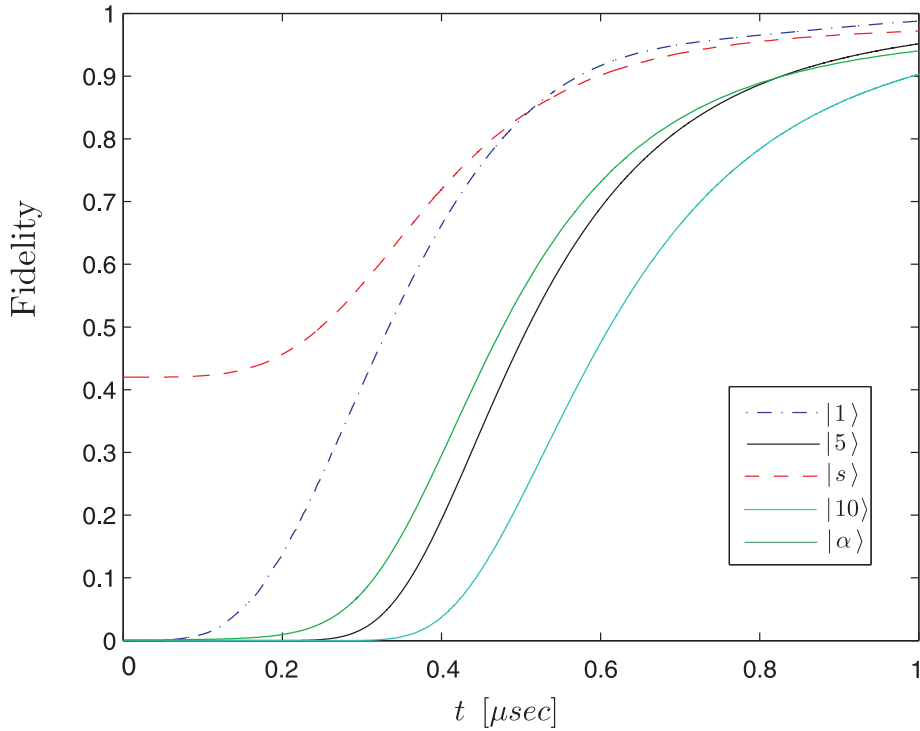


Figure 5.3: Plot of the fidelity of a variety of states versus time during the adiabatic evolution.  $|1\rangle$ ,  $|5\rangle$ ,  $|10\rangle$  denote the one, five, ten photon Fock states, respectively.  $|\alpha\rangle$  denotes the coherent state with average photon number 5 and  $|s\rangle$  the squeezed state given by equation (5.56). Details of these states can be found in the text. The total evolution time is chosen to be  $T = 1\mu s$ .

are flipped. This error is reflected in equation (5.32). Another reason is, that for the mapping of higher photon numbers, longer times are needed for the process to be adiabatic. If we do not change the time of the process, errors due to non-adiabaticity, that will be discussed in Section 5.3.3, will increase. The fidelities of the mapping of the states  $|1\rangle$  and  $|5\rangle$  are, by numerically integrating the Schrödinger equation as explained before, found to be  $F \approx 0.99$  and  $F \approx 0.95$ , respectively. For these small values of  $n$ , we find that the error is largely dominated by  $g_n$  being constant, as indicated by comparison of the fidelities following from equation (5.32), that are found to be  $F \approx 0.99$  and  $F \approx 0.95$  for one and five initial photons, respectively. To see how well superposition states are mapped we now turn to two typical states from quantum optics where relative phases are important.

### Coherent states

The properties of coherent states are discussed in Appendix B.2.1. The simulation of a coherent state  $|\alpha\rangle$  with average photon number  $|\alpha|^2 = 5$  given by

$$|\alpha\rangle = \exp\left(-\frac{|\alpha|^2}{2}\right) \sum_{k=0}^{20} \frac{\alpha^k}{\sqrt{k!}} |k\rangle, \quad (5.55)$$

where the sum  $\sum_{k=0}^{\infty}$  is cut off at  $k = 20$ , yields a mapping fidelity of  $F = 0.94$ . That shows, that erroneous phases between states with different photon numbers are small, as the fidelity for the Fock state with 5 photons,  $|5\rangle$  is  $F = 0.95$ . As the known phases  $\phi_n$  (arising from the energy  $E_{Gn}$  of the ground states) have already been compensated, the phases that states with different photon numbers acquire arise from non-adiabaticity, discussed in Section 5.3.3, and the "always on" character of  $g_n$ , discussed in Section 5.3.1.

### Squeezed states

The single-mode squeezed state simulated here is given by

$$|s\rangle = \sum_{n=0}^7 c_n |2n\rangle, \quad (5.56)$$

with

$$c_n = \frac{1}{\sqrt{\cosh(r)}} \left(-\frac{\sinh(r)}{\cosh(r)}\right)^n \sqrt{\frac{(2n-1)!!}{(2n)!!}} \quad (5.57)$$

where we set the squeezing parameter  $r = 1$  [52]. This state has a position variance given by

$$\langle(\Delta x)^2\rangle = \langle s|(x - \langle x\rangle)^2|s\rangle = \frac{1}{2}\langle s|a^\dagger a + a a^\dagger + a^\dagger a^\dagger + a a|s\rangle = 0.08, \quad (5.58)$$

where  $x = \frac{1}{\sqrt{2}}(a + a^\dagger)$ . As the state is squeezed if one of the variances is smaller than  $\frac{1}{4}$  (see equation (B.26) in Appendix B),  $|s\rangle$  is a squeezed state. This state yields a fidelity of  $F = 0.97$ .

### Average fidelity of superpositions of $|0\rangle$ and $|1\rangle$

The most important application of a quantum memory is the storage of qubits, that is the ability to store an arbitrary superposition in a 2D Hilbert space. One might be interested in the fidelity of a superposition of a state that is always mapped with perfect fidelity, namely the zero photon Fock state  $|0\rangle$ , and the one photon state  $|1\rangle$ . The average fidelity of such superposition states

$$|\psi\rangle \equiv |\theta, \phi\rangle = \frac{1}{\sqrt{2}} (\cos\theta|0\rangle + e^{i\phi}\sin\theta|1\rangle), \quad (5.59)$$

reads

$$\bar{F} = \int d \cos \theta \frac{d\phi}{2\pi} \langle \theta, \phi | M (|\theta, \phi\rangle\langle \theta, \phi|) |\theta, \phi\rangle, \quad (5.60)$$

where  $M$  denotes the mapping operation.

To compute the average fidelity  $\bar{F}$ , the projector  $\rho_{\theta, \phi} = |\theta, \phi\rangle\langle \theta, \phi|$  can be decomposed into a sum of projectors  $|\psi_x\rangle\langle \psi_x|$

$$|\theta, \phi\rangle\langle \theta, \phi| = \sum_x c_x |\psi_x\rangle\langle \psi_x|, \quad (5.61)$$

where

$$|\psi_x\rangle \in \left\{ |0\rangle, |1\rangle, \frac{1}{\sqrt{2}}(|0\rangle + |1\rangle), \frac{1}{\sqrt{2}}(|0\rangle + i|1\rangle) \right\}. \quad (5.62)$$

The coefficients  $c_x$  with

$$c_x \in \{c_{00}, c_{11}, c_{01}, c_{0i1}\}, \quad (5.63)$$

where e.g.,  $c_{01}$  denotes the coefficient of the projector  $1/2(|0\rangle + |1\rangle)(\langle 0| + \langle 1|)$ , are given by

$$\begin{aligned} c_{00} &= \cos^2 \theta - \cos \theta \sin \theta (\cos \phi + \sin \phi) \\ c_{11} &= \sin^2 \theta - \cos \theta \sin \theta (\cos \phi + \sin \phi) \\ c_{01} &= \cos \phi \sin 2\theta \\ c_{0i1} &= \sin \phi \cos 2\theta. \end{aligned} \quad (5.64)$$

As  $M$  is a linear map,  $\langle \theta, \phi | M (|\theta, \phi\rangle\langle \theta, \phi|) |\theta, \phi\rangle = \text{tr} (|\theta, \phi\rangle\langle \theta, \phi| M(\rho_{\theta, \phi}))$  can be written as

$$\text{tr} \left( \sum_x \sum_{x'} c_{x'} c_x |\psi_{x'}\rangle\langle \psi_{x'}| M(|\psi_x\rangle\langle \psi_x|) \right). \quad (5.65)$$

$M(|\psi_x\rangle\langle \psi_x|)$  can be easily simulated and the coefficients  $c_x, c'_x$  are known, thus the integral in equation (5.60) can be solved.

An average fidelity  $\bar{F} = 0.99$  for  $T = 1\mu\text{s}$  is found when simulating the mapping  $M(|\psi_x\rangle\langle \psi_x|)$  and solving the integral. Thus, the memory beats the benchmark fidelity  $\frac{2}{3}$  of a classical memory (see Section 1.3.1). We will see later how robust the state is when cavity decay is taken into account.

### Entanglement fidelity

As it has already been mentioned in Section 3.2.3, the ultimate test for a quantum memory is whether it is capable of storing part of an entangled quantum system. This will be discussed here in more detail, introducing the entanglement fidelity that measures how well an operation can preserve entanglement between a system undergoing the operation, in the following denoted by 1, and an auxiliary system

denoted by 2. Supposing that the initially joint system "12" is prepared in a pure entangled state, the entanglement fidelity as defined by [53] reads

$$F_{\text{ent}} = \langle \psi^{12} | M \otimes \mathbb{1} (|\psi^{12}\rangle\langle\psi^{12}|) | \psi^{12}\rangle, \quad (5.66)$$

where  $M$  denotes a completely positive, trace preserving map. This fidelity does not only measure how well entanglement is preserved. It is related to the average fidelity defined by

$$\bar{F} = \int \langle \psi^{12} | M (|\psi^{12}\rangle\langle\psi^{12}|) | \psi^{12}\rangle d\psi \quad (5.67)$$

by the simple relation

$$\bar{F} = \frac{BF_{\text{ent}} + 1}{B + 1}, \quad (5.68)$$

where  $B$  is the dimension of the underlying Hilbert space. For large dimensions  $B \rightarrow \infty$ ,  $\bar{F}$  and  $F_{\text{ent}}$  coincide [54]. Moreover, the maximally entangled state undergoing the operation  $M \otimes \mathbb{1}$  contains according to the Jamiolkowski isomorphism, introduced in Appendix C.2, complete information about the mapping operation, i.e., in our case about the quantum memory operation.

The entangled state that will be studied in the following is given by

$$|\phi^+\rangle = \frac{1}{\sqrt{2}}(|0_1 0_2\rangle + |1_1 1_2\rangle), \quad (5.69)$$

where the subscripts 1, 2 denote two different modes.  $|\phi^+\rangle$  is a superposition of either one or no photon in both mode 1 and mode 2. The modes could e.g., be two beams of light emerging from spontaneous parametric down conversion.

The fidelity with which one mode of the system, in the following it will be mode 1, is mapped to the nuclear spins, is given by

$$F_{\text{ent}} = \langle \phi^+ | M \otimes \mathbb{1} (|\phi^+\rangle\langle\phi^+|) | \phi^+\rangle, \quad (5.70)$$

where the map  $M$  acts on mode 1 and  $\mathbb{1}$  on mode 2.  $M \otimes \mathbb{1} (|\phi^+\rangle\langle\phi^+|)$  reads

$$\begin{aligned} M \otimes \mathbb{1} (|\phi^+\rangle\langle\phi^+|) = & \frac{1}{2} (M(|0_1\rangle\langle 0_1|) \otimes |0_2\rangle\langle 0_2| + M(|1_1\rangle\langle 1_1|) \otimes |1_2\rangle\langle 1_2| \\ & + M(|0_1\rangle\langle 1_1|) \otimes |0_2\rangle\langle 1_2| + M(|1_1\rangle\langle 0_1|) \otimes |1_2\rangle\langle 0_2|). \end{aligned}$$

As  $M(|0_1\rangle\langle 0_1|)$ ,  $M(|1_1\rangle\langle 1_1|)$ ,  $M(\frac{1}{2}(|0_1\rangle + i|1_1\rangle)(\langle 0_1| + i\langle 1_1|))$  and  $M(\frac{1}{2}(|0_1\rangle + |1_1\rangle)(\langle 0_1| + \langle 1_1|))$  are, in contrast to  $M(|1_1\rangle\langle 0_1|)$  and  $M(|0_1\rangle\langle 1_1|)$ , easy to simulate with our program, we decompose  $M(|0_1\rangle\langle 1_1|)$  into

$$\begin{aligned} \text{Re} [M(|0_1\rangle\langle 1_1|)] &= M(\frac{1}{2}(|0_1\rangle + |1_1\rangle)(\langle 0_1| + \langle 1_1|)) - \frac{1}{2}M(|0_1\rangle\langle 0_1|) - \frac{1}{2}M(|0_1\rangle\langle 0_1|) \\ \text{Im} [M(|0_1\rangle\langle 1_1|)] &= M(\frac{1}{2}(|0_1\rangle + i|1_1\rangle)(\langle 0_1| - i\langle 1_1|)) - \frac{1}{2}M(|0_1\rangle\langle 0_1|) - \frac{1}{2}M(|0_1\rangle\langle 0_1|). \end{aligned}$$

Using this decomposition, the entanglement fidelity can be computed, yielding  $F_{\text{ent}} = 0.99$  in  $T = 1\mu\text{s}$ .

## 5.5 Monte Carlo wavefunction simulation of the cavity decay

A very important source of error we did not consider so far, is the finite lifetime of the photon in the cavity. The cavity decay can be implemented with a Monte Carlo wavefunction simulation of the quantum jump approach as has been suggested in [55, 56], (for a review see [57]). The benefit of this approach is, that for systems with a large number of states  $N$ , it requires less calculation time than the master equation treatment with density matrices consisting of  $N^2$  terms. Moreover, new physical insight into the behavior of single quantum systems may be gained. As the master equation treatment is the usual way to describe the coupling between a small system and a large reservoir, it will be reviewed here very briefly.

The objective is to obtain an equation for the time evolution of the reduced density operator  $\rho_s(t) = \text{tr}_{\text{res}}(\rho)$ , where the trace is taken over the reservoir states. The master equation can be written as

$$\dot{\rho}_s(t) = L(t)\rho_s(t), \quad (5.71)$$

where  $L(t)$  is a linear operator with the form of  $L$  depending on the kind of master equation considered. In the Markov approximation, where it is assumed that the knowledge of the system at one time  $t = t_0$  is sufficient to determine  $\rho(t)$  for all  $t > t_0$ ,  $L$  is of Lindblad form and the master equation reads

$$L(t)\rho_s(t) = -i[H, \rho] + \sum_j [2A_j\rho A_j^\dagger - \rho A_j^\dagger A_j - A_j^\dagger A_j \rho] \quad (5.72)$$

where  $H$  is some hermitian operator and the  $A_j$  can be arbitrary operators acting in the space of the small system [58]. This type of the master equation is found in most quantum optics problems involving dissipation.

Another more novel treatment which is equivalent to the master equation treatment is based on the evolution of a Monte-Carlo wavefunction, where quantum jumps occur randomly and the system is evolved with a non-hermitian Hamiltonian at intermediate times between two quantum jumps, followed by renormalization of the wavefunction after this evolution. The method can be summarized as follows [57]:

- First, the probability of the emission of a photon within the time interval  $\delta t$  is determined,

$$\Delta P = \gamma \langle \psi | a^\dagger a | \psi \rangle \delta t, \quad (5.73)$$

where  $|\psi\rangle$  is a normalized state of the system and  $\gamma$  is the rate at which photons are lost by the field.

- Then, a random number  $r$  between zero and one is generated and compared to  $\Delta P$ .

- If  $r < \Delta P$ , there is an emission and the system "jumps" to the renormalized state

$$|\psi\rangle \rightarrow |\psi_{\text{em}}\rangle = \frac{a|\psi\rangle}{\sqrt{\langle\psi|a^\dagger a|\psi\rangle}}, \quad (5.74)$$

where  $a$  is the photon annihilation operator.

- If  $r > \Delta P$ , there is no emission and the system evolves according to

$$|\psi_{\text{no em}}\rangle = \frac{e^{-i\delta t H_e}|\psi\rangle}{\sqrt{\langle\psi|e^{i\delta t H_e}e^{-i\delta t H_e}|\psi\rangle}} \quad (5.75)$$

$$\approx \frac{(1-iH\delta t-(\gamma/2)\delta t a^\dagger a)|\psi\rangle}{\sqrt{1-\delta P}}, \quad (5.76)$$

with  $\hbar = 1$ , where the last equation is an approximation valid to order  $\delta t$ .

$$H_e = H - i(\gamma/2)a^\dagger a \quad (5.77)$$

is the effective non-hermitian Hamiltonian, where the second term describes the decay of the energy of the cavity field. For more details of the derivation of  $H_e$  see [57].

- The process is repeated to obtain an individual trajectory of length  $t$ .
- The observables are averaged over many such trajectories.

The evolution of the density operator of a pure state  $\rho = |\psi\rangle\langle\psi|$  within the time interval  $\delta t$  is the sum of the possible outcomes  $|\psi_{\text{em}}\rangle\langle\psi_{\text{em}}|$ , observed with probability  $\Delta P$ , and  $|\psi_{\text{no em}}\rangle\langle\psi_{\text{no em}}|$ , observed with probability  $(1 - \Delta P)$ ,

$$\begin{aligned} |\psi(t)\rangle\langle\psi(t)| &\rightarrow |\psi(t+\delta t)\rangle\langle\psi(t+\delta t)| \\ &= \Delta P |\psi_{\text{em}}\rangle\langle\psi_{\text{em}}| + (1 - \Delta P) |\psi_{\text{no em}}\rangle\langle\psi_{\text{no em}}| \\ &\approx |\psi(t)\rangle\langle\psi(t)| - i\delta t [H, |\psi(t)\rangle\langle\psi(t)|] \\ &\quad + \frac{\gamma}{2}\delta t (2a|\psi(t)\rangle\langle\psi(t)|a^\dagger - a^\dagger a|\psi\rangle\langle\psi| - |\psi\rangle\langle\psi|a^\dagger a) \end{aligned} \quad (5.78)$$

so that

$$\frac{\Delta\rho}{\Delta t} = -i[H, \rho] + \frac{\gamma}{2}(2a\rho a^\dagger - a^\dagger a\rho - \rho a^\dagger a) \quad (5.79)$$

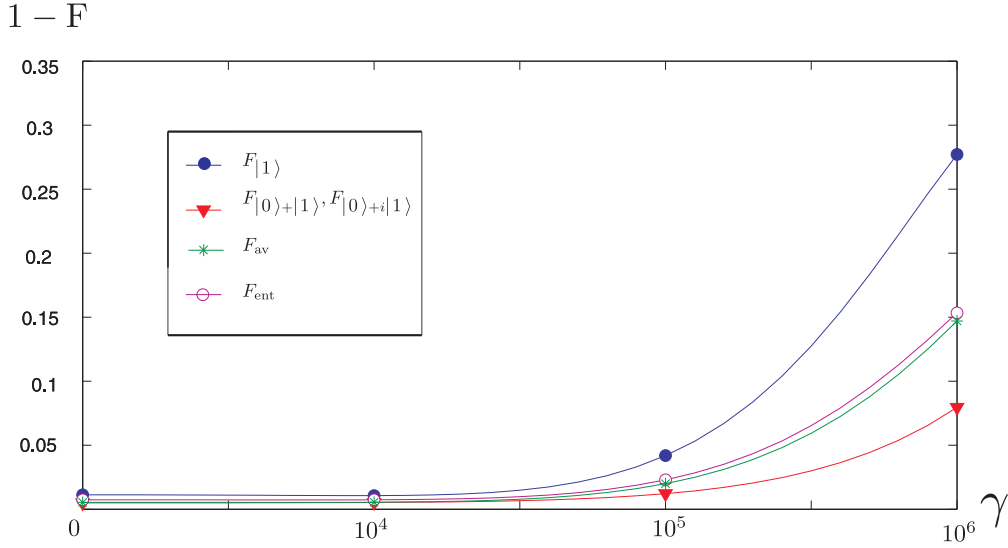
is of the form of the master equation given by equation (5.72).

The simulation follows the scheme as described here, where 2000 runs average over the trajectories. In Figure 5.5, the error "1 - F", where  $F$  is the fidelity, is plotted versus the decay rate  $\gamma_{\text{decay}}$ , the rate at which photons are lost by the cavity field. The fidelity of the states shown in Figure 5.5, i.e., of the one photon Fock state  $|1\rangle$ , of the states  $\frac{1}{\sqrt{2}}(|0\rangle + |1\rangle)$  and  $\frac{1}{\sqrt{2}}(|0\rangle + i|1\rangle)$ , the entanglement fidelity of the state  $|\phi^+\rangle = \frac{1}{\sqrt{2}}(|0_1 0_2\rangle + |1_1 1_2\rangle)$  given by equation (5.69) and the average fidelity of

the state  $|\theta, \phi\rangle = \frac{1}{\sqrt{2}} (\cos \theta |0\rangle + e^{i\phi} \sin \theta |1\rangle)$  defined by equation (5.60), are robust to cavity decay for a decay rate of up to  $\gamma = 10^5$ . For  $\gamma = 10^6$ , the fidelity for the one photon Fock state decreases by 0.38, i.e., the fidelity is given by  $F = 0.72$ . The superposition states of  $|1\rangle$  and  $|0\rangle$  are more robust as  $|0\rangle$  is mapped with perfect fidelity. The fidelity decreases with higher photon numbers as the probability that a photon is lost by the cavity increases with increasing photon number. This can be seen in Figure 5.5, where "1 - F" is plotted versus cavity decay for a 5 photon Fock state.

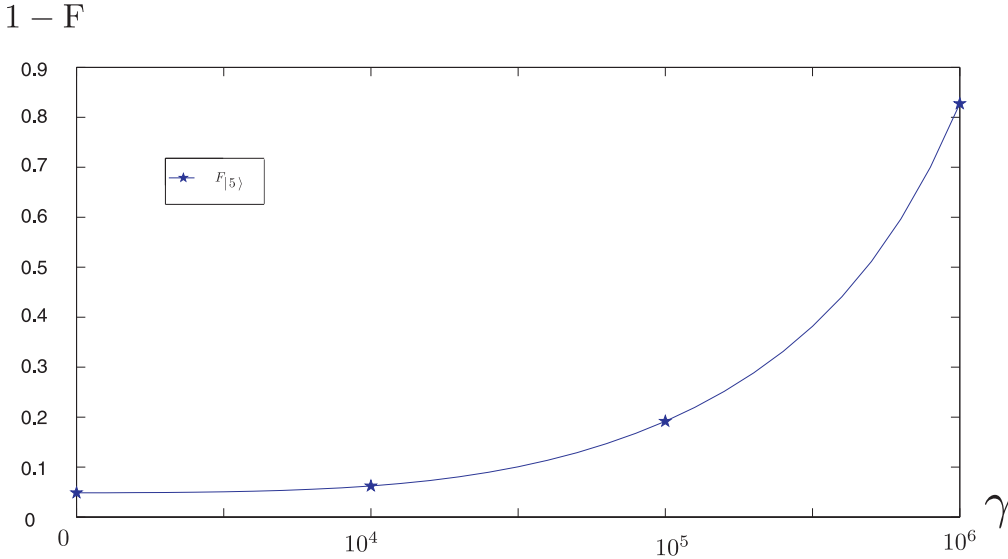
For a decay rate  $\gamma = 10^5$ , high mapping fidelities for Fock states with small photon numbers can still be achieved. Up to now, the experimentally achieved  $\gamma$  of a photonic crystal microcavity that couples to a quantum dot is of the order of  $\gamma \approx 10^{10}$ . The longest photon lifetimes of a photonic crystal nanocavity up to now, is, as mentioned before  $t = 2.1ns$  [46]. Thus, the process as suggested here cannot be implemented with today's technology. However, larger cavity and laser Rabi frequencies and cavities with higher Q-factors and larger Rabi frequencies that certainly will be achieved in the future, might reach values for which the process might become possible.

a)



a) Plot of  $1 - F$ , where  $F$  denotes the mapping fidelity, versus cavity decay rate  $\gamma$  of the one photon Fock state fidelity  $F_{|1\rangle}$ , the fidelities  $F_{|0\rangle+|1\rangle}$ ,  $F_{|0\rangle+i|1\rangle}$  of the superposition states  $\frac{1}{\sqrt{2}}(|0\rangle + |1\rangle)$ ,  $\frac{1}{\sqrt{2}}(|0\rangle + i|1\rangle)$ , the average fidelity  $F_{av}$  of the state  $|\theta, \phi\rangle = \frac{1}{\sqrt{2}}(\cos\theta|0\rangle + e^{i\phi}\sin\theta|1\rangle)$  and the entanglement fidelity  $F_{ent}$  of state  $|\phi^+\rangle = \frac{1}{2}(|0_10_2\rangle + |1_11_2\rangle)$ .

b)



b) Plot of  $1 - F$ , versus cavity decay rate  $\gamma$  of the five photon Fock state fidelity  $F_{|5\rangle}$ .

Figure 5.4: Plots of the mapping fidelities versus cavity decay rate for different types of states.

# Chapter 6

## Summary and Perspectives

A quantum interface between light pulses carrying information and matter well suited for storage and processing, is an essential building block for quantum information applications. Quantum dots are promising candidates for quantum computation, and nuclear spins are well suitable for information storage as they exhibit exceptionally long decoherence times.

In this thesis, a quantum interface between light and the nuclear spins of a semiconductor quantum dot has been studied.

To derive an operation for the mapping of the light to the nuclear spins, we followed two related approaches, the Landau-Zener model and the method of "Stimulated Raman adiabatic passage" (STIRAP). The latter method allows faster storage, as the condition that the electronic states have to be largely detuned, needed for its adiabatic elimination, was not required. For storage times on the order of  $1\mu\text{s}$ , we have demonstrated, that various states can be faithfully mapped to the nuclear spins, such as the one photon Fock state with a fidelity of 0.99, the five photon Fock state with a fidelity of 0.95, a coherent state with an average photon number of five with a fidelity of 0.94, and a single-mode squeezed state with a fidelity of 0.97.

Moreover, we have shown that our system is even capable to store part of an entangled state, while preserving the entanglement between the part of the system undergoing the memory operation with an auxiliary system.

We investigated different sources of error, such as non-perfect polarization of the nuclei, non-adiabaticity due to the finite time of the process and the error due to the constant hyperfine coupling. We modeled the cavity decay with a Monte Carlo wavefunction simulation and found that for cavity decay rates of up to  $\gamma = 10^5$ , high mapping fidelities of Fock states with small photon numbers can still be achieved.

Slightly changing the model, we found that another possible application of the system is the generation of a two-mode squeezed state of the nuclear spin-cavity system, which enables for example a light-matter interface through teleportation. The times needed for the generation of a two-mode squeezed state with squeezing parameter  $r = 1$  are of the order of  $10^{-7} - 10^{-8}$ s and thus, compared to the times for storage of a state of light in the nuclear spins, closer to the lifetimes of a photon in

a photonic crystal microcavity.

Thus, we have proposed a faithful interface between light and the nuclear spins of a quantum dot and a model that allows the generation of a two-mode squeezed state of the nuclear-spin cavity system. The problems in realizing these systems in the laboratory, are the limited lifetimes of today's cavities and the high polarization of the nuclear spins that is required. We hope that future technologies will enable higher polarization of the nuclear spins and longer cavity lifetimes.

However, other Quantum Information Processing (QIP) protocols might prove more robust to cavity losses. For example, one could employ the coupling discussed in this thesis for state preparation rather than mapping. In particular, the read-out version of the Landau-Zener or STIRAP process (i.e., the mapping of nuclear excitations to the cavity) can be used as a nuclear spin cooling process to remove nuclear spin excitations which are left over from imperfect dynamical nuclear polarization (DNP). Here cavity losses, which simply remove excitations from the system, do not affect (but even support) the polarization process.

More interestingly, it has been shown in [59] that even bad cavities can be used to generate entanglement between two distant atoms: the atoms are located in two cavities that are exposed to a two-mode squeezed vacuum state. The interplay of Jaynes-Cummings dynamics and cavity decay drives the atoms into a strongly entangled steady state. In the system studied here, the nuclei would play the role of the atoms. It would be interesting to investigate their steady state when driven by a two-mode squeezed bath and see under which conditions steady state entanglement of the nuclei can be generated.

More generally, localized nuclear spins are arguably the most promising system to store quantum information in solid stated devices while coherent coupling to optical fields offers unrivaled levels of speed and control for the manipulation of quantum systems. Therefore, further exploration of ways to combine these two techniques is of great interest for solid-state based quantum information protocols.

# Appendix A

## Adiabatic elimination

### A.1 Rotating frame

The time dependency of the Hamiltonian  $H = H_{\text{opt}} + H_{\text{NS}}$  given by equation (2.9) can be removed by turning to a rotating frame defined by the transformation

$$H' \rightarrow UHU^\dagger + i\dot{U}U^\dagger. \quad (\text{A.1})$$

To derive this transformation from the Schrödinger picture we set

$$|\varphi\rangle = U|\psi\rangle. \quad (\text{A.2})$$

Then

$$\begin{aligned} |\dot{\varphi}\rangle &= \dot{U}|\psi\rangle + U|\dot{\psi}\rangle \\ &= \dot{U}U^\dagger|\varphi\rangle - iUHU^\dagger|\varphi\rangle \end{aligned} \quad (\text{A.3})$$

and the Schrödinger equation reads

$$i|\dot{\varphi}\rangle = (UHU^\dagger + i\dot{U}U^\dagger)|\varphi\rangle, \quad (\text{A.4})$$

which yields the transformation

$$H \rightarrow UHU^\dagger + i\dot{U}U^\dagger \quad (\text{A.5})$$

for the Hamiltonian in the Heisenberg picture. It will be shown in the following that defining  $U^\dagger$  by

$$U^\dagger = \exp[-i\omega_l t(a^\dagger a + |X\rangle\langle X|)] \quad (\text{A.6})$$

leads to a time independent Hamiltonian  $H'$ . This transformation leaves the second part of the Hamiltonian  $H_{\text{NS}}$  unchanged and acts only on the Hamiltonian  $H_{\text{opt}}$  given by equation (2.3). To remind the reader it is rewritten here:

$$H_{\text{opt}} = \omega_c a^\dagger a + \omega_\uparrow |X\rangle\langle X| + g_e \mu_b B_z |\downarrow\rangle\langle \downarrow| + \frac{\Omega_c}{2} (a^\dagger |\downarrow\rangle\langle X| + \text{h.c.}) + \frac{\Omega_l}{2} (e^{+i\omega_l t} |\uparrow\rangle\langle X| + \text{h.c.}).$$

The third and the fourth term do not change under the transformation  $UH_{\text{opt}}U^\dagger$ . This is obvious for the third term, for the fourth term it can be shown by using the Baker Hausdorff Lemma

$$e^A B e^{-A} = B + [A, B] + \frac{1}{2!}[A, [A, B]] \dots \quad (\text{A.7})$$

and the commutation relations

$$[a^\dagger a, a] = -a, \quad \text{and} \quad [a^\dagger a, a^\dagger] = a^\dagger. \quad (\text{A.8})$$

The last term in  $H_{\text{opt}}$  becomes time independent under the transformation  $UH_{\text{opt}}U^\dagger$ . This can be seen by expanding  $U$  which yields

$$\begin{aligned} U \frac{\Omega_l}{2} (e^{+i\omega_l t} |\uparrow\rangle\langle X| + \text{h.c.}) U^\dagger &= \frac{\Omega_l}{2} e^{i\omega_l t(|X\rangle\langle X|)} (e^{+i\omega_l t} |\uparrow\rangle\langle X| + \text{h.c.}) e^{-i\omega_l t(|X\rangle\langle X|)} \\ &= \frac{\Omega_l}{2} [e^{+i\omega_l t} |\uparrow\rangle\langle X| + e^{-i\omega_l t} |X\rangle\langle \uparrow| + i\omega_l t (-e^{+i\omega_l t} |\uparrow\rangle\langle X| + e^{-i\omega_l t} |X\rangle\langle \uparrow|) \\ &\quad + \frac{\omega_l^2}{2} t^2 (e^{+i\omega_l t} |X\rangle\langle \uparrow| + e^{-i\omega_l t} |X\rangle\langle \uparrow|) \dots] \\ &= \frac{\Omega_l}{2} (e^{-i\omega_l t} e^{+i\omega_l t} |\uparrow\rangle\langle X| + e^{+i\omega_l t} e^{-i\omega_l t} |X\rangle\langle \uparrow|) = \frac{\Omega_l}{2} (|\uparrow\rangle\langle X| + \text{h.c.}). \end{aligned} \quad (\text{A.9})$$

The resulting Hamiltonian reads

$$H'_{\text{opt}} = \delta a^\dagger a + \Delta_e |X\rangle\langle X| + \Delta_b |\downarrow\rangle\langle \downarrow| + \frac{\Omega_c}{2} (a^\dagger |\downarrow\rangle\langle X| + \text{h.c.}) + \frac{\Omega_l}{2} (|\uparrow\rangle\langle X| + \text{h.c.})$$

where

$$\delta = \omega_c - \omega_l, \quad (\text{A.10})$$

$$\Delta_e = \omega_\uparrow - \omega_l \quad (\text{A.11})$$

and

$$\Delta_b = g_e \mu_b B_z. \quad (\text{A.12})$$

Thus the Hamiltonian  $H'$  is given by

$$H' = H'_{\text{opt}} + H_{\text{NS}}, \quad (\text{A.13})$$

with  $H_{\text{NS}}$  given by equation (2.8)

$$H_{\text{NS}} = \frac{g_n}{2} (b^\dagger S^- + S^+ b) + \frac{A}{N} \frac{\sigma_z}{2} (b^\dagger b - \frac{N}{2}). \quad (\text{A.14})$$

Shifting the energy in equation (A.13) by  $\frac{A}{4}\mathbb{1}$ , the Zeeman splitting of the electronic states due to both the external magnetic field and the field created by the polarized nuclear spins, the Overhauser field, shall be written as

$$\tilde{\Delta}_b = g_e \mu_b B_{\text{tot}}, \quad (\text{A.15})$$

where  $B_{\text{tot}}$  is given by

$$B_{\text{tot}} = \frac{1}{g_e \mu_b} \frac{A}{2} + B_{\text{ext}}, \quad (\text{A.16})$$

with the electron g-factor  $g_e$ .

Thus, the Hamiltonian given by equation (A.13) can be written as

$$\begin{aligned} H' = & \delta a^\dagger a + \Delta_e |X\rangle\langle X| + \tilde{\Delta}_b |\downarrow\rangle\langle \downarrow| + \frac{A}{N} \frac{\sigma_z}{2} b^\dagger b \\ & + \frac{\Omega_c}{2} (a^\dagger |\downarrow\rangle\langle X| + \text{h.c.}) + \frac{\Omega_l}{2} (|\uparrow\rangle\langle X| + \text{h.c.}) \\ & + \frac{g_n}{2} [b^\dagger |\downarrow\rangle\langle \uparrow| + \text{h.c.}]. \end{aligned} \quad (\text{A.17})$$

## A.2 Adiabatic elimination of the trion

If the condition

$$|\Delta_e| \gg \left| \tilde{\Delta}_b \right|, |\Omega_c|, |\Omega_l| \quad (\text{A.18})$$

holds [60], the trion can be adiabatically eliminated by projecting the Schrödinger equation onto the subspace of the electronic states

$$i \mathbb{P} |\dot{\Psi}\rangle = \mathbb{P} H' \overbrace{(\mathbb{P} + \mathbb{Q})}^{\mathbb{1}} |\Psi\rangle = (\mathbb{P} H' \mathbb{P} + \mathbb{P} H' \mathbb{Q}) |\Psi\rangle \quad (\text{A.19})$$

$$i \mathbb{Q} |\dot{\Psi}\rangle = (\mathbb{Q} H' \mathbb{Q} + \mathbb{Q} H' \mathbb{P}) |\Psi\rangle, \quad (\text{A.20})$$

where the projectors  $\mathbb{P}$  and  $\mathbb{Q}$  are defined by

$$\mathbb{P} = \mathbb{1} - |X\rangle\langle X| - |\uparrow\rangle\langle \uparrow| + |\downarrow\rangle\langle \downarrow| \quad (\text{A.21})$$

$$\mathbb{Q} = |X\rangle\langle X|. \quad (\text{A.22})$$

Defining  $|\Psi_X\rangle$  as

$$|\Psi_X\rangle := \mathbb{Q} |\Psi\rangle, \quad (\text{A.23})$$

equation (A.20) leads to the differential equation

$$i |\dot{\Psi}_X\rangle = \Delta_e |\Psi_X\rangle + \mathbb{Q} H' \mathbb{P} |\Psi\rangle$$

with the solution given by

$$|\Psi_X(t)\rangle = e^{-i\Delta_e t} |\Psi_X(0)\rangle - i \int_0^t d\tau e^{-i\Delta_e(t-\tau)} \mathbb{Q} H' \mathbb{P} |\Psi(\tau)\rangle. \quad (\text{A.24})$$

With the assumption that the trion is initially unpopulated

$$|\Psi_X(0)\rangle = 0, \quad (\text{A.25})$$

the first term in equation (A.24) vanishes. Defining  $u$  and  $v$  by

$$u := \mathbb{Q}H'\mathbb{P}|\Psi(\tau)\rangle \quad (\text{A.26})$$

$$v := \frac{1}{i\Delta_e} e^{-i\Delta_e(t-\tau)} \quad (\text{A.27})$$

$$dv = e^{-i\Delta_e(t-\tau)} d\tau, \quad (\text{A.28})$$

partial integration of the integral in (A.24) leads to

$$|\Psi_X(t)\rangle = -i \int_0^t dv u = -i \left( [uv]_0^t - \int_0^t du v \right) \quad (\text{A.29})$$

$$\begin{aligned} &= -\frac{1}{\Delta_e} \mathbb{Q}H'\mathbb{P}|\Psi(t)\rangle + \overbrace{e^{-i\Delta_e(-\tau)} \mathbb{Q}H'\mathbb{P}|\Psi(0)\rangle}^{\text{RWA}} \\ &+ \int d\tau \mathbb{Q}H'\mathbb{P}|\dot{\Psi}\rangle \frac{1}{\Delta_e} e^{-i\Delta_e(t-\tau)}. \end{aligned} \quad (\text{A.30})$$

The second, fast oscillating term in equation (A.30) can be neglected in the rotating wave approximation (RWA). The last term in equation (A.30) leads with equation (A.20) to

$$\begin{aligned} &\int_0^t d\tau \mathbb{Q}H'\mathbb{P}|\dot{\Psi}\rangle \frac{1}{\Delta_e} e^{-i\Delta_e(t-\tau)} = \int_0^t d\tau \mathbb{Q}H'(-i)(\mathbb{P}H'\mathbb{P} + \mathbb{P}H'\mathbb{Q})|\Psi\rangle \frac{1}{\Delta_e} e^{-i\Delta_e(t-\tau)} \\ &= -i \underbrace{\int_0^t d\tau \mathbb{Q}H'\mathbb{P}H'\mathbb{P}|\Psi\rangle \frac{1}{\Delta_e} e^{-i\Delta_e(t-\tau)}}_{*1} - i \underbrace{\int_0^t d\tau \mathbb{Q}H'\mathbb{P}H'\mathbb{Q}|\Psi\rangle \frac{1}{\Delta_e} e^{-i\Delta_e(t-\tau)}}_{*2}. \end{aligned} \quad (\text{A.31})$$

The first integral in equation (A.31) denoted by  $*1$  can again be solved by partial integration

$$\begin{aligned} -i \int_0^t \underbrace{\mathbb{Q}H'\mathbb{P}H'\mathbb{P}|\Psi\rangle}_u \underbrace{\frac{1}{\Delta_e} e^{-i\Delta_e(t-\tau)} d\tau}_v &= - \left[ \mathbb{Q}H'\mathbb{P}H'\mathbb{P}|\Psi\rangle \frac{1}{\Delta_e^2} \right]_0^t \\ &+ \int_0^t d\tau \mathbb{Q}H'\mathbb{P}H'\mathbb{P}|\dot{\Psi}\rangle \frac{1}{\Delta_e^2} e^{-i\Delta_e(t-\tau)}. \end{aligned} \quad (\text{A.32})$$

As

$$\mathbb{P}H'\mathbb{P} = \delta a^\dagger a + \tilde{\Delta}_b |\downarrow\rangle\langle\downarrow| - \frac{A}{N} \frac{\sigma_z}{2} b^\dagger b + \frac{g_n}{2} (b|\downarrow\rangle\langle\uparrow| + \text{h.c.}) \quad (\text{A.33})$$

and

$$\mathbb{Q}H'\mathbb{P} = \frac{\Omega_c}{2} a|X\rangle\langle\downarrow| + \frac{\Omega_l}{2} |X\rangle\langle\uparrow|, \quad (\text{A.34})$$

both the first and the second term of equation (A.32) consist of terms of the order

$$\frac{1}{\Delta_e^2} \cdot \left\{ \frac{\Omega_c \sqrt{n} \delta n}{2}, \frac{\Omega_c \sqrt{n} \tilde{\Delta}_b}{2}, \frac{\Omega_l \delta}{2}, \frac{\Omega_l g_n}{4}, \frac{\Omega_c \sqrt{n} g_n}{4}, \frac{\Omega_c \sqrt{n} A}{4N}, \frac{\Omega_l A}{4N} \right\}. \quad (\text{A.35})$$

As the condition given by equation (A.18) holds, all terms given by equation (A.35) contain the product of two energies that are assumed to be much smaller than  $\Delta_e$ , so dividing these product by  $\Delta_e^2$  yields small values and thus the integral given by equation (A.32) can be neglected.

Using the expression given by equation (A.30)

$$|\Psi_X(t)\rangle = -\frac{1}{\Delta_e} \mathbb{Q}H'\mathbb{P}|\Psi(t)\rangle + \int d\tau \mathbb{Q}H'\mathbb{P}|\dot{\Psi}\rangle \frac{1}{\Delta_e} e^{-i\Delta_e(t-\tau)}, \quad (\text{A.36})$$

the second integral in equation (A.31), denoted by  $*^2$ , can be solved:

$$-i \int d\tau \mathbb{Q}H'\mathbb{P}H' \overbrace{\mathbb{Q}|\Psi\rangle}^{|\Psi_X\rangle} \frac{1}{\Delta_e} e^{-i\Delta_e(t-\tau)} \quad (\text{A.37})$$

$$= -i \int d\tau \mathbb{Q}H'\mathbb{P}H'\mathbb{Q} \left[ -\frac{1}{\Delta_e} \mathbb{Q}H'\mathbb{P}|\Psi(t)\rangle + \int d\tau' \mathbb{Q}H'\mathbb{P}|\dot{\Psi}\rangle \frac{1}{\Delta_e} e^{-i\Delta_e(\tau-\tau')} \right] \frac{1}{\Delta_e} e^{-i\Delta_e(t-\tau)}.$$

All terms in equation (A.38) are of the order of

$$\frac{1}{\Delta_e^2} \cdot \left\{ \left( \frac{\Omega_c \sqrt{n}}{2} \right)^2, \left( \frac{\Omega_l}{2} \right)^2 \right\}. \quad (\text{A.38})$$

With the same argument as used before, the integral given by equation (A.37) can be neglected.

Thus, the last part of equation (A.30) can be neglected, leading to

$$|\Psi_X(t)\rangle = -\frac{1}{\Delta_e} \mathbb{Q}H'\mathbb{P}|\Psi(t)\rangle. \quad (\text{A.39})$$

Now, the projection of the Schrödinger equation (A.30) onto the subspace of the electronic states can be written as

$$i\mathbb{P}|\dot{\Psi}\rangle = \mathbb{P}H'(\mathbb{P} + \mathbb{Q})|\Psi\rangle = (\mathbb{P}H'\mathbb{P} + \mathbb{P}H' \overbrace{\mathbb{Q}}^{|\Psi_X\rangle})|\Psi\rangle \quad (\text{A.40})$$

$$= \mathbb{P}H'\mathbb{P} - \mathbb{P}H'\mathbb{Q} \frac{1}{\mathbb{Q}H'\mathbb{Q}} \mathbb{Q}H'\mathbb{P}|\Psi\rangle \quad (\text{A.41})$$

$$= \mathbb{P}H'\mathbb{P} - \mathbb{P}H'\mathbb{Q} \frac{1}{\Delta_e} \mathbb{Q}H'\mathbb{P}|\Psi\rangle. \quad (\text{A.42})$$

Defining the projection of  $|\Psi\rangle$  on  $\mathbb{P}$  as

$$\mathbb{P}|\Psi\rangle = |\phi\rangle, \quad (\text{A.43})$$

equation (A.40) reads

$$i|\dot{\phi}\rangle = H_{\text{eff}}|\phi\rangle, \quad (\text{A.44})$$

where  $H_{\text{eff}}$  is given by

$$\begin{aligned} H_{\text{eff}} &= \mathbb{P}H'\mathbb{P} - \mathbb{P}H'\mathbb{Q}\frac{1}{\Delta_e}\mathbb{Q}H'\mathbb{P}|\Psi\rangle \\ &= \tilde{\Delta}_b|\downarrow\rangle\langle\downarrow| + \delta a^\dagger a + \frac{A}{N}\frac{\sigma_z}{2}b^\dagger b + \frac{g_n}{2}(b^\dagger|\downarrow\rangle\langle\uparrow| + \text{h.c.}) \\ &\quad - \left(\frac{\Omega_c}{2}a^\dagger|\downarrow\rangle\langle X| + \frac{\Omega_l}{2}|\uparrow\rangle\langle X|\right)\frac{1}{\Delta_e}\left(\frac{\Omega_c}{2}a|X\rangle\langle\downarrow| + \frac{\Omega_l}{2}|X\rangle\langle\uparrow|\right), \end{aligned} \quad (\text{A.45})$$

which yields

$$\begin{aligned} H_{\text{eff}} &= \delta a^\dagger a + \left(\tilde{\Delta}_b - \frac{\Omega_c^2}{4\Delta_e}a^\dagger a - \frac{A}{2N}b^\dagger b\right)|\downarrow\rangle\langle\downarrow| - \left(\frac{\Omega_l^2}{4\Delta_e} - \frac{A}{2N}b^\dagger b\right)|\uparrow\rangle\langle\uparrow| \\ &\quad - g_a(a|\uparrow\rangle\langle\downarrow| + \text{h.c.}) + \frac{g_n}{2}(b^\dagger|\downarrow\rangle\langle\uparrow| + \text{h.c.}), \end{aligned} \quad (\text{A.46})$$

where

$$g_a = \frac{\Omega_c\Omega_l}{4\Delta_e}. \quad (\text{A.47})$$

Shifting the energy by adding  $\frac{\Omega_l^2}{4\Delta_e}\mathbb{1}$ , leads to

$$\begin{aligned} H_{\text{eff}}'' &= \delta a^\dagger a + \left(\tilde{\Delta}_b - \frac{\Omega_c^2}{4\Delta_e}a^\dagger a - \frac{A}{2N}b^\dagger b + \frac{\Omega_l^2}{4\Delta_e}\right)|\downarrow\rangle\langle\downarrow| + \frac{A}{2N}b^\dagger b|\uparrow\rangle\langle\uparrow| \\ &\quad + \frac{g_n}{2}(b^\dagger|\downarrow\rangle\langle\uparrow| + \text{h.c.}) - g_a(a|\uparrow\rangle\langle\downarrow| + \text{h.c.}) \end{aligned} \quad (\text{A.48})$$

### A.3 Adiabatic elimination of the electronic states

To get an effective interaction between light and nuclear spins, we want to adiabatically eliminate the electronic spin-down state  $|\downarrow\rangle$  by projecting the Schrödinger equation on the subspace of the electronic spin-up state  $|\uparrow\rangle$ . This can be done, if the splitting of the electronic states is large compared to the couplings  $g_a$  and  $g_n$ , i.e., if condition

$$|\Delta_2| \gg |g_a|, |g_n| \quad (\text{A.49})$$

holds, where

$$\Delta_2 = \tilde{\Delta}_b - \frac{\Omega_c^2}{4\Delta_e}n - \frac{A}{2N}n_k + \frac{\Omega_l^2}{4\Delta_e}, \quad (\text{A.50})$$

with  $n$  denoting the photon number and  $n_k$  the number of nuclear spins flipped with respect to the polarized sample.

Defining the projectors  $\mathbb{P}'$  and  $\mathbb{Q}'$  by

$$\mathbb{P}' = |\uparrow\rangle\langle\uparrow| \quad (\text{A.51})$$

$$\mathbb{Q}' = 1 - \mathbb{P}' = |\downarrow\rangle\langle\downarrow| \quad (\text{A.52})$$

and projecting the Schrödinger equation on the electron spin-up subspace

$$i\mathbb{P}'|\dot{\Psi}\rangle = \mathbb{P}'H''_{\text{eff}}\overbrace{(\mathbb{P}' + \mathbb{Q}')}^{\mathbb{1}}|\Psi\rangle, \quad (\text{A.53})$$

where  $H''_{\text{eff}}$  is the Hamiltonian given by equation (A.48), the effective Hamiltonian

$$\tilde{H}_{\text{eff}} = \mathbb{P}'H''_{\text{eff}}\mathbb{P}' - \mathbb{P}'H''_{\text{eff}}\mathbb{Q}'\frac{1}{\mathbb{Q}'H''_{\text{eff}}\mathbb{Q}'}\mathbb{Q}'H''_{\text{eff}}\mathbb{P}' \quad (\text{A.54})$$

can be derived in the same way as it has been done for the adiabatic elimination of the trion. With

$$\Delta_2 = \mathbb{Q}'H''_{\text{eff}}\mathbb{Q}' = \tilde{\Delta}_b - \frac{\Omega_c^2}{4\Delta_e}\langle a^\dagger a \rangle - \frac{A}{2N}\langle b^\dagger b \rangle + \frac{\Omega_l^2}{4\Delta_e}, \quad (\text{A.55})$$

$\tilde{H}_{\text{eff}}$  is given by

$$\begin{aligned} \tilde{H}_{\text{eff}} &= \delta a^\dagger a - \left(\frac{g_n}{2}b - g_a a\right)\frac{1}{\Delta_2}\left(\frac{g_n}{2}b^\dagger - g_a a^\dagger\right) \\ &= \delta a^\dagger a - \frac{g_a^2}{\Delta_2}aa^\dagger - \frac{g_n^2}{4\Delta_2}bb^\dagger + \frac{g_n g_a}{2\Delta_2}(a^\dagger b + \text{h.c.}). \end{aligned} \quad (\text{A.56})$$

With a shift of  $\frac{g_a^2}{\Delta_2}\mathbb{1}$ , we finally obtain

$$\tilde{H}_{\text{eff}} = \left(\delta - \frac{g_a^2}{\Delta_2}\right)a^\dagger a - \frac{g_n^2}{4\Delta_2}bb^\dagger + \frac{g_n g_a}{2\Delta_2}(a^\dagger b + \text{h.c.}) \quad (\text{A.57})$$

where  $g_a = \frac{\Omega_l \Omega_c}{4\Delta_e}$ .



# Appendix B

## Gaussian states and transformations

### B.1 Preliminaries

We consider a quantum system consisting of  $N$  canonical (bosonic) degrees of freedom (or modes) in phase space  $\mathbb{R}^{2N}$ , described by the vector

$$R = (R_1, \dots, R_{2N}) = (X_1, \dots, X_N, P_1, \dots, P_N) \quad (\text{B.1})$$

of the position and momentum operators (field quadratures). The canonical commutation relations for the  $R_i$  read

$$[R_k, R_l] = i\sigma_{k,l}\mathbb{1}, \quad (\text{B.2})$$

where the skew symmetric, block diagonal  $2N \times 2N$ -matrix  $\sigma$  is given by

$$\sigma = \begin{pmatrix} 0 & \mathbb{1}_N \\ -\mathbb{1}_N & 0 \end{pmatrix}. \quad (\text{B.3})$$

Here,  $\mathbb{1}_N$  is the  $N$ -dimensional identity matrix. The structure of  $\sigma$  reflects that the position and momentum operators of the same mode do not commute. It is called symplectic matrix. The annihilation and creation operators  $a_i$  and  $a_i^\dagger$ ,  $i = 1 \dots N$  are related to the field quadratures of each mode by the relation

$$X_i = (a_i + a_i^\dagger)/\sqrt{2}, \quad P_i = -i(a_i - a_i^\dagger)/\sqrt{2}. \quad (\text{B.4})$$

They obey the standard commutation relations

$$[a_l, a_k^\dagger] = \delta_{lk}\mathbb{1} \quad \text{and} \quad [a_l, a_k] = [a_l^\dagger, a_k^\dagger] = 0. \quad (\text{B.5})$$

Equation (B.1) and  $(a_1, \dots, a_N, a_1^\dagger, \dots, a_N^\dagger)$  are related by

$$(a_1, \dots, a_N, a_1^\dagger, \dots, a_N^\dagger)^T = \Omega(X_1, \dots, X_N, P_1, \dots, P_N)^T, \quad (\text{B.6})$$

where the unitary matrix  $\Omega$  is given by

$$\Omega = \frac{1}{\sqrt{2}} \begin{pmatrix} \mathbb{1}_N & i\mathbb{1}_N \\ \mathbb{1}_N & -i\mathbb{1}_N \end{pmatrix}. \quad (\text{B.7})$$

A useful tool for the description of states in phase space are the Weyl or displacement operators defined by

$$W_\xi = e^{i\xi^T \sigma R} \quad (\text{B.8})$$

with  $\xi \in \mathbb{R}^{2N}$ . Weyl operators satisfy the Weyl relations

$$W_\xi W_\eta = e^{-\frac{i}{2}\xi^T \sigma \eta} W_{\xi+\eta}, \quad (\text{B.9})$$

which constitute the exponentiated form of the commutation relations.

Weyl operators correspond to translations in phase space, which is reflected in the relation

$$W_\xi R_k W_\xi^* = R_k + \xi_k \mathbb{1}. \quad (\text{B.10})$$

The state of a system with canonical coordinates can be specified by a suitable phase space function. One such function is the characteristic function which completely determines a state given by its density operator  $\rho$ . It is defined by the expectation value of the Weyl operator

$$\chi(\xi) = \text{tr}[W_\xi \rho]. \quad (\text{B.11})$$

## B.2 Gaussian states

Gaussian states, i.e., states with Gaussian characteristic functions, play a central role in continuous variable systems as they are the most easily prepared states currently used in continuous-variable quantum computation and quantum communication. Important examples for Gaussian states are vacuum, coherent, squeezed, thermal and squeezed-thermal states of the electromagnetic field. Gaussian states are fully characterized by the first and second moments of the canonical operators. The first moments are the expectation values of the canonical coordinates, the displacement, given by

$$d_k = \text{tr}[\rho R_k]. \quad (\text{B.12})$$

The second moments are embodied in the covariance matrix having the entries

$$\gamma_{kl} := \langle R_i R_j + R_j R_i \rangle - 2\langle R_i \rangle \langle R_j \rangle. \quad (\text{B.13})$$

Note that not every matrix  $\gamma$  is the covariance matrix of a physical state. The covariance matrix of a physical state has to be real, symmetric and has to fulfill<sup>1</sup>

$$\gamma + i\sigma \geq 0, \quad (\text{B.14})$$

---

<sup>1</sup>There exist other equivalent conditions

which is the Heisenberg uncertainty principle expressed in a basis independent way.

Let us define Gaussian states now:

*A state  $\rho$  is called Gaussian or quasifree, if its characteristic function is a Gaussian function in phase space, i.e., if it is of the form*

$$\chi(\rho) = \exp(-\xi^T \gamma \xi / 4 + i d^T \xi). \quad (\text{B.15})$$

A Gaussian state with covariance matrix  $\gamma$  is pure iff one of the following (equivalent) five conditions holds:

- (i)  $\det(\gamma) = 1$
- (i)  $\text{rank}[\gamma + i\sigma] = N$
- (iii)  $(\gamma^{-1}\sigma)^2 = -\mathbb{1}$ .

Examples for pure Gaussian states that are used within the present work are coherent states and squeezed states which will be studied in more detail in the following.

### B.2.1 Coherent states

Coherent states are right eigenvectors of the annihilation operator

$$a|\alpha\rangle = \alpha|\alpha\rangle, \quad \alpha \in \mathbb{C}. \quad (\text{B.16})$$

They can be expanded in terms of number states

$$|\alpha\rangle = \exp\left(-\frac{|\alpha|^2}{2}\right) \sum_{n=0}^{\infty} \frac{\alpha^n}{\sqrt{n!}} |n\rangle. \quad (\text{B.17})$$

As it can be seen for example in [42], expression (B.17) can be rewritten in the form

$$|\alpha\rangle = D(\alpha)|0\rangle, \quad (\text{B.18})$$

where the displacement operator  $D(\alpha) = e^{a\alpha^\dagger - \alpha^*a}$  is acting on the vacuum state  $|0\rangle$ . The covariance matrix of a coherent state is given by the covariance matrix of the vacuum state

$$\gamma = \mathbb{1} \quad (\text{B.19})$$

and the displacement

$$d_a = (\langle a \rangle, \langle a^\dagger \rangle) = (\alpha, \alpha^*), \quad (\text{B.20})$$

in terms of the annihilation and creation operators  $a$  and  $a^\dagger$ . Thus, like all Gaussian states, the coherent state can be fully described by its first and second moments given by

$$(\gamma, d_a) = (\mathbb{1}, \alpha). \quad (\text{B.21})$$

This reflects the relation given in equation (B.18), where the coherent state is described by a displacement operator acting on the vacuum.

Using the relation introduced in equation (B.6), the displacement operator in terms of  $R_k$  is simply given by

$$d_R = \Omega^\dagger d_a = \sqrt{2}(\operatorname{Re}(\alpha), \operatorname{Im}(\alpha))^T. \quad (\text{B.22})$$

### B.2.2 Squeezed states

**Squeezing criterion:** *A state of  $N$  modes with covariance matrix  $\gamma$  is squeezed iff  $\gamma$  has at least one eigenvalue smaller than one.*

The covariance matrix of a squeezed state written in terms of  $R_k$  is given by

$$\gamma = R(\theta)^T \begin{pmatrix} e^{-2r} & 0 \\ 0 & e^{2r} \end{pmatrix} R(\theta), \quad (\text{B.23})$$

where

$$R = \begin{pmatrix} \cos(\theta) & -\sin(\theta) \\ \sin(\theta) & \cos(\theta) \end{pmatrix} \quad (\text{B.24})$$

is a rotation by  $\theta$  in the phase plane.

For  $d = 0$ , the states are called squeezed vacuum states. In such a state the variance of the operator  $X_\theta := \cos(\theta)X + \sin(\theta)P$  is reduced, whereas the variance in  $P_\theta$  is increased by the same factor, so that their product yields the minimum value of the uncertainty relation

$$\langle(\Delta X_\theta)^2\rangle\langle(\Delta P_\theta)^2\rangle = \frac{1}{4}. \quad (\text{B.25})$$

A squeezed state with  $d > 0$  is obtained if one of the variances is smaller than  $\frac{1}{4}$

$$\langle(\Delta Y)^2\rangle < \frac{1}{4}, \quad (\text{B.26})$$

where  $\Delta Y \in \{\Delta X_\theta, \Delta P_\theta\}$ .

## B.3 Gaussian unitaries

The simplest Gaussian channel is a *lossless* unitary evolution. A Gaussian unitary transformation is of the form

$$\rho \rightarrow U\rho U^\dagger, \quad U = e^{(\frac{i}{2}\sum_k H_{k,l}R_kR_l)}, \quad (\text{B.27})$$

with  $H$  being a real symmetric  $2N \times 2N$  matrix. Such unitaries correspond to a representation of the real symplectic group  $SP(2N, \mathbb{R})$ . It is formed by those real matrices for which

$$S\sigma S^T = \sigma, \quad (\text{B.28})$$

i.e., by linear transformations that preserve the commutation relations. Thus, the unitary is given by  $S = e^{H\sigma}$ . The covariance matrix and the displacement of the transformed state are given by

$$(S\gamma S^T, S^T d). \quad (\text{B.29})$$

Two different scenarios, namely passive and active transformations will be studied in the following.

### B.3.1 Passive transformations

In an optical context, Gaussian unitaries that preserve the total photon number are called passive transformations. Prominent examples are beam splitters and phase shifters.

**Beamsplitter:** A beamsplitter interferes two input modes and creates two output modes. The beamsplitter Hamiltonian is given by

$$H = \pm\theta(X_2P_1 - X_1P_2). \quad (\text{B.30})$$

The corresponding unitary  $S_{\text{BS}}$  is given by

$$S_{\text{BS}} = \begin{pmatrix} \cos(\theta) & \sin(\theta) & 0 & 0 \\ -\sin(\theta) & \cos(\theta) & 0 & 0 \\ 0 & 0 & \cos(\theta) & \sin(\theta) \\ 0 & 0 & -\sin(\theta) & \cos(\theta) \end{pmatrix}, \quad (\text{B.31})$$

where  $T = \cos(\theta)$  is the transmittivity and  $R = \sin\theta$  the reflectivity of the beam splitter. The transformations on  $R_k$  can thus be written as

$$X_{out1} = TX_1 + RX_2 \quad (\text{B.32})$$

$$X_{out2} = -RX_1 + TX_2 \quad (\text{B.33})$$

$$P_{out1} = TP_1 + RP_2 \quad (\text{B.34})$$

$$P_{out2} = -RP_1 + TP_2. \quad (\text{B.35})$$

**Phase shift:** A phase shifter changes either the relative phase between two spatial modes or the phase between two orthogonal modes in the same spatial direction.

The Hamiltonian is given by

$$H = \phi(X^2 + P^2) \quad (\text{B.36})$$

The corresponding unitary  $S_{\text{PS}}$  is given by

$$S_{\text{PS}} = \begin{pmatrix} \cos(\phi) & \sin(\phi) \\ -\sin(\phi) & \cos(\phi) \end{pmatrix}. \quad (\text{B.37})$$

### B.3.2 Active transformations

Gaussian unitaries that do not preserve the total photon number are called active transformations. The most prominent example is squeezing.

**Squeezer:** *Single mode-squeezing* is usually done by using a degenerate optical amplifier that is pumped by a strong field and produces two modes which both have half the pump-frequency, called the signal and the idler modes. The Hamiltonian is given by

$$H = \pm r(XP + PX) \quad (\text{B.38})$$

with squeezing parameter  $r$  (more general, the squeezing parameter is given by  $\xi = re^{i\theta}$ . Here we consider  $\theta = 0$ ). The corresponding unitary  $S_{\text{SQ}}$  is given by

$$S_{\text{SQ}} = \begin{pmatrix} e^{\pm r} & 0 \\ 0 & e^{\mp r} \end{pmatrix}. \quad (\text{B.39})$$

The transformations on  $R_k$  can be written as

$$X_{\text{out}} = e^{+r} X \quad (\text{B.40})$$

$$P_{\text{out}} = e^{-r} P. \quad (\text{B.41})$$

The effect of the squeezing operator on an arbitrary pair of quadratures is the attenuation of one quadrature and the amplification of the other. Using  $r \geq 0$ , the position mode is squeezed and the momentum mode is stretched.

In terms of annihilation and creation operators these relations read

$$a_{\text{out}} = a \cosh(r) + a^\dagger \sinh(r) \quad (\text{B.42})$$

$$a_{\text{out}}^\dagger = a^\dagger \cosh(r) + a \sinh(r), \quad (\text{B.43})$$

which correspond to the output state of degenerate parametric amplification, in which signal and idler frequencies both equal half the pump frequency. The corresponding Hamiltonian reads

$$H = i \frac{r}{2} ((a^\dagger)^2 - a^2). \quad (\text{B.44})$$

*Two-mode squeezing:* The two-mode squeezing Hamiltonian in terms of  $R_k$  is given by

$$H = 2r (X_1 P_2 + X_2 P_1). \quad (\text{B.45})$$

The quadrature operators of the two-mode state can be written as

$$X_{\text{out},1} = \frac{1}{\sqrt{2}}(X_1 e^r + X_2 e^{-r}) \quad (\text{B.46})$$

$$P_{\text{out},1} = \frac{1}{\sqrt{2}}(P_1 e^{-r} + P_2 e^r) \quad (\text{B.47})$$

$$X_{\text{out},2} = \frac{1}{\sqrt{2}}(X_1 e^r - X_2 e^{-r}) \quad (\text{B.48})$$

$$P_{\text{out},2} = \frac{1}{\sqrt{2}}(P_1 e^{-r} - P_2 e^r) \quad (\text{B.49})$$

The individual quadratures  $X_{out,1}$ ,  $P_{out,1}$  become very noisy for large squeezing  $r$ , however, the relative position and the total momentum become sharp

$$X_{out,1} - X_{out,2} = \sqrt{2}e^{-r} X_2 \quad (\text{B.50})$$

$$P_{out,1} + P_{out,2} = \sqrt{2}e^{-r} P_1. \quad (\text{B.51})$$

The Hamiltonian in terms of the annihilation and creation operators reads

$$H = ir \left( a_1^\dagger a_2^\dagger - a_1 a_2 \right). \quad (\text{B.52})$$

A two-mode squeezed state produced by parametric down-conversion, where  $a_1$  and  $a_2$  refer to the signal and idler modes emerging at two sidebands around half the pump frequency and having different polarizations, is utilized by quantum teleportation protocols [61]. The annihilation and creation operators of the two-mode squeezed state read

$$a_{out,1} = a_1 \cosh(r) + a_2^\dagger \sinh(r) \quad (\text{B.53})$$

$$a_{out,2} = a_2 \cosh(r) + a_1^\dagger \sinh(r). \quad (\text{B.54})$$

Two-mode squeezed states are bipartite entangled states. In the following Sections, some properties of bipartite Gaussian states and entanglement of Gaussian states will be reviewed.

## B.4 Bipartite Gaussian states

In the foregoing chapter an example for a pair of entangled systems shared by two parties, a bipartite state, has been considered. Two systems held by two different parties live on the space that is spanned by the tensor product of the Hilbert spaces of the two systems. In phase space, the tensor product structure of the Hilbert space corresponds to the direct sum of the phase space of those systems. Thus, a covariance matrix  $\gamma$  of a bipartite system, where system I is composed of  $N$  modes and system II of  $M$  modes, corresponds to a  $2N + 2M$  square matrix which can be written as

$$\gamma = \begin{pmatrix} A & C \\ C^T & B \end{pmatrix}. \quad (\text{B.55})$$

Here,

$$A_{X_1, P_1} = \begin{pmatrix} 2\langle X_1^2 \rangle & \langle \{X_1 P_1\} \rangle \\ \langle \{X_1 P_1\} \rangle & 2\langle P_1^2 \rangle \end{pmatrix}, \quad A_{a, a^\dagger} = \Omega A \Omega^\dagger = \begin{pmatrix} \langle a a^\dagger \rangle & \langle a a \rangle \\ \langle a^\dagger a^\dagger \rangle & \langle a^\dagger a \rangle \end{pmatrix} \quad (\text{B.56})$$

is a  $2N$  covariance matrix describing the reduced state of system I, expressed in quadrature operators and annihilation and creation operators, respectively, where  $\langle \{ab\} \rangle = \langle ab + ba \rangle$ .

$$B_{X_2, P_2} = \begin{pmatrix} 2\langle X_2^2 \rangle & \langle \{X_2 P_2\} \rangle \\ \langle \{X_2 P_2\} \rangle & 2\langle P_2^2 \rangle \end{pmatrix}, \quad B_{b, b^\dagger} = \Omega B \Omega^\dagger = \begin{pmatrix} \langle bb^\dagger \rangle & \langle bb \rangle \\ \langle b^\dagger b^\dagger \rangle & \langle b^\dagger b \rangle \end{pmatrix} \quad (\text{B.57})$$

is a  $2M$  covariance matrix describing the reduced state of system II, and

$$C_{X_1, P_1, X_2, P_2} = \begin{pmatrix} 2\langle X_1 X_2 \rangle & \langle X_1 P_2 \rangle \\ \langle P_1 X_2 \rangle & 2\langle P_1 P_2 \rangle \end{pmatrix}, \quad C_{a, a^\dagger, b, b^\dagger} = \Omega C \Omega^\dagger = \begin{pmatrix} \langle ab^\dagger \rangle & \langle ab \rangle \\ \langle a^\dagger b^\dagger \rangle & \langle a^\dagger b \rangle \end{pmatrix} \quad (\text{B.58})$$

is a  $2N \times 2M$  covariance matrix describing the (quantum and classical) correlations between system I and II. The displacement  $d$  of the bipartite system is given by the direct sum of the displacements of system I and II:

$$d = d_I \oplus d_{II}. \quad (\text{B.59})$$

When studying properties of bipartite (or multipartite) systems, local equivalence is an important concept. It is defined as follows:

**Definition:** *Two states  $\rho, \rho'$  on  $\mathcal{H}_A \otimes \mathcal{H}_B$  are called locally equivalent if there exist unitaries  $U_A, U_B$  on  $\mathcal{H}_A, \mathcal{H}_B$ , respectively, such that  $\rho' = U_A \otimes U_B \rho U_A^\dagger \otimes U_B^\dagger$ .*

Locally equivalent states have identical entanglement properties. An example are Gaussian states that have identical covariance matrices but different displacements. They can be converted into each other by local displacement operations.

It has been shown by Duan, Giedke et al. (2000)[62] and Simon (2000)[45] that every covariance matrix of a bipartite Gaussian state can be transformed by local quasifree transformations into a standard form. The one proposed by Simon reads

$$\gamma = \begin{pmatrix} a & 0 & c & 0 \\ 0 & a & 0 & c' \\ c & 0 & b & 0 \\ 0 & c' & 0 & b \end{pmatrix}. \quad (\text{B.60})$$

An important example for a covariance matrix in the standard form is the covariance matrix of a two-mode squeezed state. In terms of the quadrature operators  $R_k$  it is given by

$$\gamma_s = \begin{pmatrix} \cosh(2r) & 0 & \sinh(2r) & 0 \\ 0 & \cosh(2r) & 0 & -\sinh(2r) \\ \sinh(2r) & 0 & \cosh(2r) & 0 \\ 0 & -\sinh(2r) & 0 & \cosh(2r) \end{pmatrix}. \quad (\text{B.61})$$

In terms of the annihilation and creation operators  $a$  and  $a^\dagger$  it reads:

$$\gamma'_s = \Omega \gamma_s \Omega^\dagger = \begin{pmatrix} \cosh(2r) & 0 & 0 & \sinh(2r) \\ 0 & \cosh(2r) & \sinh(2r) & 0 \\ 0 & \sinh(2r) & \cosh(2r) & 0 \\ \sinh(2r) & 0 & 0 & \cosh(2r) \end{pmatrix}. \quad (\text{B.62})$$

As already mentioned before, a two-mode squeezed state is an entangled state. Entanglement of Gaussian states will be studied in Appendix C.



# Appendix C

## Entanglement

Entanglement can be considered to be the most nonclassical manifestation of the quantum formalism. Classically, complete knowledge of a system composed of two subsystems implies complete information on the state of the subsystems. In quantum mechanics however, there exist states for which the complete knowledge of a composite system does not mean knowledge of its subsystems. It might even happen that the state of the subsystem is completely undetermined. This is the case for maximally entangled states. Let us formally define entanglement now:

Consider  $n$  quantum systems  $V_1, \dots, V_n$  with the corresponding Hilbert spaces given by  $H_{V_1}, \dots, H_{V_n}$ . The Hilbert space of the total system  $H$  is given by the tensor product  $H = H_{V_1} \otimes H_{V_2} \otimes \dots \otimes H_{V_n}$ . The state of a system composed of several subsystems can be written in the form

$$|\psi\rangle = \sum_{i_1, \dots, i_n} b_{i_1, \dots, i_n} |\varphi_{i_1}\rangle \otimes |\varphi_{i_2}\rangle \otimes \dots \otimes |\varphi_{i_n}\rangle \quad (\text{C.1})$$

with  $|\varphi_{i_j}\rangle \in H_{V_j}$ . In general  $|\psi\rangle$  is not a product of states  $|\psi_j\rangle \in H_{V_j}$  of the subsystems,  $|\psi\rangle \neq |\psi_1\rangle \otimes |\psi_2\rangle \otimes \dots \otimes |\psi_n\rangle \equiv |\psi_1 \psi_2 \dots \psi_n\rangle$ . In this case it is in an entangled state and entanglement can be defined as follows:

**Entanglement** *A pure state of a composed quantum system is called entangled if it cannot be written as a product of states of the individual subsystems.*

A simple example for an entangled state is the singlet state

$$|\psi\rangle = \frac{|01\rangle - |10\rangle}{\sqrt{2}}, \quad (\text{C.2})$$

where  $|0\rangle$  and  $|1\rangle$  are orthonormal states.

In case of mixed states, the situation is more difficult and entanglement is not equivalent to being non-product. Rather, a mixed state  $\rho$  of  $n$  subsystems is called

entangled if it cannot be written as a convex combination of product states [63]:

$$\rho \neq \sum_i a_i \rho_{i_1} \otimes \rho_{i_2} \otimes \cdots \otimes \rho_{i_n}. \quad (\text{C.3})$$

In the following we will focus on bipartite systems.

For pure bipartite systems, to determine whether a system is entangled or not, one has to consider the Schmidt decomposition [64]. If the system has more than one Schmidt coefficient it is entangled.

For mixed states it is much harder to determine whether a state is entangled or not. A range of entanglement criteria has been developed in recent years. The entanglement criteria that will be discussed in the following are the partial transposition criterion and its generalization to arbitrary positive maps. Moreover an entanglement measure, namely the logarithmic negativity, will be considered.

## C.1 The positive partial transpose criterion

The partial transposition criterion was provided by A. Peres (1996) [65]. It is called "positive partial transpose" (ppt) and requires the following definition.

**Partial transpose:** *The quantum state of a bipartite system be given in terms of the density operator  $\rho$ . Let the matrix elements of  $\rho$  in a particular basis be  $\langle m\mu|\rho|n\nu\rangle$ , with  $|m\rangle, |n\rangle$  and  $|\mu\rangle, |\nu\rangle$  as basis vectors of the first and second subsystem respectively: The density operator  $\rho^{T_2}$  with matrix elements*

$$\langle m\mu|\rho^{T_2}|n\nu\rangle \equiv \langle m\nu|\rho|n\mu\rangle$$

*is called the partial transpose of  $\rho$  with respect to the second subsystem.*

Note that although the partial transposition depends on the basis in which  $\rho$  is written, the eigenvalues of  $\rho^{T_2}$  are basis independent. With this definition, the ppt criterion can be formulated as follows:

**Positive partial transpose criterion:**  $\rho$  separable  $\Rightarrow \rho^{T_2} = \sum_i p_i \rho_{i_1} \otimes \rho_{i_2}^T$  and  $\rho^{T_2} \geq 0$ .

This means that entanglement of a bipartite state  $\rho$  can easily be detected by finding the eigenvalues of its partial transposition  $\rho^{T_2}$ . If at least one of them is negative, the system is entangled. Note, that bipartite systems are considered here. For arbitrary dimension, the ppt criterion is only *sufficient* but not *necessary*. Only for the special cases of  $\mathcal{C}^2 \otimes \mathcal{C}^2$  and  $\mathcal{C}^2 \otimes \mathcal{C}^3$  it is sufficient and necessary [66]. The partial transpose can be seen as a time reversal on one subsystem. Thus, the ppt criterion has a physical interpretation in the sense that separable states do not

correlate local time flows. If the time reversal on just one subsystem leads to a non-physical state of the total system, the time flows must have been correlated and the state entangled.

## C.2 Positive maps and entangled states

The ppt criterion is a special case that can be deduced from a more general theorem which was proven by M.&P.&R.Horodecki [66] and reads:

**Separability condition with positive maps** *A state  $\rho \in \mathcal{B}(\mathcal{H}_a \otimes \mathcal{H}_b)$  (where  $\mathcal{B}(\mathcal{H})$  is the space of operators, also having Hilbert space structure) is separable iff for any positive map<sup>1</sup>  $\epsilon : \mathcal{B}(\mathcal{H}_b) \rightarrow \mathcal{B}(\mathcal{H}_c)$  we have*

$$(\mathbb{1}_a \otimes \epsilon) \rho \geq 0. \quad (\text{C.4})$$

Obviously transposition  $T$  is a positive map, thus the partial transposition is of the form  $(\mathbb{1}_a \otimes \epsilon)$ .

Next, the Jamiołkowski isomorphism is introduced.

**Jamiołkowski isomorphism** [64]: *"Given an operator  $E \in \mathcal{B}(\mathcal{H}_B \otimes \mathcal{H}_C)$  we define a map by*

$$\epsilon : \mathcal{B}(\mathcal{H}_B) \rightarrow \mathcal{B}(\mathcal{H}_C), \quad (\text{C.5})$$

where

$$\epsilon(\rho) = \text{tr}_B(E\rho^{T_B}). \quad (\text{C.6})$$

*This shows how to construct the map  $\epsilon$  from the given operator  $E$ . To construct an operator from a given map we use the state*

$$|\Phi^+\rangle = \frac{1}{\sqrt{D}} \sum_{i=1}^D |i\rangle_{B'} |i\rangle_B \quad (\text{C.7})$$

(where  $D = \dim \mathcal{H}_B$ ) to get

$$D(\mathbb{1}_{B'} \otimes \epsilon)(|\Phi^+\rangle\langle\Phi^+|) = E. \quad (\text{C.8})$$

This "1-1" relation between maps and operators has the property that:

*$E \geq 0$  iff  $\epsilon$  is a completely positive map.*

---

<sup>1</sup>A linear self-adjoint map  $\epsilon$  is called positive if  $\forall \rho \in \mathcal{B}(\mathcal{H}), \rho \geq 0 \implies \epsilon(\rho) \geq 0$ . A positive map therefore maps positive operators onto positive operators.

### C.3 Entanglement measures

For the *quantification* of entanglement of mixed states, several criteria exist that measure entanglement. Examples are the *entanglement cost* [67], which measures the asymptotic entanglement of the pure state that is required to create  $\rho$  and the *entanglement of distillation*, which measures the entanglement that can asymptotically be extracted from  $\rho$  by local operations and classical communication (LOCC) [68].

However, for practical applications, computable measures have to be found. An example for a computable measure is the *concurrence* proposed by Wootters [69]. Another criterion that is computable and can be equally well applied to pure and mixed states is the *negativity* and *logarithmic negativity* that has been derived by Vidal and Werner (2002) [44]. It is based on the trace norm of the partial transpose  $\rho^{T_1}$  of a bipartite system and reads as follows:

**Logarithmic negativity:**

$$E_{\mathcal{N}}(\rho) = \log_2 \|\rho^{T_1}\|_1 \quad (\text{C.9})$$

where  $\|\cdot\|_1$  denotes the trace norm.

It expresses the degree to which the partial transpose of a state fails to be positive and is thus a quantitative version of Peres' ppt criterion. While  $E_{\mathcal{N}}$  is not convex, it was recently proven to be nonincreasing under positive partial transpose preserving operations, of which LOCC operations are a subset. Therefore it is a good entanglement measure [70]. The logarithmic negativity for Gaussian states is used in the present work and will be discussed in Section C.4.3.

### C.4 Entanglement of Gaussian states

One might think that the characterization of entanglement of continuous variables is a much more difficult task than the one for finite dimensional systems. However, it turns out that for the special class of continuous variable states, the Gaussian entangled states, the theoretical description simplifies a lot. Here we focus on bipartite entanglement of both pure and mixed Gaussian states.

The prime example for an entangled Gaussian state is the pure two-mode squeezed state, described by the covariance matrix given by equation (B.61).

Instead of the continuous variable basis, it may also be written in the discrete photon number (Fock) basis.

$$\sqrt{1-\lambda} \sum_{n=0}^{\infty} \lambda^{n/2} |n\rangle |n\rangle \quad (\text{C.10})$$

where  $\lambda = (\tanh(r))^2$ . Equation (C.10) shows that the two modes of the two-mode squeezed state are also quantum correlated in photon number. For  $r \rightarrow \infty$ ,  $\tanh(r) \rightarrow 1$  and the two-mode squeezed state of equation (C.10) approaches a *maximally* entangled state. For finite  $r$  the two-mode squeezed state is a nonmaximally entangled state.

### C.4.1 Pure entangled Gaussian states

As any bipartite pure multimode Gaussian state corresponds to a tensor product of pure two-mode squeezed states up to local Gaussian unitary transformations [71], its entanglement can be quantified via the partial von Neumann entropy [32]. This will not be discussed in more detail as it goes beyond the scope of this work.

### C.4.2 Mixed entangled Gaussian states

As it has been discussed in Section C.1, the partial transpose criterion can be used to decide whether a state is entangled or not. The question is now, how it can be applied to Gaussian states. Transposition of a hermitian density operator corresponds to complex conjugation, and complex conjugation of a quantum system described by the Schrödinger equation is equivalent to time reversal,  $i\partial/\partial t \rightarrow -i\partial/\partial t$ . Thus it can be seen, that transposition of a density operator means time reversal. This has already been mentioned in Section C.1. For continuous variable systems, time reversal corresponds to a sign change of the momentum variable [45]. In phase space, this transformation corresponds to

$$\xi^T \rightarrow \Gamma \xi^T = (X_1, -P_1, X_2, -P_2, \dots, X_N, -P_N)^T. \quad (\text{C.11})$$

The second-moment covariance matrix (the first moment, i.e., the displacement does not affect the entanglement properties of the system as mentioned before) transforms according to

$$\gamma \rightarrow \Gamma \gamma \Gamma. \quad (\text{C.12})$$

For the *partial* transposition of a bipartite Gaussian system, the transformation corresponds to

$$\Gamma_A = \Gamma_A \otimes \mathbb{1}_B, \quad (\text{C.13})$$

meaning that the sign of the momentum variables of system A changes, whereas system B is left unchanged.

The continuous-variable version of Peres' ppt criterion is given by

$$\Gamma_A \gamma_{AB} \Gamma_A \not\geq i\sigma, \quad (\text{C.14})$$

which is a sufficient condition for system A and B to be entangled. For Gaussian states and if both systems A and B have only one mode, i.e., their covariance matrices are  $2 \times 2$  matrices, or if one system has one mode and the other one has arbitrary many modes, condition (C.14) is necessary and sufficient [72].

### C.4.3 Entanglement measure for Gaussian states

In Section C.3 the logarithmic negativity has been introduced. Here, it will be discussed for the special case of bipartite Gaussian states [44].

**Logarithmic negativity of bipartite Gaussian states** *Let  $\rho$  be a Gaussian density operator with covariance matrix  $\gamma$ , and let  $(\tilde{c}_1, \dots, \tilde{c}_n)$  be the symplectic spectrum of  $\gamma^{T_1}$ . Then*

$$E_{\mathcal{N}} = \sum_{\alpha=1}^n F(\tilde{c}_\alpha) \quad (\text{C.15})$$

where  $F(c) = \log_2 \|\rho_c\|_1$ , and  $\rho_c$  is the operator whose Wigner function is a Gaussian with covariance  $\text{diag}(c, c)$ .

In order to compute the trace norm of such an operator, the covariance matrix  $\gamma$  has to be brought in a standard form called normal-mode decomposition or symplectic diagonalization. In order to understand what this means, we consider first the Hilbert space level of the system. Normal-mode decomposition means, that the state is transformed into a tensor product of independent harmonic oscillators. For the covariance matrix, normal mode decomposition means, that it is brought to the form  $\gamma = \text{diag}(c_1, \dots, c_n)$  by canonical linear transformations. The diagonal form of the covariance matrix reflects that the system is composed of a set of independent harmonic oscillators. The  $c_1, \dots, c_n$  are called the symplectic spectrum of  $\gamma$ . A very easy and fast way to compute it is to compute the eigenvalues of  $\sigma^{-1}\gamma$  which yields  $\pm ic_1, \dots, \pm ic_n$ .

It is shown in [44] that  $F(c)$  can be determined by

$$F(c) = \begin{cases} 0 & \text{for } c \geq 1 \\ -\log_2(c) & \text{for } c < 1 \end{cases} .$$

Now, we have everything at hand to easily compute the logarithmic negativity of a Gaussian state. This will be done in Chapter 3.

# Bibliography

- [1] B. Julsgaard, J. Sherson, I. Cirac, J. Fiurasek and E.S. Polzik. Experimental demonstration of quantum memory for light, *Nature* **432**, 482 (2004).
- [2] D. Loss and D.P. DiVincenzo. Quantum Computation with Quantum Dots, *Phys. Rev. A* **57**, 120 (1998).
- [3] A. Imamoglu, D.D. Awschalom, G. Burkard, D.P. DiVincenzo, D. Loss, M. Sherwin and A. Small. Quantum information processing using quantum dot spins and cavity-QED, *Phys. Rev. Lett.* **83**, 4204 (1999).
- [4] F. Meier and B. Zhakharchenya, editors *Optical Orientation*, , volume 8 of *Modern Problems in Condensed Matter Sciences* North-Holland, Amsterdam, 1984.
- [5] A. Imamoglu, E. Knill, L. Tian and P. Zoller. Optical Pumping of Quantum-Dot Nuclear Spins, *Phys. Rev. Lett.* **91**, 017402 (2003).
- [6] J.M. Taylor, C.M. Marcus and M.D. Lukin. Long-Lived Memory for Mesoscopic Quantum Bits, *Phys. Rev. Lett.* **90**, 206803 (2003).
- [7] J.M. Taylor, A. Imamoglu and M.D. Lukin. Controlling a mesoscopic spin environment by quantum bit manipulation, *Phys. Rev. Lett.* **91**, 246802 (2003).
- [8] H. Haug and S.W. Koch: *Quantum Theory of the Optical and Electronic Properties of Semiconductors*, 4. edition. World Scientific, Singapore, 2004.
- [9] P. Harrison: *Quantum Wells, Wires and Dots*, Wiley, 2005.
- [10] M. Winger: *Towards spin-flip Raman scattering in self-assembled quantum dots*, ETH Zürich, Diplomarbeit, 2005.
- [11] H.Ibach and H. Lüth: *Solid-State Physics*, Springer Verlag, 1993.
- [12] F. Rossi, editor *Semiconductor Macroatoms*, Imperial College Press, 2005.
- [13] A.J. Shields. Semiconductor quantum light sources, *Nature Photonics* **1**, 215 (2007).

- [14] E. Biolatti, I. D'Amico, P. Zanardi and F. Rossi. Electro-optical properties of semiconductor quantum dots: Application to quantum information processing, *Phys. Rev. B* **65**, 075306 (2002).
- [15] A. Stoneham: *Theory of Defects in Solids*, Oxford University Press, 1975/2001.
- [16] E. Fermi. Ueber die magnetischen Momente der Atomkerne, *Z. Phys.* page 320 (1930).
- [17] J. Schliemann, A. Khaetskii and D. Loss. Electron spin dynamics in quantum dots and related nanostructures due to hyperfine interaction with nuclei, *J. Phys.: Cond. Mat.* **15**, R1809 (2003).
- [18] D. Paget, G. Lampel, B. Sapoval and V.I. Safarov. Low field electron-nuclear spin coupling in Gallium Arsenide under optical pumping conditions, *Phys. Rev. B* **15**, 5780 (1977).
- [19] A.S. Bracker, E.A. Stinaff, D. Gammon, M.E. Ware, J.G. Tischler, A. Shabaev, A.L. Efros, D. Park, D. Gershoni, V.L. Korenev and I.A. Merkulov. Optical pumping of electronic and nuclear spin in single charge-tunable quantum dots, *Phys. Rev. Lett.* **94**, 047402 (2005).
- [20] C.W. Lai, P. Maletinsky, A. Badolato and A. Imamoglu. Knight Field Enabled Nuclear Spin Polarization in Single Quantum Dots, *Phys. Rev. Lett.* **96**, 167403 (2006).
- [21] I.A. Akimov, D.H. Feng and F. Henneberger. Electron Spin Dynamics in a Self-Assembled Semiconductor Quantum Dot: The Limit of Low Magnetic Fields, *Phys. Rev. Lett.* **97**, 056602 (2006).
- [22] G. Jundt, L. Robledo, A. Högele, S. Fält and A. Imamoglu. Observation of dressed excitonic states in a single quantum dot, *preprint: arXiv:0711.4205* (2007).
- [23] H. Christ, J.I. Cirac and G. Giedke. Quantum Description of Nuclear Spin Cooling in a Quantum Dot, *Phys. Rev. B* **75**, 155324 (2007).
- [24] F.T. Arecchi, E. Courtens, R. Gilmore and H. Thomas. Atomic Coherent States in Quantum Optics, *Phys. Rev. A* **6**, 2211 (1972).
- [25] H. Christ, J.I. Cirac and G. Giedke. Nuclear Spin Polarization in Quantum Dots-The Homogeneous Limit, *Solid State Sciences* (2007).
- [26] P. Maletinsky, A. Badolato and A. Imamoglu. Dynamics of Quantum Dot Nuclear Spin Polarization Controlled by a Single Electron, *Phys. Rev. Lett.* **99**, 056804 (2007).

- [27] H. Christ, G. Giedke and I. Cirac *unpublished*.
- [28] Z. Song, P. Zhang, T. Shi and C.P. Sun. Effective boson-spin model for nuclei-ensemble-based universal quantum memory, *Phys. Rev. B* **71**, 205314 (2005).
- [29] T. Holstein and H. Primakoff. Field dependence of the intrinsic domain magnetization of ferromagnet, *Phys. Rev.* **58**, 1098 (1940).
- [30] H. Christ: *unpublished*, Max-Planck-Institut für Quantenoptik, Dissertation, 2007.
- [31] K. Hammerer, M. Wolf, E. Polzik and J. Cirac. Quantum benchmark for storage and transmission of coherent states, *Phys. Rev. Lett.* **94**, 150503 (2005).
- [32] S.L. Braunstein and P. van Loock. Quantum information with continuous variables, *Rev. Mod. Phys.* **77**, 513 (2005).
- [33] C.H. Bennett, G. Brassard, C. Crepeau, R. Jozsa, A. Peres and W.K. Wootters. Teleporting an unknown quantum state via dual classical and Einstein-Podolsky-Rosen channels, *Phys. Rev. Lett.* **70**, 1895 (1993).
- [34] L. Vaidman. Teleportation of quantum states, *Phys. Rev. A* **49**, 1473 (1994).
- [35] M.A. Nielsen and I.L. Chuang: *Quantum Computation and Quantum Information*, Cambridge University Press, Cambridge, 2000.
- [36] F. Grosshans and P. Grangier. Quantum cloning and teleportation criteria for continuous quantum variables, *Phys. Rev. A* **64**, R010301 (2001).
- [37] K. Hennessy, A. Badolato, M. Winger, D. Gerace, M. Atature, S. Gulde, S. Fält, E.L. Hu and A. Imamoglu. Quantum nature of a strongly coupled single quantum dot-cavity system, *Nature* **445**, 896 (2007).
- [38] M. Woldeyohannes and S. John. Coherent control of spontaneous emission near a photonic band edge, *J. Opt. B: Quantum Semiclass. Opt.* **5**, R43 (2003).
- [39] K.M. Birnbaum, A. Boca, R. Miller, A.D. Boozer, T.E. Northup and H.J. Kimble. Photon blockade in an optical cavity with one trapped atom, *Nature* **436**, 87 (2005).
- [40] L. Landau. Zur Theorie der Energieübertragung bei Stößen, *Physikalische Zeitschrift der Sowjetunion* **1**, 88 (1932).
- [41] C. Zener. Non-adiabatic crossing of energy levels, *Proc. Roy. Soc. London* **137**, 696 (1932).
- [42] M.O. Scully and M.S. Zubairy: *Quantum Optics*, Cambridge University Press, 1997.

- [43] H. Scutaru. Transition Probabilities for Quasifree States, *J. Math. Phys.* **39**, 6403 (1998).
- [44] G. Vidal and R.F. Werner. A computable measure of entanglement, *Phys. Rev. A* **65**, 032314 (2002).
- [45] R. Simon. Peres-Horodecki separability criterion for continuous variable systems, *Phys. Rev. Lett.* **84**, 2726 (2000).
- [46] Y. Takahashi, H. Hagino, Y. Tanaka, B.S. Song, T. Asano and S. Noda. High-Q nanocavity with a 2-ns photon lifetime, *Opt. Express* **15**, 17206 (2007).
- [47] K. Bergmann, H. Theuer and B.W. Shore. Coherent population transfer among quantum states of atoms and molecules, *Rev. Mod. Phys.* **70**, 1003 (1998).
- [48] A.S. Parkins, P. Marte, P. Zoller, O. Carnal and H.J. Kimble. Quantum-state mapping between multilevel atoms and cavity light fields, *Phys. Rev. A* **51**, 1578 (1995).
- [49] F. Schwabl: *Quantenmechanik*, Springer-Lehrbuch, 1990.
- [50] A. Messiah: *Quantenmechanik Band 2*, de Gruyter, 1985.
- [51] Y. Shi. Perturbative formulation and nonadiabatic corrections in adiabatic quantum-computing schemes, *Phys. Rev. A* **69**, 024301 (2004).
- [52] L. Mandel and E. Wolf: *Optical Coherence and Quantum Optics*, Cambridge University Press, 1995.
- [53] B. Schumacher. Sending entanglement through noisy quantum channels, *Phys. Rev. A* **54**, 2614 (1996).
- [54] D. Kretschmann and R.F. Werner. Tema con variazioni: quantum channel capacity, *New Journal of Physics* **6**, 26 (2004).
- [55] J. Dalibard, Y. Castin and K. Mølmer. Wave-function approach to dissipative processes in quantum optics, *Phys. Rev. Lett.* **68**, 580 (1992).
- [56] C.W. Gardiner, A.S. Parkins and P. Zoller. Wave-function quantum stochastic differential equations and quantum-jump simulation methods, *Phys. Rev. A* **46**, 4363 (1992).
- [57] M.B. Plenio and P.L. Knight. The Quantum Jump Approach to Dissipative Dynamics in Quantum Optics, *Rev. Mod. Phys.* **70**, 101 (1998).
- [58] C.W. Gardiner and P. Zoller: *Quantum Noise*, 2. edition. Springer Verlag, Berlin, 2000.

- 
- [59] B. Kraus and J.I. Cirac. Discrete entanglement distribution with squeezed light, *Phys. Rev. Lett.* **92**, 013602 (2004).
- [60] E. Brion, L.H. Pedersen and K. Molmer. Adiabatic Elimination in a Lambda System, *arXiv.org:quant-ph/0610056* (2006).
- [61] S.L. Braunstein and H.J. Kimble. Teleportation of Continuous Quantum Variables, *Phys. Rev. Lett.* **80**, 869 (1998).
- [62] L.M. Duan, G. Giedke, J.I. Cirac and P. Zoller. Inseparability criterion for continuous variable systems, *Phys. Rev. Lett.* **84**, 2722 (2000).
- [63] L.F. Haruna, M.C. de Oliveira and G. Rigolin. Minimal Set of Local Measurements and Classical Communication for Two-Mode Gaussian State Entanglement Quantification, *Phys. Rev. Lett.* **98**, 150501 (2007).
- [64] D. Bruss and G. Leuchs, editors *Lectures on Quantum Information*, Wiley-VCH, 2007.
- [65] A. Peres. Separability Criterion for Density Matrices, *Phys. Rev. Lett.* **77**, 1413 (1996).
- [66] M. Horodecki, P. Horodecki and R. Horodecki. Separability of mixed states: necessary and sufficient conditions, *Phys. Lett. A* **223**, 1 (1996).
- [67] P.M. Hayden, M. Horodecki and B.M. Terhal. The asymptotic cost of preparing a quantum state, (2000).
- [68] C.H. Bennett, D.P. DiVincenzo, J.A. Smolin and W.K. Wootters. Mixed-state entanglement and quantum error correction, *Phys. Rev. A* **54**, 3824 (1996).
- [69] W.K. Wootters. Entanglement of formation and concurrence, *J. Quant. Inf. Comp.* **1**, 27 (2001).
- [70] M.B. Plenio. Logarithmic Negativity: A Full Entanglement Monotone That is not Convex, *Phys. Rev. Lett.* **95**, 090503 (2005).
- [71] G. Giedke, J. Eisert, J.I. Cirac and M.B. Plenio. Entanglement transformations of pure Gaussian states, *J. Quant. Inf. Comp.* **3(3)**, 211 (2003).
- [72] R.F. Werner and M.M. Wolf. Bound entangled Gaussian States, *Phys. Rev. Lett.* **86**, 3658 (2001).



# Acknowledgements

First of all, I want to thank Prof. Dr. Ignacio Cirac for giving me the opportunity to do my diploma thesis in his group, for his constant support, for many enlightening and motivating discussions, for all the time he spent helping me with my work and great and friendly guidance throughout all the time.

I want to thank both Prof. Dr. Ignacio Cirac and my supervisor Dr. Géza Giedke for providing such a highly interesting topic for my thesis.

Sincere thank to my supervisor Dr. Géza Giedke for his great support, his always open door, innumerable discussions, his patience, inspiration, and for all the time he has spent with me explaining and teaching me so many things and for constantly providing me with very good hints and ideas. Moreover I want to thank him for his non-profit sweet shop that kept me alive during late evenings but also during the day.

I want to thank Prof. Dr. Claus Zimmermann for being my external supervisor at the University of Tübingen and thus making this work possible, and for being the second reader of this thesis. Moreover I want to thank him for first awaking my interest in the field of quantum optics with his lecture during my studies in Tübingen.

Furthermore, I owe thanks to all my colleagues and friends in our working group who all contributed to the great and friendly atmosphere in this group. I spent many enjoyable hours with group members in the institute, in the evenings and on two great workshops.

My special thanks goes to Dr. Roman Schmied, Henning Christ, Dr. Ines de Vega, Dr. Diego Porras and Dr. Mari Carmen Banuls for fruitful discussions and Dr. Géza Giedke, Christian Schmid, Dr. Roman Schmied, Henning Christ, Eric Kessler for perusal of (parts of) my thesis.

I am very grateful to Christian Schmid for his great support during the last weeks.

I want to thank my roommates Christian Mendl, Mikel Sanz and Sébastien Perseguers who helped me with LaTeX, Mathematica and Matlab and who all created a nice and funny atmosphere in our office. Special thanks to Valentin Murg for his help and patience with my problems using the Cluster computer.

I also thank Verena Maier for her great support with all organizational tasks and for nice chats. Thanks to Maria Eckhold Perotti for the great time we spent together on the Summer School in Ireland and in Munich.

To my parents and sister I give them my deepest thank for their love and support they have given me all the way.



# Erklärung

Hiermit erkläre ich, die vorliegende Arbeit selbstständig verfasst und nur die angegebenen Quellen und Hilfsmittel verwendet zu haben.

Heike Schwager  
Garching, den 2. Januar 2008